Appendix `UALcode`: Development of the UAL/ETEAPOT Code for the Proton EDM Experiment

Nikolay Malitsky, John Talman,
and Richard Talman

August 7, 2014

Abstract

A proposed experiment to measure the proton electric dipole moment (EDM) uses protons stored in a fully electrostatic storage ring. The main bending field is produced by applying a voltage between inner and outer chamber walls. The full ring consists of repetitions of these wedge-shaped sector bends separated by drifts, quadrupoles, RF cavities and so on.

For simulating the design and performance of the EDM ring, a code UAL/ETEAPOT is being developed. New code is required because of the implicit assumption in existing code that the major deflections occur in magnets, with the result that particle speeds change only in RF cavities. In electric fields it is the *total* energy, mechanical plus potential that is conserved; $\mathcal{E} = \gamma mc^2 + eV(\mathbf{x})$. For the initially assumed (but now superceded) electrode shape (curved-planar) the radial electric field dependence is $E \sim 1/r$. For this dependence the dispersion, as conventionally defined, is *infinite*. This serves as a warning that the electric formalism has to be very different from the existing magnetic formalism.

Due to changes in potential energy the mechanical energy $\gamma m_p c^2$ changes on the same "fast" betatron time scale as the horizontal and vertical displacements. This breaks the customary paradigm in which energy oscillations are slow while betatron oscillations are fast. This has required UAL/ETEAPOT to deviate conceptually from UAL/TEAPOT.

Benchmarking of the code for an idealized lattice shows agreement at the one percent level between the (exact) ETEAPOT code and an (approximate, entirely independent) linearized transfer matrix code.

The strong coupling between speed and position is only present within electric bending element. Outside bending elements, where the electric potential vanishes, the motion more nearly resembles motion in a magnetic ring.

Contents

1 Introduction

1.1 Code Requirements for the EDM Experiment

UAL (Universal Accelerator Libraries) is an open source library of accelerator simulation codes accessible at `http://code.google.com/p/ual`. This report provides documentation for the development of UAL/ETEAPOT which is to be used for simulation of the electric lattice required for the proton electric dipole moment (EDM) experiment.[1]

The purpose for accelerator simulation codes is to simulate effects that are too complicated to be calculated analytically; for example dynamic aperture, sensitivity to errors, space charge effects, IBS and so on. All these effects, and others, will eventually be included in the UAL/ETEAPOT code.

Initially though, for the experimental planning phase, there are three less ambitious requirements:

1. Evaluation of linearized lattice functions such as tunes, the Twiss, α, β, and γ, dispersion function, chromatic dependence of these functions, and their sensitivity to imperfections.

2. Short term tracking, for confirmation of the lattice function, for determining dynamic aperture, and for investigating the performance of analytically derived compensation schemes.

3. Guaranteed to be *stable*, long term tracking. The EDM experiment requires the spin coherence time (SCT) to be 1000 s or longer. During this time every particle executes about 10^9 betatron oscillations. The code is required to be "stable" (no spurious growth or decay) for this interval of time.

The breakdown of the fast/slow, betatron/synchrotron paradigm was emphasized in the abstract. This has seriously complicated the first of the three requirements. The fast/slow separation into betatron and synchrotron amplitudes has become fundamental to the conventional (Courant-Snyder) formalism. But, in an electric lattice the mechanical energy varies on the same time scale as the transverse amplitudes. When re-expressed in terms of total energy instead of mechanical energy, a similar fast/slow separation can be anticipated. Such a formalism is not yet available, and the existing UAL/TEAPOT formalism needs serious revision for such a separation to be reconstituted.

The sloshing between horizontal betatron motion and mechanical energy is exhibited in Figure 1. It is probably not wrong to visualize every bend element as being a mini DC cavity, briefly decelerating or accelerating a particle, but averaging to zero in the long run.

In the magnetic formalism one is accustomed to treating the energy as constant for times short compared to the synchrotron period. Alternatively one can interpret the transverse treatment as being averaged over times long compared to the synchrotron period. For the time being we have to use this averaged interpretation when comparing electric lattice performance to expectations based on experience with magnetic lattices. That is to say we compare transverse behavior averaged over fast energy deviations.

Because of this longitudinal complication, each of the three listed requirements for the proton EDM experiment requires a somewhat different implementation in UAL. Requirement 1., lattice function determination, uses a truncated power series formalism in UAL/TEAPOT that is not applicable to electric elements. Requirement 3., long term stability, requires the *exact tracking in approximate lattice* feature of TEAPOT. Both of these capabilities are present in UAL/TEAPOT. But translating some of the power series formalism from magnetic to electric is a long ($\sim$one year) task. To cover all three tasks on the time scale required for experimental planning we have, therefore, had to take multiple tracks.

The first track starts by implementing "exact" tracking in the (now known to be unacceptable) inverse square law potential electrical field between spherical electrodes, with *real* quadrupoles present in the lattice to provide vertical focusing. To be applicable to the E_r approximately independent-of-r field dependence now thought to be optimal, it is necessary to introduce *artificial* quadrupoles in the interior of bend elements. Causing only "kicks", these elements preserve symplecticity. Meeting the TEAPOT

[1] For the record, all results in this report were obtained using ETEAPOT/Cylindrical distributed in version svn:472 of the UAL code. This version number changes almost daily and any version later than 472 should produce equivalent results.

standard, the subsequent tracking is then *exact*. We refer to this computational track as *Spherical*. This track will allow requirements 2. and 3. to be met.

An earlier version of the code, referred to as *Cylindrical*, performed only approximated tracking in and electric field E_r having the logarithmic potential established between cylindrical electrodes. For this field it is quite a good approximation to treat horizontal and vertical betatron motion as uncoupled. By tracking particles with judiciously chosen initial parameters the tunes Q_x, Q_y and Q_s could be obtained to good accuracy, by tracking over many turns followed by FFT processing. An example is shown in Fig. 1. Since (linearized) transfer matrices are not used this code could not extract Twiss functions. However, tunes and Twiss functions can be obtained (to amply satisfactory accuracy) using FFT and MIA (model-independent) analysis. (See Section 2.1.)

The *Spherical* code removes the blemish of treating horizontal and vertical motion as uncoupled. Artificial thin kicks are still be required to implement the actual radial field dependence. This is similar to the (well-tested) treatment of combined function magnets by TEAPOT.

1.2 Electric Lattice Formalism: Qualitative Discussion

Analytic evolution formulas for electric elements have been obtained for the simplest ($1/r^2$ and $1/r$) electric field variations. See Sections 3, 4, and 3. Closed form expressions describing propagation through thick elements are derived for these two special radial dependencies. Appendix 6.2 descibes how (with delta function kicks) "exact" tracking can be performed for other, in general non-integer, field indices using one or the other of the two analytic formulations. The ($1/r^2$) formulas are both analytic and exact (relativistic Kepler problem). The ($1/r$) formulas become exact only after (quite accurate) redefinition of the radial dependence.

As in magnetic TEAPOT, perturbative focusing effects can be incorporated by thin element kicks without sacrificing long term stability. This includes handling the true, typically non-integer, field index case. Since the ($1/r$) case is closer to the actual experimental field, using it amounts to reducing the size of the perturbation used in modeling the true field. In any case, both formalisms are derived in this report. Treatment of the artificial quadrupoles, as well as true quadrupoles, sextupoles, and so on is described in Appendix 7.

In spite of being both exact and fully relativistic, the $1/r^2$ law case generalizes in full the analytic Newton/Kepler formulas familiar from planetary orbits and the hydrogen atom. A similarly powerful analysis in the $1/r$ case is only applicable (and exact) after minor field modification (which has only minor effect for the realistic EDM lattice). A linearized, transfer matrix description adequate for discussion of orbit stability is given. But this description is insufficient since compensation of spin decoherence requires nonlinear analysis to at least sextupole order.

Analytic evolution formulas, valid for orbits of arbitrarily great amplitude relative to the central orbit are derived. Based on these formulas a reduction to quadratures solution is obtained for the Thomas/BMT equation governing the evolution of the in-plane spin component.

Numerical computational algorithms are needed for "exact" (and hence symplectic) orbit and spin evolution in idealized lattice elements. As well as thick bends, this includes thin multipole elements, especially quadrupoles and sextupoles. This capability is needed for various technical reasons specific to the proton EDM experiment. The $1/r^2$ field provides unnecessarily strong vertical focusing and undesirably large mechanical energy discontinuities at element ends. The $1/r$ field provides no vertical focusing; this is the reason there need to be vertically focusing quadrupoles present in the lattice. The infinite dispersion problem mentioned in the abstract makes the cylindrical case very tricky however.

Assuming (as we do) that idealized, zero length elements can be approximately replicated with finite length elements, it is hoped that long term evolution (especially spin coherence time) can be reliably predicted for the billion or so turns needed for the effect of the miniscule electric dipole moment to make its presence felt.

This report, now intended to serve as documentation for the UAL/ETEAPOT simulation code, was originally a chapter in the March 2011, BNL review of the EDM experiment. Numerical examples and graphs specific to the realistic EDM ring are mainly contained in the "Ring Lattice" chapter for the same BNL review.

1.3 Evolution Strategy

The February, 2011, baseline proton EDM lattice is almost circular, only slightly racetrack-shaped, with (approximate) superperiodicity of eight, and true periodicity of two, as well as mirror symmetry about both diameters. Identical electrostatic sector bends are interspersed with drifts, quadrupoles and other elements. The first task is to evolve proton orbits through one such sector bend. After that, orbit evolution through other elements, and spin evolution is treated.

For faithful long term treatment of the evolution of proton orbits in electric elements the general strategy is to mimic, but improve upon, the strategy employed by TEAPOT for following orbits in magnetic fields. To preserve symplecticity, *exact* ("to machine precision") orbits have to be found. Here the (controversial) term "exact" is used as shorthand for the longer TEAPOT principle of "exact tracking in an approximate lattice" which is to be contrasted with the more common "approximate tracking in an exact lattice". That is, the physical lattice model has to be sufficiently idealized that its mathematically exact orbits can be found. (In appropriate variables) the solutions are pure sinusoids that can be said to be exact for infinite time, at least as regards stability.

In (magnetic) TEAPOT all quadrupoles, sextupoles, and multipoles are segmented finely enough to be represented by delta functions (thereby preserving symplecticity). Even uniform magnetic field sector bends are segmented sufficiently finely to be represented as thin elements. This step, taken when TEAPOT was first developed, though not wrong for sufficiently fine element slicing, has later been found to be unnecessarily crude. Our electric approach proceeds less clumsily.

Similar comments apply to the evolution of spin orientation. It has to be calculated exactly (to guarantee symplecticity). The spin evolution is simpler in at least one way. Though the spin orientation is in locked response to the particle orbit, the particle orbit is unaffected by the spin orientation. (As far as we know, Stern-Gerlach particle deflections can always be neglected in the present context.)

We are not particularly interested in the sort of polarization that develops over long times in electron rings. Rather we are interested in tracking beams that, initially, are at least partially polarized. Generally speaking, the accelerators of interest are designed to preserve this polarization, in the face of decoherence mechanisms that are conspiring to destroy the polarization. For the EDM experiment a compensation scheme to preserve the polarization has been designed. It is described in the accompanying Ring Lattice chapter. An important early task for the ETEAPOT simulation tool will be to faithfully track the polarization so that the efficacy of this or other compensation schemes can be evaluated and improved.

References [1] through [7] are useful for deriving formulas for the (relativistic) Kepler orbits we have to deal with. Møller[1], probably following Einstein or Darwin, in the context of perihelion advance of Mercury, derives the fully relativistic inverse square law orbit equation and solves it perturbatively. Aguirregabiria[5] derives the orbit equation for arbitrary power law fields, and describes circular and near-circular orbits; this is equivalent to an accelerator physicist's paraxial transfer matrix description. Boyer[7] solves the relativistic orbit equation in general, but with emphasis on the anomalous spiraling-in of high energy, low angular momentum orbits, absent non-relativistically, but permitted by relativity.

2 Preliminary Results

2.1 Orbit Tracking

Particle tracking results for the lattice `E_FirstTest.sxf` are shown in Figs. 1, 2, and 3. The "`E_`" prefix to the file name serves only as a reminder that the lattice only makes sense when its elements are interpreted as being electric. Otherwise the file is indistinguishable from a magnetic lattice description file.

There are various lattice exchange formats, of which "`.sxf`" is one. Using MADX, lattice descriptions in this format can be produced from lattices in the "`.mad`" format, such as the baseline proton EDM lattice `E_pEDM-rtr1.mad` lattice described in the accompanying chapter (for the March, 2011, BNL Review) entitled "Ring Lattice for Proton EDM Measurement"[13].

The plots are explained in the captions to the figures. Apart from illustrating present code capabilities these plots are primarily intended to illustrate the phase space sloshing between horizontal betatron and longitudinal mechanical energy (γmc^2).

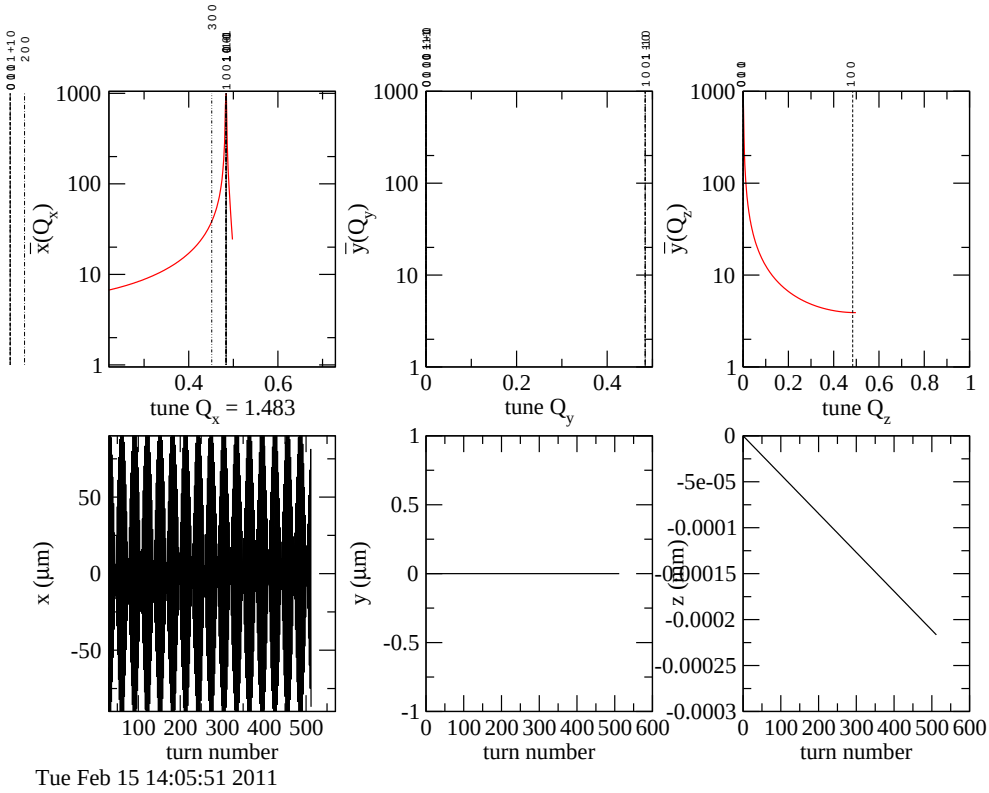

Figure 1: Tracking results for purely horizontal motion of one particle in an idealized "first test" ring. The lower row gives time domain, turn-by-turn displacements, horizontal, vertical and longitudinal. The upper row shows tune domain spectra obtained by FFT processing the corresponding data in the lower row. Since there is no RF cavity in the ring, the lower right hand figure shows the particle's inexorable longitudinal drift. The lower left graph exhibits horizontal betatron motion at the expected horizontal tune of $Q_x = 1.48$ (as read from the curve above it) but modulated by the sloshing between betatron oscillation and mechanical energy $\gamma m_p c^2$. The upper right hand figure does not show this sloshing because it is the FFT of turn-by-turn values of total energy $\mathcal{E}$, which is conserved rather than the mechanical energy, which is not.

The `E_FirstTest.sxf` is a simple example of the simplest possible electrode design (curved planar electrodes). Except for its having no sextupoles this lattice is the same as the version (viii) EDM lattice described in reference [21]. Weak vertically focusing quadrupoles, needed to stabilize the vertical motion, are the only quadrupoles in the ring. This lattice has extravagantly long straight sections and extravagantly short cell lengths compared to the current baseline design. Its properties have been thoroughly studied using transfer matrices. Its infinite dispersion function and the fact that its orbits can be calculated analytically make it both a clean and a stringent test of the ETEAPOT code.

The most striking *physics* result obtained so far is the sloshing between phase space degrees of freedom, shown most clearly in Fig. 3. The presence of coupling between horizontal and longitudinal degrees of freedom has been understood for some time. What is new is the near perfect mixing of the four degrees of freedom in the design plane of the ring.

Recall that the $1/r$ field variation case being analysed is also the singular, logarithmic potential, "infinite dispersion" case. It might be said that mother nature protects herself from singularity by shoving amplitude from the singular degree of freedom into other degrees of freedom. It remains to be seen whether there will be as good mixing for the non-singular, such as $r^{0.2}$, field variation.

There is further discussion of these results in Section 2.2.

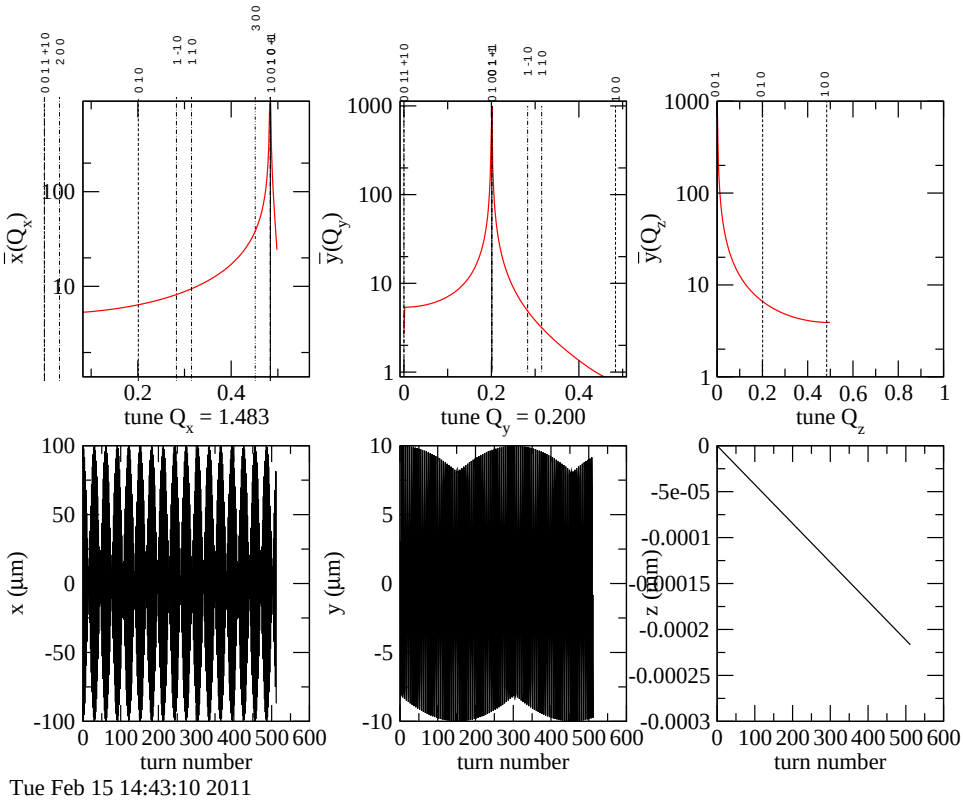

Figure 2: Tracking results for simultaneous vertical and horizontal motion of one particle in an idealized "first test" ring. The same sloshing between horizontal and longitudinal phase space as in Figure 1 is observed. The much weaker sloshing away from vertical may be due to the fact that the vertical focusing strength of the quadrupoles is modulated by oscillation of the particle momentum. The vertical dashed lines in these plots give resonance indices. So "1 0 0" labels the horizontal fundamental and "0 1 0" labels the vertical fundamental. The absence of peaks at "1 1 0" or "1 -1 0" (or anyplace else for that matter) indicates that resonance is playing no role. The weakness of the sloshing is consistent with our treating horizontal and vertical motion as independent.

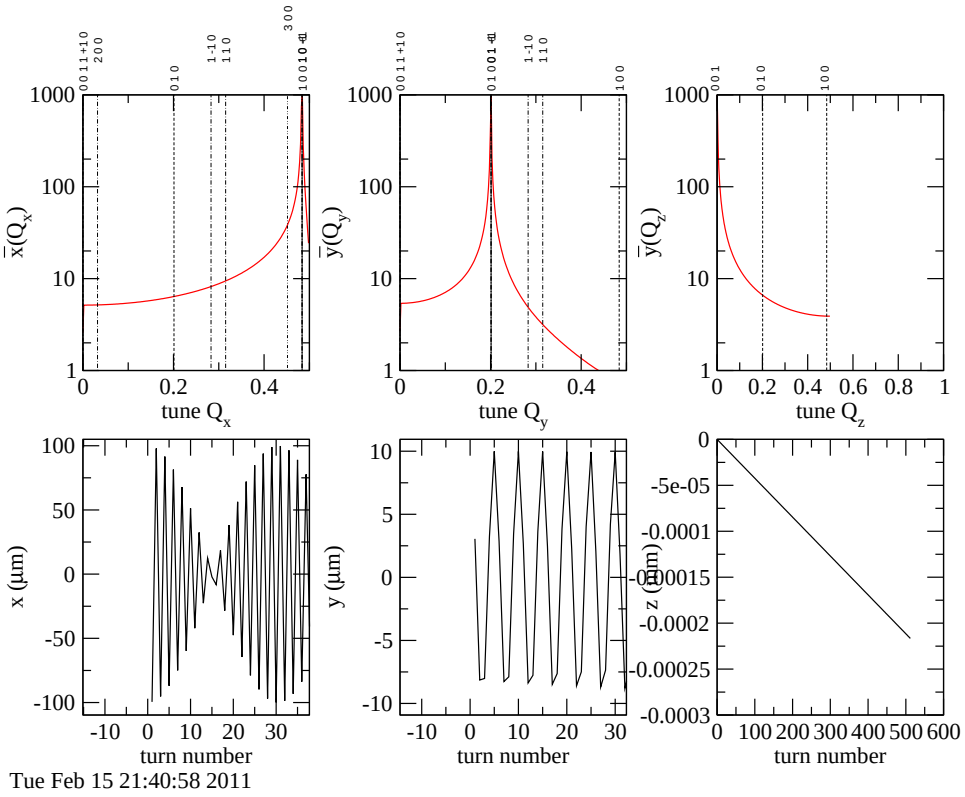

Figure 3: This is the same as Figure 2, except only a brief time interval is displayed so that individual turns can be observed. This is how the integer portion of the tunes have been inferred (though protection against aliasing requires more than one sampling per turn). The beat pattern is obvious for horizontal oscillations, but there is the merest hint of a pattern for vertical oscillations.

2.2 Comparisons With Analytic Results

Initial requirements for tracking protons in the EDM experiment were listed in Section 1.1. This was interpreted to mean, primarily, comparisons with the lattice functions of the baseline proton EDM lattice described in reference [13]. That reference, using linearized transverse transfer matrices, produced the sorts of Twiss function plots and other lattice functions that one is accustomed to seeing for magnetic lattices.

Using the transfer matrix formalism formalism (described in Section 8.1.7), the tunes for the `E_FirstTest.sxf` are predicted to be $Q_x = 1.52$, $Q_y = 0.200$. Using the *cylindrical* version of ETEAPOT, the tunes for the same lattice are predicted to be $Q_x = 1.48$, $Q_y = 0.200$, as shown on axis labels in Fig. 2. Even without allowing for the fast/slow issue just discussed, we regard these values sufficiently close to provide mutual corroboration of both approaches (which, admittedly, are produced by the same team.) A tune comparison between truly independent workers has been documented by Semertzidis[22].

Note added in proof: while editing the figure caption to Fig. 3 it was realized that the $Q_x = 1.48$ tune identification might be being fooled by incorrect alias deciphering. Since the `E_FirstTest.sxf` has perfect forty-fold supersymmetry, it was possible to sample more finely by a factor of forty. This gave $Q_x = 1.515$, in nearly perfect agreement with the transfer matrix determination—the correct tune is 2 minus the (insufficiently finely sampled) FFT displayed tune rather than 1 plus that displayed tune. The numerical value $Q_x = 1.483$ shown in Figs. 1 and 2 is therefore wrong; it should be $Q_x = 1.517$.

Detailed comparisons with other lattice functions have not yet been produced. Given that the tunes are simple averages of the (inverse) beta functions, and the variation ranges of the beta functions are not great, it is obvious that the beta functions obtained by the two independent approaches are also in very good agreement.

In any case comparisons between linearized transfer matrix results (which neglect coupling between longitudinal and horizontal) with ETEAPOT results (which make no such assumption) can only be approximate.

2.3 Spin Tracking

Development of spin tracking in ETEAPOT has been deferred until orbitry is well in hand. Though we are approaching this state we are not yet there.

It should be noted though that the rapid sloshing between horizontal and longitudinal amplitudes has important implications for the proton EDM experiment. The most ideal dynamics for long spin coherence time would have perfect mixing of all three degrees of frequency. (If every particle is like every other, then their spins would all precess coherently.) Such mixing could be imposed externally but that would surely violate the conditions on which Liouville's theorem is based and could only be accompanied by emittance growth.

The "mixing" caused by electric bend elements is "lossless". That is, it is Hamiltonian and meets the requirements of Liouville's theorem.

The "effective RF" provided by each electric bend causes every particle velocity to "dither" about its central value, with a fractional range of about one part in 10^4. A similar dithering, over a not much greater range, will be caused by the oscillations produced by the RF cavity in the ring. This mode of operation is required to preserve long spin coherence time, but at the cost of requiring the beam to be bunched. (An RF cavity is also required for various beam manipulations needed for the experiment, and for other technical reasons.) In principle, under ideal (and hence almost surely unachievable) conditions, the automatic dithering produced by the electric elements could preserve quite long spin coherence times even for unbunched beams.

Even neglecting vertical motion this mixing will not cause every particle to be equivalent to every other on the average. Rather the best one can expect is a kind of foliation (like an onion, not like an artichoke) in which all particles on the same leaf are all equivalent (averaged over time). Even this much mixing should markedly relax the spin coherence time compensation scheme requirements.

3 Electric Field Varying as $1/r$

An electric field with index m power law dependence on radius r for y=0 is

$$\mathbf{E}(r,0) = -E_0 \, \frac{r_0^{1+m}}{r^{1+m}} \, \hat{\mathbf{r}}, \tag{1}$$

and the electric potential $V(r)$, adjusted to vanish at $r = r_0$, is

$$V(r) = -\frac{E_0 r_0}{m} \left(\frac{r_0^m}{r^m} - 1 \right). \tag{2}$$

The "cleanest" case has m=1, in which case it is known as the Kepler or the Coulomb electric field. Our case is a bit more general than this terminology suggests, since our treatment is necessarily relativistic. For m=1 the Kepler problem can be solved with the same generality in the relativistic as in the nonrelativistic case; the orbits are no longer exactly elliptical, nor exactly closed however.

The equations are most easily assimilated and checked for m=1. (The offset of 1 in the definition of this index is inherited from the unfortunate historical choice of $1/r$ as the radial variation of choice for the EDM experiment.) The EDM experiment is now known to need $m \neq 0$. We therefore start with an arbitrary m formulation.

The (now deprecated) curved-planar electrodes produce an electric field having m=0 as the field index. The task is to determine the exact general orbit, which is the bold curve in Fig. 4. Its initial radial displacement (from the design orbit) and its radial slope are x_0 and x_0'. The initial vertical slope is y_0'. Any particular orbit will also have some initial vertical displacement y_0. But y_0 can be set to zero without loss of generality, since the apparatus has vertical translational symmetry. (This is only true for $m = 0$.) The orbit is also influenced by the proton's initial fractional total (mechanical plus potential) energy deviation from nominal, $\Delta\mathcal{E} = \mathcal{E} - \mathcal{E}_0$. This makes, altogether, four independent initial conditions. Unlike in a magnetic field, the magnitude of the momentum is *not* conserved in the electric bend. Given initial conditions $X(\theta = 0) = \big(x_0, x_0', y_0', \Delta\mathcal{E}_0\big)$, the task is to solve for $X(\theta) = \big(x(\theta), x'(\theta), y'(\theta), \Delta\mathcal{E}_0\big)$. Note, here, that the fourth component does not change—with potential energy included in the definition of total energy, $\mathcal{E}$ *is conserved*. But the mechanical energy, conveniently represented as $\gamma m_p c^2$, is not conserved in general; only the sum of mechanical and potential energy is conserved. On entering or exiting a bending element it is necessary to account for the changes in potential energy.

The central, or design, orbit is a circle of radius r_0, midway between the circular cylinder electrodes of radii $r_0 \pm g/2$. Defining the electric field on the central orbit as E_0, the field is given by[2]

$$\mathbf{E}(r,\theta,y) = -E_0 \, \frac{r_0}{r} \, \hat{\mathbf{r}}. \tag{3}$$

The electric potential $V(r)$, adjusted to vanish on the design orbit, is

$$V(r) = E_0 r_0 \ln \frac{r}{r_0} = E_0 r_0 \ln r - E_0 r_0 \ln r_0. \tag{4}$$

The design parameters are related by

$$eE_0 r_0 = \beta_0 p_0 c = m_p c^2 \Big(\gamma_0 - \frac{1}{\gamma_0} \Big), \tag{5}$$

where p, v, and β are proton momentum, velocity, and v/c. The momentum vector components are defined by

$$\mathbf{p} = p_r \hat{\mathbf{r}} + p_\theta \hat{\theta} + p_y \hat{\mathbf{y}} = \frac{m_p \dot{r}}{\sqrt{1 - v^2/c^2}} \, \hat{\mathbf{r}} + \frac{m_p r \dot{\theta}}{\sqrt{1 - v^2/c^2}} \, \hat{\theta} + \frac{m_p \dot{y}}{\sqrt{1 - v^2/c^2}} \, \hat{\mathbf{y}}. \tag{6}$$

[2] To be scrupulously careful at this point the radial coordinate r and the radial unit vector $\hat{\mathbf{r}}$ would be assigned subscripts c, standing for "cylindrical" to distinguish them from spherical coordinates that will enter later. For y=0, r_c and r_s coordinates are identical and, at least in an accelerator, they will always be at least approximately equal. Somewhat confusingly, in this section, whereas r is the radial cylindrical coordinate, $\mathbf{r}$, the three dimensional radius vector, can have a non-vanishing y-component.

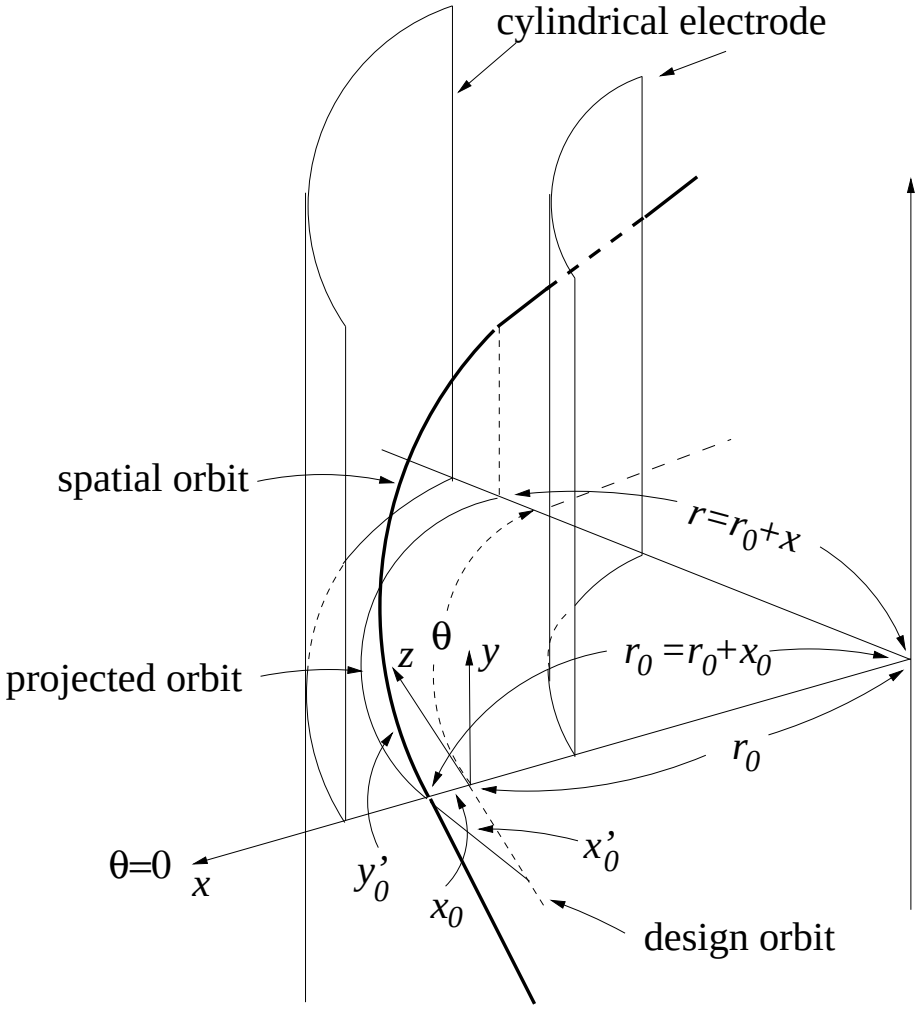

Figure 4: The bold curve shows a proton orbit passing through a curved-planar cylindrical electrostatic bending element. The electrode spacing is g and the design orbit is centered between the electrodes.

The electric force alters only the radial momentum component

$$\frac{dp_r}{dt} = -eE_0\frac{r_0}{r}. \tag{7}$$

It is essential to exploit the invariance of the system to translation along the y-axis, which causes p_y to be conserved, and to rotation around the central axis, which causes L_y, the vertical component of angular momentum, to be conserved. For a particle in the horizontal plane containing the origin the angular momentum vector is

$$\mathbf{L} = \mathbf{r}\times\mathbf{p} = -\frac{m_p r\dot{y}}{\sqrt{1-v^2/c^2}}\,\hat{\theta} + \frac{m_p r^2\dot{\theta}}{\sqrt{1-v^2/c^2}}\,\hat{\mathbf{y}} = L_\theta\hat{\theta} + L_y\hat{\mathbf{y}}. \tag{8}$$

The design orbit angular momentum is

$$L_0 = m_p c\beta_0\gamma_0 r_0. \tag{9}$$

We seek the orbit differential equation giving dependent variable r as a function of independent variable θ. The (conserved) total proton energy $\mathcal{E}$ is the sum of the mechanical energy and the potential energy

$$\mathcal{E} = \sqrt{p_r^2c^2 + p_\theta^2c^2 + p_y^2c^2 + m_p^2c^4} + eV(r). \tag{10}$$

Squaring this equation yields

$$\big(\mathcal{E} - eV(r)\big)^2 = p_r^2c^2 + p_\theta^2c^2 + p_y^2c^2 + m_p^2c^4. \tag{11}$$

The terms on the right hand side of this equation can be expressed in terms of r, $dr/d\theta$, and conserved quantities. From Eqs. (6) and (8),

$$p_\theta = \frac{L_y}{r}. \tag{12}$$

p_r can be expressed similarly using Eq. (6);

$$\frac{p_r}{p_\theta} = \frac{\dot{r}}{r\dot{\theta}} = \frac{1}{r}\,\frac{dr}{d\theta}, \quad \text{and hence} \quad p_r = \frac{L_y}{r^2}\,\frac{dr}{d\theta}. \tag{13}$$

Making these substitutions yields

$$\big(\mathcal{E} - eV(r)\big)^2 = \left(\frac{L_y c}{r^2}\frac{dr}{d\theta}\right)^2 + \frac{L_y^2c^2}{r^2} + p_y^2c^2 + m_p^2c^4. \tag{14}$$

Following treatments of relativistic Kepler orbits such as [1], we change variables from r to a dimensionless variable ξ, which is proportional to x for small x, and substitute

$$\xi = 1 - \frac{r_0}{r} = \frac{x}{r_0+x} = \frac{x}{r}, \quad \text{and} \quad \frac{d\xi}{d\theta} = \frac{r_0}{r^2}\,\frac{dr}{d\theta}, \quad \text{or} \quad \frac{d\xi}{d\theta} = \frac{r_0^2}{r^2}\,\frac{dr}{ds}, \tag{15}$$

since $s = r_0\theta$. Inverse relations are

$$x = \frac{r_0\xi}{1-\xi}, \quad \text{and} \quad \frac{dx}{ds} = \frac{r_0 d\xi/ds}{(1-\xi)^2} = \frac{d\xi/d\theta}{(1-\xi)^2}. \tag{16}$$

With ξ regarded as a function of θ and x as a function of s, sometimes one uses the abbreviations $\xi' = d\xi/d\theta$ and $x' = dx/ds$, so $x' = \xi'/(1-\xi^2)$.

Eq. (14) becomes

$$\big(\mathcal{E} + eE_0r_0\ln(1-\xi)\big)^2 = \frac{L_y^2c^2}{r_0^2}\left(\frac{d\xi}{d\theta}\right)^2 + \frac{L_y^2c^2}{r_0^2}(1-\xi)^2 + p_y^2c^2 + m_p^2c^4. \tag{17}$$

Differentiating this equation with respect to θ and dividing through by $d\xi/d\theta$ yields

$$\begin{aligned}\frac{d^2\xi}{d\theta^2} &= 1-\xi-\mathcal{E}\,\frac{eE_0r_0^3}{L_y^2c^2}\,\frac{1}{1-\xi}-\frac{e^2E_0^2r_0^4}{L_y^2c^2}\,\frac{\ln(1-\xi)}{1-\xi}\\ &= 1-\xi-\frac{\mathcal{E}/e}{L_yc/(er_0)}\,\frac{E_0r_0}{L_yc/(er_0)}\,\frac{1}{1-\xi}-\left(\frac{E_0r_0}{L_yc/(er_0)}\right)^2\frac{\ln(1-\xi)}{1-\xi}\\ &= 1-\xi-\frac{\mathcal{E}}{\mathcal{E}_0}\,\frac{L_0^2}{L_y^2}\,\frac{1}{1-\xi}-\frac{L_0^2}{L_y^2}\,\beta_0^2\,\frac{\ln(1-\xi)}{1-\xi}.\end{aligned} \tag{18}$$

Here L_0 and $\mathcal{E}_0$ represent the design orbit angular momentum and total energy. The final step has used Eq. (5). This is the "orbit equation" to be solved for every particle passing through every bend element.

3.0.1 Solution of the $E \sim 1/r$ Orbit Equation

For the paraxial motion appropriate for an accelerator the variable ξ will always be close to x/r_0. The ratios L_0/L_y and $\mathcal{E}/\mathcal{E}_0$ will also be very close to 1.

For the proton EDM experiment the "magic" kinematic parameters satisfy

$$g = 2G+2, \tag{19}$$

$$\gamma_0 = \sqrt{\frac{g}{g-2}} = \sqrt{1+\frac{1}{G}}, \tag{20}$$

where all fundamental parameters are stored in `$UAL/codes/UAL/src/UAL/common/Def.hh`, and yield the following kinematic quantities:

```
mcsq :=              0.938272046 GeV
G :=                 1.79284736
c :=                 2.99792458e8 m/s
g := 2G + 2 =        5.58569472
gamma0 :=            1.248107354
Escr0 := gamma0*mcsq 1.171064241 GeV
K0 := Escr0 - mcsq   0.232792195 GeV
p0c :=               0.7007403404 GeV
beta0 :=             0.5983790777
```

(Occasionally the symbol "a" is used instead of the symbol "G".) These numbers are fixed by the "frozen-spin" requirement of the experiment. For the baseline lattice adopted in early-2011, $r_0 = 40.0\,\mathrm{m}$. For this value $L_0c/e = r_0p_0c/e = 28.0\,\mathrm{GV\text{-}m}$.

Though nonlinear and formidable-looking, Eq. (18) has the simplifying feature that all terms on the right hand side are functions only of the dependent variable ξ. The physicist's approach to this situation is to introduce an "effective potential" whose derivative yields the "effective force" on the right hand side of the equation. This provides a "reduction to quadratures" solution. The mathematician's approach is to find an integrating factor followed by the same reduction to quadratures. The integrating factor is

$$\mu = \frac{d\xi}{d\theta} \equiv \xi'. \tag{21}$$

(Note that prime " ' " here, when applied to ξ, is being used as abbreviation for "$d/d\theta$" which is not the same as its usual (accelerator jargon) meaning of "d/ds", where s is longitudinal position. One consequence of this is that phase space coordinates ξ and ξ' will have identical physical dimensions here. Also the Twiss parameters will acquire familiar units only after θ has been converted to $s = r_0\theta$ and the Twiss parameters altered accordingly.)

The reduction to quadratures approach gives θ as a function of ξ, but we need the inverse, giving ξ as a function of θ. Unfortunately the reduction to quadrature integral cannot be evaluated analytically. It

will be necessary, therefore, to obtain some form of analytical approximation. Failing that, it would be necessary to perform the integral numerically. This would probably be too slow for long term tracking.

Taylor approximating the quadrature solution denominator factor and dropping terms beyond quadratic alters the value of the denominator factor by only 3×10^{-7} for an orbit just striking inner and outer electrodes. Furthermore the integral can be performed and the result inverted to give $\xi(\theta)$ in a sinusoidal form having the same simple properties as will be obtained next, Taylor expanding the right hand side of the orbit equation itself. The quadrature integral can be evaluated in terms of elliptic integral functions even after keeping one more term in the denominator. This leads to absurdly high accuracy (with hopeless complexity) that can be perhaps be used for testing the accuracy of the simpler solutions.

A simpler approach we now take is to approximate the right hand side of orbit equation (18) by Taylor expansion;

$$(1-\xi)^{-1} = 1 + \xi + \xi^2 + \ldots, \quad \frac{\ln(1-\xi)}{1-\xi} = -\xi - \frac{3}{2}\,\xi^2 + \ldots. \tag{22}$$

The orbit equation becomes

$$\frac{d^2\xi}{d\theta^2} = 1 - \frac{L_0^2}{L_y^2}\,\frac{\mathcal{E}}{\mathcal{E}_0} - \left(1 + \frac{L_0^2}{L_y^2}\Big(\frac{\mathcal{E}}{\mathcal{E}_0} - \beta^2\Big)\right)\xi - \frac{L_0^2}{L_y^2}\left(\frac{\mathcal{E}}{\mathcal{E}_0} - \frac{3}{2}\,\beta^2\right)\xi^2 + \ldots \tag{23}$$

$$\approx -Q^2(\xi - \xi_{\rm co}), \tag{24}$$

where

$$Q^2 = 1 + \frac{L_0^2}{L_y^2}\Big(\frac{\mathcal{E}}{\mathcal{E}_0} - \beta^2\Big), \quad \text{and} \quad \xi_{\rm co} = \frac{1 - \frac{L_0^2}{L_y^2}\,\frac{\mathcal{E}}{\mathcal{E}_0}}{Q^2}. \tag{25}$$

After this simplification the equation has been reduced to offset simple harmonic motion. $\xi_{\rm co}$ is the value ξ-value for which the r.h.s. vanishes for the parameters appearing in the equation.

Our approach will be to take Eq. (25), only an approximation to the true system though it may be, as being the differential equation for a redefined physical system approximating the original. By solving the redefined equations exactly one preserves exact symplecticity, even for propagation through thick elements. Furthermore, energy conservation will be preserved explicitly at every transition at the edges of bend elements.

It is important to realize that the parameters in Eq. (25) need to be worked out on a particle-by-particle basis. In particular $\xi_{\rm co}$ is *not* the ξ-value of an incident particle being tracked; rather (after multiplication by Q^2) it is the constant term on the r.h.s. of the equation appropriate for the particle being tracked. The coefficient Q, though approximately constant, depends on the dynamic variables $\mathcal{E}$, L_y, and β, which also depend on the coordinates of the particle being tracked.

3.0.2 Tracking the Full Transverse Oscillation Amplitude

For propagating $\Delta\xi = \xi - \xi_{\rm co}$, one introduces cosine-like trajectory $C_\xi(\theta)$ satisfying $C_\xi(0) = 1$, $C'_\xi(0) = 0$ and sine-like trajectory $S_\xi(\theta)$ satisfying $S_\xi(0) = 0$, $S'_\xi(0) = 1$. They are given by

$$\begin{aligned} C_\xi(\theta) &= \cos(Q\theta) \\ C'_\xi(\theta) &= -Q\,\sin(Q\theta) \\ S_\xi(\theta) &= \frac{\sin(Q\theta)}{Q} \\ S'_\xi(\theta) &= \cos(Q\theta). \end{aligned} \tag{26}$$

For describing evolution of (ξ, ξ') from its initial values $(\xi_{\rm in}, \xi'_{\rm in})$ at $\theta = 0$ to its values at θ one can use the "transfer matrix" defined by

$$\mathbf{M}_\xi\,(\theta) = \begin{pmatrix} C_\xi(\theta) & S_\xi(\theta) \\ C'_\xi(\theta) & S'_\xi(\theta) \end{pmatrix}, \tag{27}$$

to give

$$\begin{pmatrix} \xi(\theta) \\ \xi'(\theta) \end{pmatrix} = \begin{pmatrix} \xi_{\rm co} \\ \xi'_{\rm co} \end{pmatrix} + \mathbf{M}_\xi(\theta) \begin{pmatrix} \xi_{\rm in} - \xi_{\rm co} \\ \xi'_{\rm in} - \xi'_{\rm co} \end{pmatrix}. \tag{28}$$

or

$$\begin{aligned} \xi(\theta) &= \xi_{\rm co} + C_\xi(\theta)(\xi_{\rm in} - \xi_{\rm co}) + S_\xi(\theta)(\xi'_{\rm in} - \xi'_{\rm co}), \\ \xi'(\theta) &= \xi'_{\rm co} + C'_\xi(\theta)(\xi_{\rm in} - \xi_{\rm co}) + S'_\xi(\theta)(\xi'_{\rm in} - \xi'_{\rm co}). \end{aligned} \tag{29}$$

Using Eq. (15) initial conditions $(\xi_{\rm in}, \xi'_{\rm in})$ can be expressed in terms of initial x conditions;

$$\xi_{\rm in} = \frac{x_{\rm in}}{r_0 + x_{\rm in}}, \quad \xi'_{\rm in} = \frac{r_0^2 x'_{\rm in}}{(r_0 + x_{\rm in})^2}. \tag{30}$$

Substitution from Eqs. (30) into Eqs. (29) gives a description of the evolution of $(\xi(\theta), \xi'(\theta))$, from initial conditions $(x_{\rm in}, x'_{\rm in})$. Finally the x evolution is obtained by substitution into Eqs. (16).

Because of the Taylor expansion in Eq. (24) these equations are not exact. The similar manipulations for the inverse square law field will not require this Taylor expansion.

For the proton EDM experiment the value of radius r_0 will be, say, 40 m. An initial value $x_{\rm in} = 1$ m would be unrealistically large. It is better therefore to use centimeter units. Then $r_0 = 4000$ cm. With the gap width being 3 cm, a typical amplitude is 0.1 in these units, and (allowing for radial offset due to momentum) a maximal surviving amplitude is about 1. Even at this amplitude the nonlinear correction, for example in the denominators of Eq. (30), is only 1 part in 4000.

3.0.3 Vertical Motion

The formalism so far has assumed that horizontal and vertical motions are decoupled. For our present $m = 0$, cylindrical electrode case, this an excellent, but not perfect, approximation. There are two reasons why it is so good. With cylindrical electrodes there is no vertical field so the vertical component of momentum is conserved. Also, for the EDM experiment, the vertical beta function is huge (certainly greater than 100 m) and the vertical emittance is tiny, $\epsilon_y \approx 0.0001$ m. A typical vertical angle is therefore $\sqrt{10^{-6}} = 1$ mr, which makes the vertical speed nonrelativistic. The only change in vertical velocity is due to a change in the relativistic mass. The vertical displacement error from this source while traversing one bending element cannot exceed $10^{-11}\, m$ and averages to zero to far higher accruracy than this. It is therefore an excellent approximation to use

$$y = y_0 + y'_0 s, \tag{31}$$

to model the vertical motion. The vertical motion has a similarly negligible effect on the horizontal motion.

The distinction between short and long term stability was introduced in the introduction. This decoupling of horizontal and vertical motion assumed here is almost surely legitimate even for long term stability and, without doubt, is adequate for short term behavior. The long term treatment is based on the $1/r^2$ formalism, for which the horizontal/vertical coupling is treated exactly.

3.0.4 Fast/Slow, Betatron/Synchrotron Separation

An alternate interpretation of Eq. (25) is to evaluate Q^2 and $\xi_{\rm co}$ on the design orbit and to treat them as being the same for all particles. Or better, Q^2 and $\xi_{\rm co}$ can be treated as functions of the energy offset. This produces the standard, linearized, description of the motion as being the sum of a betatron and a synchrotron part, with the betatron part quickly varying and the synchrotron part slowly varying. However, this separation is not very well motivated for electric lattices since the mechanical energy of each particle varies on the betatron oscillation time scale. This invalidates the conventional betatron/synchrotron separation paradigm.

The general solution of Eq. (24) can be written as the sum of a general solution of the homogeneous part and a specific solution of the inhomogeneous part, where the term $Q^2\xi_{\rm co}$ on the r.h.s. of Eq. (25) is the inhomogenous term.

The homogeneous solution will be referred to as "betatron oscillation", which will also be referred to as "fast" oscillation (in spite of the fact that, for the proton EDM experiment, the betatron tune will be of order 1, which would usually be reqarded as a fairly low tune.) The inhomogeneous solution will be referred to as "synchrotron oscillation", which will also be referred to as "slow" oscillation.

For theoretical discussion, including determination of the lattice Twiss and dispersion functions, the separation into betatron and synchrotron oscillations is both conventional and convenient. For particle tracking in UAL/ETEAPOT, the coefficients Q and $\xi_{\rm co}$ are being tracked constantly on a particle by particle basis. This makes the betatron/synchrotron separation just a nuisance. (Actually it is more than just a nuisance, since the separation into closed orbit part and small oscillation part is equivalent only to first order in x and ξ spaces.) These notes therefore spell out separately a combined approach for tracking and, after that, a separated approach for theoretical discussion. Since cosine-like and sine-like amplitudes will be used in both approaches it will be necessary to distinguish their symbols. $C_\xi(\theta)$ and $S_\xi(\theta)$ will be used for the full amplitudes. $C_\beta(\theta)$ and $S_\beta(\theta)$ will be used for the betatron amplitudes. These quantities will appear as matrix elements in transfer matrix representations of the motion. Similar functions could also be defined for synchrotron oscillations. But this formalism is rarely used for synchrotron oscillation (for example, because they are inherently nonlinear, as well as being slow).

3.0.5 Betatron Transfer Matrix Description

We can express ξ as the sum of a "betatron" part and a closed-orbit part

$$\xi = \xi_\beta + \xi_0, \tag{32}$$

where ξ_0 was defined along with Eq. (30). With $\xi_0 = 0$, the betatron equation simplifies to

$$\frac{d^2\xi_\beta}{d\theta^2} = -Q^2\xi_\beta, \tag{33}$$

Cosine-like trajectory $C_\xi(\theta)$ satisfies $C_\xi(0) = 1$, $C'_\xi(0) = 0$ and sine-like trajectory $S_\xi(\theta)$ satisfies $S_\xi(0) = 0$, $S'_\xi(0) = 1$. They are given by

$$\begin{aligned} C_\xi(\theta) &= \cos(Q\theta) \\ C'_\xi(\theta) &= -Q\,\sin(Q\theta) \\ S_\xi(\theta) &= \frac{\sin(Q\theta)}{Q} \\ S'_\xi(\theta) &= \cos(Q\theta). \end{aligned} \tag{34}$$

These are formally identical to Eqs. (26) but, as discussed earlier, the parameters Q^2 and ξ_0 (peviously called $\xi_{\rm co}$) are now either the same for all particles or, at most, functions only of the particle energy.

For describing evolution of (ξ, ξ') from its initial values (ξ_0, ξ'_0) at $\theta = 0$ to its values at θ one can use the "transfer matrix" defined by

$$\mathbf{M}_\beta\,(\theta) = \begin{pmatrix} C_\beta(\theta) & S_\beta(\theta) \\ C'_\beta(\theta) & S'_\beta(\theta) \end{pmatrix}. \tag{35}$$

to give, for the betatron part of the motion,

$$\begin{pmatrix} \xi_\beta(\theta) \\ \xi'_\beta(\theta) \end{pmatrix} = \mathbf{M}_\beta \begin{pmatrix} \xi_{\beta,0} \\ \xi'_{\beta,0} \end{pmatrix}. \tag{36}$$

With the electrode spacing being 2 cm, and cm units being used, this unit-amplitude, cosine-like trajectory happens to have something like a maximal amplitude.

The oscillation "frequency" Q is the square root of the "restoring coefficient", namely

$$Q_\xi = \sqrt{2-\beta_0^2} = \sqrt{1+1/\gamma_0^2}; \tag{37}$$

with the independent variable being the *angle* θ, Q_ξ is, in fact, the lattice "tune" Q_ξ. (For motion $\xi \sim \cos Q_\xi\theta = \cos Q_\xi\theta$, an angular period of 2π corresponds to $Q_\xi = 1$). This agrees with the tune determination, using transfer matrices, in Section 8.1.6. There the tune is inferred from the x-motion. Here it is inferred from the ξ-motion which, to linear order, is proportional to x. But, from its definition in Eq. (15), ξ and x deviate in higher order.

3.0.6 Off-Energy Equilibrium Orbits

There is a conventional accelerator physics formalism for defining off-energy equilibrium orbits in magnetic rings; a "dispersion function" is defined which describes the incremental horizontal displacement accompanying an incremental change in energy. We now have to face up to the fact that this description becomes singular (i.e. breaks down) for precisely the logarithmic potential case we are studying.

The simplest possible ring has alternating drifts and sector bends. Off-energy closed orbits continue to be circlular in bend regions, that enter and exit normal to the element ends. Since their x coordinates are constant through drifts, their paths in the next bend element just amount to continuation of the circle from the previous bend. and described by Eq. (5), now generalized to off-energy;

$$\beta pc = eE_0 r_0 = m_p c^2 \frac{\gamma^2-1}{\gamma}. \tag{38}$$

Because of the potential energy discontinuity at the end of a bend element it is necessary to distinguish, by subscripts I and O, between kinematic variables respectively inside and outside the bend element. (If we are completely consistent in using the subscript I, as in γ^I, for particles inside the element, then we can afford to drop the O, as in just γ. The point is that being "outside" a magnet and being "outside" an electric element is the same thing—so formalism should carry over unchanged from magnetic to electric rings, as long as we are in free space regions.) One simplifying fact is that, since the potential is zero by definition on the design orbit, then $\gamma^I = \gamma_0$ on the design orbit, whether inside or outside the element.

Generalizing to a circular orbit with radius increased from r_0 to $r_0 + x$, but with the electric field unchanged, exploiting the constancy of the central member of Eq. (38) yields

$$\frac{{\gamma^I}^2-1}{\gamma^I} = \frac{\gamma_0^2-1}{\gamma_0}. \tag{39}$$

As a result $\gamma^I = \gamma_0$, irrespective of which particular off-energy design orbit is being considered. This implies that the dispersion function, as conventionally defined, is infinite—an arbitrarily small shift of γ^I causes a finite shift in equilibrium radius. This may or may not be fatal.

Introducing deviation $\Delta\gamma^I = \gamma^I - \gamma_0$, using Eq. (4), and tolerating $\gamma^I \equiv \gamma_0$,

$$\Delta\gamma^O = \frac{eV(r)}{m_p c^2} = \frac{eE_0 r_0}{m_p c^2}\,\ln\left(1+\frac{x}{r_0}\right) = \frac{\gamma_0^2-1}{\gamma_0}\,\ln\left(1+\frac{x}{r_0}\right) \approx \frac{\gamma_0^2-1}{\gamma_0}\,\frac{x}{r_0}. \tag{40}$$

(For higher than linear order in x the second last form should be used.) The closed orbit offset is given by

$$\frac{x_0}{r_0} = \frac{m_p c^2}{eE_0 r_0}\,\Delta\gamma^O \approx \frac{\gamma_0 m_p c^2}{eE_0 r_0}\,\frac{\Delta\gamma^O}{\gamma_0} = \frac{1}{\beta_0^2}\,\frac{\Delta\gamma^O}{\gamma_0}. \tag{41}$$

Signifying by superscript (O) and subscript γ, the referencing to γ^O, such that fraction offset $\Delta\gamma^O$ results in orbit displacement $D_\gamma^{(O)}\Delta\gamma^O$, the dispersion function is

$$D_\gamma^{(O)} = \frac{m_p c^2/e}{E_0} \quad \left(\overset{\text{e.g.}}{=} \frac{938\text{Mv}}{17\text{Mv/m}} = 55\,\text{m}\right). \tag{42}$$

With x being conserved on transition from inside to outside, one can, taking care to reference to outside energy, define the dispersion function inside, as being the same as outside.

Even for a ring with no drift sections, to keep infinite dispersion function out of the formalism, we propose to use γ^O to differentiate individual particles, whether the particle is inside or outside. (As mentioned already, the O could be dropped, except for the (high) risk that the resulting γ might then be interpreted as the valid-inside relativistic factor, in spite of the fact that γ is implicitly defined to stand for the valid-outside relativistic factor of a particular particle.) [3]

Chromaticity. For betatron oscillations relative to off-energy closed orbits it is necessary to evaluate Q from Eq. (25). We have that for circular orbits in the $1/r$ field mechanical parameters, such as γ^I are constant and hence cannot be used to label different circular orbits. But, as long as the closed orbits are circles they can labelled by x_0 or by γ^O. On these circles, from Eqs. (9) and (41),

$$\frac{L_{y,\mathrm{c.o.}}}{L_0} = 1 + \frac{x_0}{r_0} = 1 + \frac{m_p c^2}{eE_0 r_0}\,\Delta\gamma^O \approx 1 + \frac{1}{\beta_0^2}\,\frac{\Delta\gamma^O}{\gamma_0}.. \tag{43}$$

(In the definition of angular momentum as momentum times radius, the radius has gone frorm r_0 to $r_0 + x_0$ but the momentum has not changed. The energy ratio can be similarly expressed,

$$\frac{\mathcal{E}_0|_{x_{co}=x_0}}{\mathcal{E}_0} = 1 + \frac{eE_0 x_0}{\mathcal{E}_0} \approx 1 + \frac{\Delta\gamma^O}{\gamma_0} \approx 1 + \beta_0^2\,\frac{x_0}{r_0}. \tag{44}$$

Substituting one or the other of these expressions into Q, as given by Eq. (25), one obtains the chromaticity (dependence of focusing on energy offset);

$$Q \approx 2 - \beta_0^2 + \Big(-1 + \frac{1}{\beta_0^2}\Big)\,\frac{\Delta\gamma^O}{\gamma_0}. \tag{45}$$

Revolution Period of Off-Energy Orbits. In a ring consisting only of repetitions of alternating circular arcs and drifts, the revolution period of off-energy closed orbits around the ring can be calculated easily. The sum of the arc lengths is $2\pi(r_0 + x_0)$ and all velocities within bend elements are identical; $\beta_0 c$. Let $D_{\mathrm{tot.}}$ stand for the sum of the lengths of the drift sections. The outside speed is given by

$$\beta^O = \sqrt{1 - \frac{1}{(\gamma_0 + \Delta\gamma_0^O)^2}}, \tag{46}$$

where

$$\Delta\gamma_0^O = \frac{\gamma_0^2 - 1}{\gamma_0}\,\ln\Big(1 + \frac{x_0}{r_0}\Big), \quad \text{or} \quad \frac{x_0}{r_0} = \exp\Big(\frac{\gamma_0 \Delta\gamma_0^O}{\gamma_0^2 - 1}\Big) - 1. \tag{47}$$

(Neglecting fringe field effects) this is valid even if accuracy higher than linear in x_0 is required. The total revolution period is then

$$cT(\Delta\gamma_0) = \frac{2\pi r_0(1 + x_0/r_0)}{\beta_0} + \frac{D_{\mathrm{tot.}}}{\beta^O}. \tag{48}$$

[3] These issues are not entirely academic, since the closest thing to a "nominal" EDM lattice assumes cylindrical electrodes, which give precisely the logarithmic potential behavior being discussed. Injection into such a lattice may present problems. To avoid mismatch it seems as if the injected proton beam must have energy and transverse displacement correlated exactly as required by the dispersion function. It seems unavoidable that finite energy spread at fixed displacement ("slice emittance" would be the phrase used for beams in bunch compressors) will lead to magnified horizontal betatron oscillations. i.e. horizontal emittance growth. This will place a premium on achieving extremely small energy spread, perhaps by precooling of some kind.

3.0.7 Kinematic Variables in Terms of Initial Conditions

For cylindrical electrodes the electric potential is given by Eq. (4);

$$V(r) = E_0 r_0 \ln\Big(1 + \frac{x}{r_0}\Big). \tag{49}$$

From the known (conserved) total energy $\mathcal{E} = eV + \gamma^I m_p c^2$, this gives,

$$m_p c^2 \gamma^I(\theta) = \mathcal{E} - eE_0 r_0 \ln\Big(1 + \frac{x}{r_0}\Big). \tag{50}$$

From this formula one can obtain β^I using

$$\beta^{I\,2}(\theta) = 1 - \frac{1}{\gamma^{I\,2}(\theta)}. \tag{51}$$

For motion in the horizontal plane, the angular velocity can be obtained starting from the y-component of Eq. (8);

$$\frac{d\theta}{dt} = \frac{L}{m_p r^2 \gamma^I}. \tag{52}$$

(Warning: check sign of L.) The right hand side of this equation can be expressed in terms of θ, invariants and initial conditions using Eq. (50). This relation is useful primarily to obtain the flight time through bend elements. After rearrangement, the flight time $t_o - t_i$ from input to output of a bend element is given by

$$t_o - t_i = \frac{m_p}{L} \int_{\theta_i}^{\theta_o} r^2(\theta')\gamma^I(\theta')\, d\theta' \approx \frac{m_p r_0^2}{L} \int_{\theta_i}^{\theta_o} \big(1 + 2x(\theta')/r_0\big)\gamma^I(\theta')\, d\theta'. \tag{53}$$

Here, because it is conserved, L has been taken outside the integral. But, depending as it does on initial conditions x_0 and x_0', the integral has to be individually evaluated for every particle being tracked.

4 Electric Field Varying as $1/r^2$

Particle propagation in an electric field between spherical electrodes is shown in Figure 5.

4.1 Solution of Equation of Motion

Throughout much of this section formulas of Muñoz and Pavic[2] will be transcribed unchanged, except for bringing symbols into consistency with the rest of this report. The Muñoz/Pavic formulation, though consistent with various other formalisms describing relativistic Coulomb orbits, is especially appropriate for our relativistic accelerator application. They show that the "generalized"-Hamilton vector

$$\widetilde{\mathbf{h}} = \widetilde{h_r}\,\hat{\mathbf{r}} + \widetilde{h_\theta}\,\hat{\boldsymbol{\theta}} \tag{54}$$

is especially powerful in describing 2D, relativistic Kepler orbits. Our 3D application can be formulated in such a way as to use only such 2D orbits.

(The overhead tildes in Eq. (54) have been added for our later convenience. Eventually, for our accelerator application, we will wish to redefine the generalized-Hamilton vector slightly, for example making it dimensionless rather than a velocity, by dividing by a constant characteristic velocity chosen to bring the formalism more into conformity with standard accelerator terminology. Except for these overhead tildes, in this section, quantities and formulas will be largely copied from M & P; this includes using the abbreviation f' for $df/d\theta$. When the formulas have finally been interpreted in accelerator context, the usual accelerator definition of the prime symbol, with f' standing for df/ds, where s is arc length, will be adopted. On the design orbit of radius r_0, where θ and s are both defined, one has $s = r_0\theta$, and this redefinition merely introduces constant factors r_0 into the formulas.)

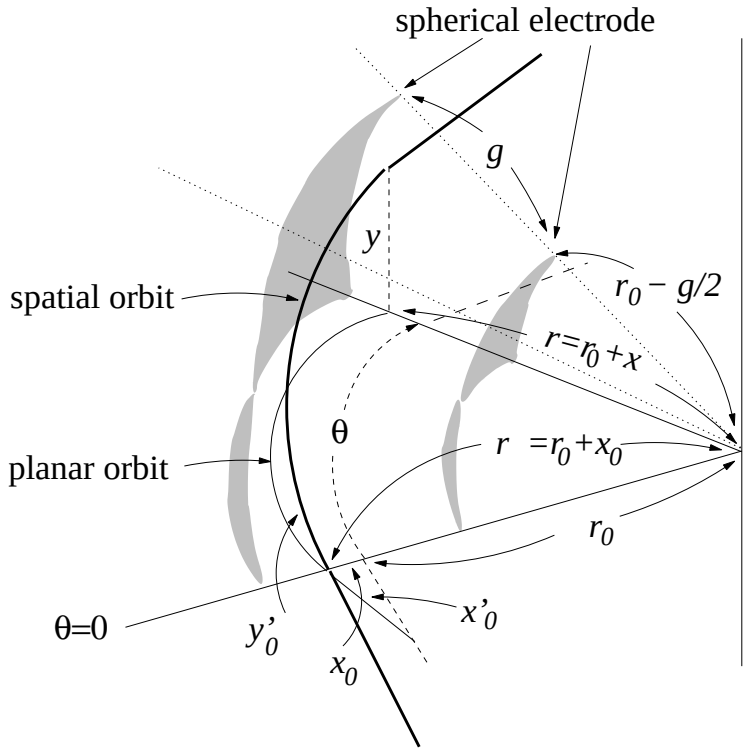

Figure 5: The bold curve shows a proton orbit passing through a spherical electrostatic bending element. The figure is grossly distorted.

We will refer to $\widetilde{\mathbf{h}}$ as the "MP-vector" since, as far as we know, Muñoz and Pavic intoduced it. In the non-relativistic regime $\widetilde{\mathbf{h}}$ is related to the (nonrelativistically conserved) Laplace-Runge-Lenz vector. As generalized by Muñoz and Pavic, though not quite conserved in the relativistic regime, $\widetilde{\mathbf{h}}$ satisfies a very simple equation of motion, whose exact solutions are sinusoids. In the accelerator context $\widetilde{h}_\theta$ is linearly related (with offset) to the relativistic factor γ^I. (As elsewhere, the superscript "I" serves as a reminder that it refers to "inside" bend elements.) This permits other orbit quantities to be expressed analytically. For example, the orbit period $T_{\text{rev.}}$, so important for spin coherence analysis, can be expressed in terms of integrals that can be evaluated in closed form. When expressed in terms of $\widetilde{h}_\theta$, the time of flight through a bend element can be obtained in closed form. (See Eq. (154).) In accelerator context the evolution of $\widetilde{\mathbf{h}}$ for any particular particle will turn out to be interpretable as the phase space evolution of that particle.

Though $\widetilde{\mathbf{h}}$ is not conserved in general, Muñoz and Pavic show that $\widetilde{\mathbf{h}}$ *is conserved if and only if the orbit is circular.* For the proton EDM lattice the design orbit is circular within bends. Also, neglecting the effects of the very weak, vertically focusing quads, off-momentum closed orbits are also circles. Along with its simple evolution, exactly sinusoidal, the use of $\widetilde{\mathbf{h}}$ is conceptually attractive. For example, the relativistic factor γ^I is given by a constant plus a term proportional to its θ component $\widetilde{h}_\theta$. (See Eq. (74).) This is especially important for an electric ring in which γ^I varies as the particle's potential energy changes. It is also possible to define an implicit transfer map (where "implicit" implies the matrix elements depend on particle coordinates) incorporating the strong coupling between kinetic energy and horizontal position in an electric ring. No such tool is needed for magnetic rings.

But $\widetilde{\mathbf{h}}$ also has a potential numerical disadvantage. Transverse displacements (the normally significant aspect of accelerator dynamics) need, at least superficially, to be described by expressions having large cancellations. This makes it essential to proceed exactly, avoiding any series approximations, or even the paraxial approximation that is so prevalent in linearized magnetic accelerator formalisms. It also makes it important to organize the evolution formulas in such a way as to avoid approximately cancelling differences. These same considerations complicate the derivation of an explicit (meaning the elements

are independent of particle coordinates) transfer matrix description from the generalized Hamilton vector evolution.

The Lorentz force equation is

$$\frac{d\mathbf{p}}{dt} = -k\,\frac{\hat{\mathbf{r}}}{r^2}, \tag{55}$$

where k is the same as the customary MKS notation for $1/(4\pi\epsilon_0)$ except for implicitly containing also a charge factor. On the central orbit the centripetal force equation is

$$\frac{(p_0c/e)\beta_0}{r_0} = \frac{k/e}{r_0^2} \overset{\text{also}}{=} E_0. \tag{56}$$

As in MAD, in UAL energies like "p_0c" are always expressed numerically in units such that their value in the computer is $10^{-9}p_0c/e$, which has "GV" units—an MKS unit. From Eq. (56), k/e=$(p_0c/e)\beta_0 r_0$ and "k" is always expressed in the computer as $10^{-9}k/e$, which gives it "GV-m" units—also an MKS unit. The on-axis electric field E_0 is measured in GV/m units. In these units $k = E_0 r_0^2$, numerically, with r_0 measured in meters.

The angular momentum is

$$\mathbf{L} = \mathbf{r} \times \mathbf{p}. \tag{57}$$

In terms of the design momentum p_0 and the design radius r_0, $L_0 = r_0 p_0$, and

$$\frac{k}{L_0 c} = \beta_0 \quad (= 0.598379 \text{ for pEDM}). \tag{58}$$

Like k, internally (i.e. in the computer), L_0c is expressed numerically as $10^{-9}L_0c/e$. For internal numerical values to be most easily substituted into an analytic external documentation formula, factors should be grouped as pc/e, Lc/e, k/e, etc. or, as here, $k/(Lc)$, and factors of 10^9 (for eV to GeV conversion) put in "by hand". (The UAL code itself may be notationally inconsistent: for example "q" may stand for the charge in units of the electron charge.)

In SXF files the RF parameter "V" actually stands for 10^{-9} times the maximum energy change in eV of charge e passing through the RF cavity.

Eq. (58) is also useful in the form

$$k = \gamma_0 m_p c^2 r_0 \beta_0^2. \tag{59}$$

One shows easily that both the total energy

$$\mathcal{E} = \left(\gamma^I m_p c^2 - \frac{k}{r}\right) + \frac{k}{r_0} \equiv \mathcal{E}_M + \frac{k}{r_0}, \tag{60}$$

and

$$L = \gamma^I m_p r^2 \dot{\theta}, \tag{61}$$

are constants of the motion. It has been necessary to distinguish between the Muñoz potential energy V_M and our potential energy eV, because our potential vanishes on the design orbit, while his vanishes at infinity. For the design orbit, using Eqs. (59) and (60), one obtains

$$\mathcal{E}_{M,0} = \frac{m_p c^2}{\gamma_0}. \tag{62}$$

Using the relations (valid for rotation with angle θ increasing)

$$\hat{\boldsymbol{\theta}}' = -\hat{\mathbf{r}}, \quad \text{and} \quad \hat{\mathbf{r}}' = \hat{\boldsymbol{\theta}}, \tag{63}$$

where primes stand for $d/d\theta$, the Lorentz equation can be re-expressed as

$$\frac{d\mathbf{p}}{dt} = \frac{k}{r^2}\,\frac{d\hat{\boldsymbol{\theta}}}{d\theta}. \tag{64}$$

Defining (covariant) velocity $\mathbf{u} = \gamma^I \mathbf{v}$, and using Eq. (61) to express $d\theta/dt$ in terms of L, the $\mathbf{u}$ equation of motion is

$$\frac{d\mathbf{u}}{d\theta} = \frac{k\gamma^I}{L}\,\frac{d\hat{\boldsymbol{\theta}}}{d\theta}. \tag{65}$$

Muñoz and Pavic then introduce the generalized Hamilton vector

$$\widetilde{\mathbf{h}} = \mathbf{u} - \frac{k\gamma^I}{L}\,\hat{\boldsymbol{\theta}}, \quad \text{or} \quad (\widetilde{h}_\theta, \widetilde{h}_r) = \Big(u_\theta - \frac{k\gamma^I}{L}, u_r\Big), \tag{66}$$

which we refer to as the MP-vector. It is specially tailored so that the differential equation for $\widetilde{\mathbf{h}}$ reduces to

$$\frac{d\widetilde{\mathbf{h}}}{d\theta} = -\frac{k}{L}\,\frac{d\gamma^I}{d\theta}\,\hat{\boldsymbol{\theta}}. \tag{67}$$

(The previously mentioned constancy of $\widetilde{\mathbf{h}}$ on circular orbits is evident from this equation.) Using

$$u_\theta = \frac{L}{m_p r}, \qquad \widetilde{h}_\theta = \frac{L}{m_p r} - \frac{k\gamma^I}{L} \overset{\text{also}}{=} \frac{\kappa^2 L}{m_p r} - \frac{k}{L}\,\frac{\mathcal{E}_M}{m_p c^2}, \tag{68}$$

where the new parameter κ is defined by

$$\kappa^2 = 1 - \left(\frac{k}{Lc}\right)^2. \tag{69}$$

On the design orbit

$$\kappa_0 = \sqrt{1-\beta_0^2} = \frac{1}{\gamma_0} \quad (= \ 0.801213 \text{ for pEDM}). \tag{70}$$

(Of course κ_0 will not be controlled to this accuracy in practice.) Solving Eq. (68) for r, the orbit equation can be expressed in terms of $\widetilde{h}_\theta$;

$$r = \frac{\lambda}{1 + \bar{\epsilon}\widetilde{h}_\theta}, \tag{71}$$

where

$$\lambda = \frac{L^2 c^2 \kappa^2}{k\mathcal{E}_M} \quad \text{and} \quad \bar{\epsilon} = \frac{m_p c^2}{\mathcal{E}_M}\,\frac{L}{k}. \tag{72}$$

The parameter λ is especially important in the storage ring context, where the second term in the denominator of Eq. (71) is both small compared to the first, and oscillatory. As a result λ can be thought of as an average radial position, at least in some approximate sense. In component form Eq. (67) is

$$\widetilde{h}_r' - \widetilde{h}_\theta = 0, \quad \widetilde{h}_\theta' + \widetilde{h}_r = -\frac{k}{L}\,\gamma^{I\prime}. \tag{73}$$

The relativistic factor γ^I (equal to $(\mathcal{E}_M + k/r)/(m_p c^2)$) can be expressed in terms of $\widetilde{h}_\theta$. First, eliminate r in favor of u_0 using the first of Eqs. (68), then eliminate u_0 if favor of $\widetilde{h}_\theta$, and, finally, solve for γ^I;

$$\gamma^I = \frac{\mathcal{E}_M}{\kappa^2 m_p c^2} + \frac{k}{\kappa^2 L c^2}\,\widetilde{h}_\theta, \tag{74}$$

Needed for Eqs. (73), differentiating this equation yields

$$\gamma^{I\prime} = \frac{k}{\kappa^2 L c^2}\,\widetilde{h}_\theta'. \tag{75}$$

(After several lines of algebra) Eqs. (73) reduce to

$$\boxed{\begin{aligned} \widetilde{h}_r' &= \widetilde{h}_\theta, \\ \widetilde{h}_\theta' &= -\kappa^2\,\widetilde{h}_r. \end{aligned}} \tag{76}$$

These are the equations that justify having introduced the generalized Hamilton vector. Their general solution can be written as

$$\widetilde{h}_\theta = \widetilde{\mathcal{C}}\,\cos\kappa(\theta-\theta_0)$$
$$\widetilde{h}_r = \frac{\widetilde{\mathcal{C}}}{\kappa}\,\sin\kappa(\theta-\theta_0). \tag{77}$$

where θ is a running angle in the interior of the bend and θ_0 is an angle to be determined, along with $\widetilde{\mathcal{C}}$, by matching to the known initial conditions. These are the functions to be used for smoothly fitting the true, particle by particle, orbits over short arcs. (As explained elsewhere, the effects of the small deviations of the actual electric field from the Coulomb field are to be corrected for by delta function kicks between bend slices.) Concentrating on $\widetilde{h}_\theta$, and *defining* θ to be zero at the bend entrance, we have

$$\widetilde{h}_0 \equiv \widetilde{h}_\theta|_{\theta=0} = \widetilde{\mathcal{C}}\cos\kappa\theta_0,$$
$$\widetilde{h}'_0 \equiv \widetilde{h}'_\theta|_{\theta=0} = \widetilde{\mathcal{C}}\kappa\sin\kappa\theta_0. \tag{78}$$

These equations determine $\widetilde{\mathcal{C}}$ and θ_0 to satisfy

$$\widetilde{\mathcal{C}} = \sqrt{\widetilde{h}_0^2 + \frac{(\widetilde{h}'_0)^2}{\kappa^2}}, \quad \text{and} \quad \tan\kappa\theta_0 = \frac{\widetilde{h}'_0}{\kappa\widetilde{h}_0}. \tag{79}$$

(To obtain $\widetilde{h}_0$ one uses the middle one of Eqs. (68). To obtain $\widetilde{h}'_0$ one starts from the defining relation, $\widetilde{h_r} = u_r = \gamma^I\dot{r}$, used in the second of Eqs. (76;

$$\frac{d\widetilde{h}}{d\theta} = -\kappa^2 u_r = -\kappa^2\gamma^I\frac{d}{dz}(r_0+x)\,v_z = -\kappa^2\,\frac{L}{m_p r}\,p[1]. \tag{80}$$

)

The latter equation can be used to fix θ_0, but this also requires resolving the multiple-valued nature of the inverse tangent function. It seems this can be done by requiring r to be "smooth" (continuous and continuous slope) across the bend entrance edge. Even this is tricky, at least in principle since, for non-normal incidence, there is a refractive deflection at the boundary. But this deflection is small, especially for near-normal incidence, which is valid in our case, and in which case x' is continuous across the boundary. To resolve the inverse tangent ambiguity for non-normal incidence one can choose the value for which the slope is most nearly continuous. (Note, though, that a simple-minded ambiguity resolution prescription like this would be incompatible with polymorphic, high order map generation.)

From Eq. (71) our radial coordinates are related by

$$r = \frac{\lambda}{1+\epsilon\cos\kappa(\theta-\theta_0)}, \quad \text{where} \quad \epsilon = \widetilde{\mathcal{C}}\bar{\epsilon}. \tag{81}$$

Borrowing terminology from solar planetary orbits about the sun, from its structure, one sees that θ_0 is either the angle at perihelion, or aphelion, depending on the sign of ϵ. Using Eqs. (72), (79), and (81),

$$\epsilon = \widetilde{\mathcal{C}}\,\frac{m_p c^2}{\mathcal{E}_M}\,\frac{L}{k} = \sqrt{\widetilde{h}_0^2 + \frac{(\widetilde{h}'_0)^2}{\kappa^2}}\,\frac{m_p c^2}{\mathcal{E}_M}\,\frac{L}{k}. \tag{82}$$

By expressing the small parameter ϵ, proportional to the small Hamilton vector value and slope (or rather their quadrature sum), this formula is essential to the implementation of the Muñoz/Pavic approach. (These "small" quantities can even be infinitesimal.)

The initial conditions of $\widetilde{h}_\theta$ need to be determined from the known proton coordinates just as it enters the bend region. From its defining Eq. (66),

$$\widetilde{h}_0 = u_0 - \frac{k\gamma^I}{L}, \tag{83}$$

Note that γ, like L, is a running particle-specific probe variable. updated on every entry to or exit from a bend element. When inside the bend it is equal to γ^I. In Eq. (68), for any particular particle, r is the only factor which is not a constant of the motion. We therefore have

$$\widetilde{h}_0' = \frac{d\widetilde{h}}{d\theta}\Big|_{\theta=0} = -\kappa^2 \frac{L}{m_p r^2} \frac{dr}{d\theta}\Big|_{\theta=0} = -\kappa^2 \frac{L}{m_p r^2} r_0 \frac{dx}{ds}\Big|_{\theta=0}. \tag{84}$$

From these equations one has obtained convenient analytic solutions for $x(\theta)$ and $\gamma^I(\theta)$. In particle tracking one knows $x_{\rm in}$ to high accuracy and wishes to find $x_{\rm out}$, also to high accuracy. Their difference is given by

$$\begin{aligned} x_{\rm out} - x_{\rm in} &= \frac{\lambda}{1+\bar{\epsilon}\,\widetilde{h}_\theta} - r_0 - \frac{\lambda}{1+\bar{\epsilon}\,\widetilde{h}_0} + r_0 \\ &= \frac{\widetilde{h}_0 - \widetilde{h}_\theta}{(1+\bar{\epsilon}\,\widetilde{h}_\theta)(1+\bar{\epsilon}\,\widetilde{h}_0)}\,\lambda\bar{\epsilon}. \end{aligned} \tag{85}$$

This manipulation has avoided the harmful cancellation exhibited in Eq. (81) which gives r rather that the radial displacement from the design orbit. Eventually, when deviation from $1/r^2$ electric field dependence is modeled by artificial thin quadrupoles, to improve precision, one will slice the bends finer and finer. In the context of accelerator physics one can ask for the similar evolution equations for vertical coordinate y. But this question is inappropriate; the Kepler orbit lies, by definition, in a single plane and we always choose the propagation plane to be the plane containing the incident velocity vector. Instead of keeping track of y we have to keep track of the orbit plane or, equivalently, the normal to the orbit plane. This vector changes discontinuously (but only by a tiny angle) in passing through thin multipole elements. It is undefined in drift regions and is constant in bend elements. Keeping track of the orbit plane is one of the subjects of later sections.

4.2 Rescaling of the MP-Vector and Updating the Horizontal Slope

For updating the horizontal slope component, we introduce the previously-anticipated redefinition of the MP-vector;

$$\mathbf{h} \equiv \frac{\widetilde{\mathbf{h}}}{\gamma_0 v_0}. \tag{86}$$

Dividing by the design velocity v_0 has rendered $\mathbf{h}$ dimensionless, and the further factor of γ_0 in the denominator will yield useful simplification. At this time we also switch definitions of the prime operator notation so that $f' \equiv df/ds$, where s is arc length along the design orbit. With this revised notation Eqs. (76) become

$$\boxed{\begin{aligned} h_r' &= \frac{1}{r_0}\, h_\theta, \\ h_\theta' &= -\frac{1}{r_0}\,\kappa^2\, h_r, \end{aligned}} \tag{87}$$

and Eq. (116) reduces to

$$p_x = \gamma_0 m_p v_0\, h_r, \quad \text{or} \quad x' \equiv \frac{dx}{ds} = \mathtt{p[1]} = \frac{p_x}{p_z} = h_r, \tag{88}$$

where $p_0 = \gamma_0 m_p v_0$ is the design momentum and `p[1]` is the symbol used for x' internally in the UAL code. (Some components in the chain of equalities in Eq. (88) may assume paraxial approximation, even if for no reason other than that the definition of x is unambiguous only in the paraxial limit.) So h_r is nothing other than the phase space "momentum" component dx/ds.

The value of x' given by Eq. (88) would better have been called $x'_{{\rm out},-}$, since the refractive compensation associated with exiting the bend still needs to be made to produce `p[1]` valid just outside the bend

exit. But this comment is somewhat gratuitous at this point since the corresponding compensation should have been made at the bend entrance. i.e. the refractive corrections are not currently in ETEAPOT.

A compact way to update the 2D phase space coordinates is to work directly from Eq. (81). For bend angle $\Delta\theta$, the argument $\theta - \theta_0$ is $\Delta\theta$. The increment in x from input to output is

$$x_{\rm out} - x_{\rm in} = \lambda\epsilon \, \frac{\cos\kappa\theta_0 - \cos\kappa\Delta\theta}{(1+\epsilon\cos\kappa\Delta\theta)(1+\epsilon\cos\kappa\theta_0)} \tag{89}$$

Differentiating Eq. (81) produces

$$\frac{dx}{d\theta}(\theta) = \lambda\epsilon\kappa \, \frac{\sin\kappa(\theta-\theta_0)}{\big(1+\epsilon\cos\kappa(\theta-\theta_0)\big)^2}. \tag{90}$$

Including the change of independent variable from θ to z, the increment from input to output is

$$\frac{dx}{dz}\Big|_{\rm out} - \frac{dx}{dz}\Big|_{\rm in} = \frac{\lambda\epsilon\kappa}{r_0}\left(\frac{\sin\kappa\Delta\theta}{(1+\epsilon\cos\kappa\Delta\theta)^2} + \frac{\sin\kappa\theta_0}{(1+\epsilon\cos\kappa\theta_0))^2}\right). \tag{91}$$

4.3 Determination of the MP Bend Plane

In order to reserve x for radial displacement in the MP bend plane we now use overhead bars to designate conventional Courant-Snyder (CS) coordinates. Angular momentum is related to CS (Frenet) variables in Fig. 6. At a location where the longitudinal coordinate has been shifted to be $z = 0$, the particle position $(\bar{x}, \bar{y}, 0)$ is given by

$$\frac{\mathbf{r}}{r_0} = \Big(1 + \frac{\bar{x}}{r_0}\Big)\,\hat{\bar{\mathbf{x}}} + \frac{\bar{y}}{r_0}\,\hat{\bar{\mathbf{y}}}. \tag{92}$$

Scaled momentum components $\tilde{p}_{\bar{x}} = (p_{\bar{x}}/p_0)/(1+\delta p/p_0)$, and $\tilde{p}_{\bar{y}} = (p_{\bar{y}}/p_0)/(1+\delta p/p_0)$, are defined by

$$\tilde{\mathbf{p}} = \tilde{p}_{\bar{x}}\hat{\bar{\mathbf{x}}} + \tilde{p}_{\bar{y}}\hat{\bar{\mathbf{y}}} + \Big(1 - \frac{\tilde{p}_{\bar{x}}^2}{2} - \frac{\tilde{p}_{\bar{y}}^2}{2}\Big)\,\hat{\bar{\mathbf{z}}}, \tag{93}$$

where terms of fourth order and beyond have been dropped. (For the EDM experiment such terms have numerical values such as $(0.01/20)^4 \approx 10^{-13}$.) This has been arranged so that $\tilde{\mathbf{p}}$ is a unit vector. The p[1] and p[3] MAD/UAL coordinates being tracked in the computer are close to, but not exactly equal to $\tilde{p}_{\bar{x}}$ and $\tilde{p}_{\bar{y}}$. In fact

$$\tilde{p}_{\bar{x}} = \frac{\mathtt{p[1]}}{1+\delta p/p_0}, \qquad \tilde{p}_{\bar{y}} = \frac{\mathtt{p[3]}}{1+\delta p/p_0}. \tag{94}$$

Scaled angular momentum components are then given by

$$\begin{aligned}\tilde{\mathbf{L}} = \frac{\mathbf{L}}{r_0 p_0} = \frac{\mathbf{r}\times\mathbf{p}}{r_0 p_0} &= \det\begin{pmatrix} \hat{\bar{\mathbf{x}}} & \hat{\bar{\mathbf{y}}} & \hat{\bar{\mathbf{z}}} \\ 1+\bar{x}/r_0 & \bar{y}/r_0 & 0 \\ \tilde{p}_{\bar{x}} & \tilde{p}_{\bar{y}} & \tilde{p}_{\bar{z}} \end{pmatrix} \\ &= \frac{\bar{y}}{r_0}\,\tilde{p}_{\bar{z}}\,\hat{\bar{\mathbf{x}}} - \Big(1+\frac{\bar{x}}{r_0}\Big)\,\tilde{p}_{\bar{z}}\,\hat{\bar{\mathbf{y}}} + \Big(\tilde{p}_{\bar{y}} + \frac{\bar{x}}{r_0}\,\tilde{p}_{\bar{y}} - \frac{\bar{y}}{r_0}\,\tilde{p}_{\bar{x}}\Big)\,\hat{\bar{\mathbf{z}}}.\end{aligned} \tag{95}$$

The scaled central angular momentum is $\tilde{\mathbf{L}}_{\mathbf{0}} = -\hat{\bar{\mathbf{y}}}$, and the perpendicular component $\tilde{\mathbf{L}}_\perp$ is

$$\begin{aligned}\tilde{\mathbf{L}}_\perp &= \frac{\bar{y}}{r_0}\Big(1 - \frac{\tilde{p}_{\bar{x}}^2}{2} - \frac{\tilde{p}_{\bar{y}}^2}{2}\Big)\,\hat{\bar{\mathbf{x}}} + \Big(\tilde{p}_{\bar{y}} + \frac{\bar{x}}{r_0}\,\tilde{p}_{\bar{y}} - \frac{\bar{y}}{r_0}\,\tilde{p}_{\bar{x}}\Big)\,\hat{\bar{\mathbf{z}}} \\ &\equiv \sin\phi_{\bar{z}}\,\hat{\bar{\mathbf{x}}} - \sin\phi_{\bar{x}}\hat{\bar{\mathbf{z}}},\end{aligned} \tag{96}$$

which defines two (small) angles the tilted bend plane makes with true vertical. This equation determines the (small) rotation angles about transverse axes that rotate the horizontal plane into the MP plane. The trigonometry is not exact. But it is expected to be accurate enough for the extremely small angles involved. This will have to be checked later.

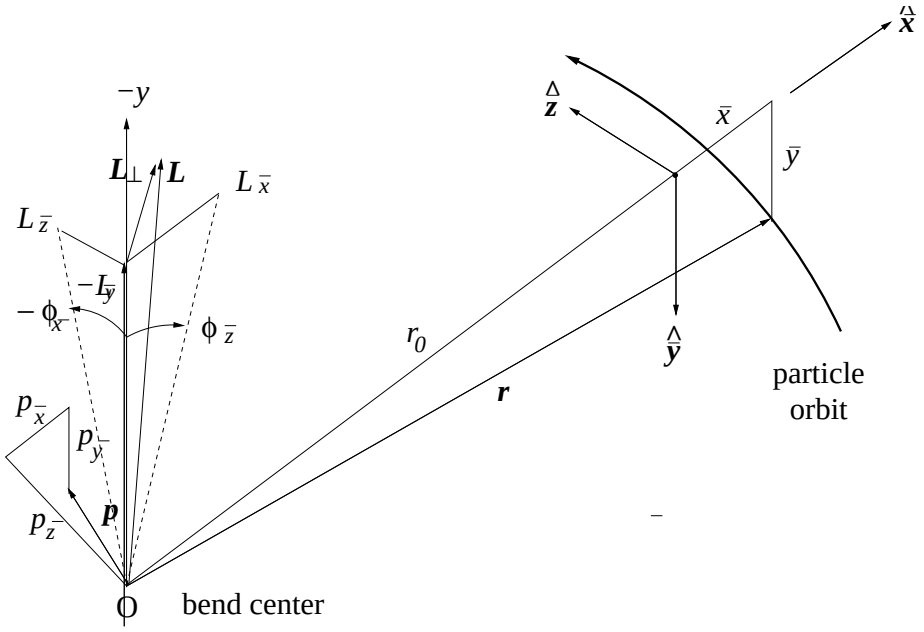

Figure 6: Figure relating angular momentum componenents $(L_{\bar{x}}, L_{\bar{y}}, L_{\bar{z}})$ to Courant-Snyder coordinates $(\bar{x}, p_{\bar{x}}, \bar{y}, p_{\bar{y}})$.

4.4 Merging MP-Tracking into Three Dimensions

With the orbit geometry already worked out in the 2D MP plane, it remains necessary to transform into the 3D Frenet frame.

The local coordinate system with origin at the bend center is shown in Figure 6. The goal of a tracking calculation is to obtain the output particle radius vector $\mathbf{r}_{\rm out}$ for a given input particle radius vector $\mathbf{r}_{\rm in}$. The corresponding unit vector evolution is from $\hat{\mathbf{r}}_{\rm in} = (\hat{x}_{\rm in}, \hat{y}_{\rm in}, 0)$ to $\hat{\mathbf{r}}_{\rm out}$. We calculate this unit vector evolution first.

On the design orbit the input and output vectors are $\mathbf{d}_{\rm in} = (1, 0, 0)$ and $\mathbf{d}_{\rm out} = (\cos\theta, 0, \sin\theta)$, both lying in the horizontal (xz)-plane. With the design bend angle defined to be θ, one has

$$\hat{\mathbf{d}}_{\rm in} \cdot \hat{\mathbf{d}}_{\rm out} = \cos\theta. \tag{97}$$

The particle-specific bend angle ϕ satisfies

$$\hat{\mathbf{r}}_{\rm in} \cdot \hat{\mathbf{r}}_{\rm out} = \cos\phi, \tag{98}$$

where ϕ is close to, but not equal to, θ in general. Letting a and $b = \pm|b| = \pm\sqrt{1-a^2}$ be the components of $\hat{\mathbf{r}}_{\rm out}$ along $\hat{\mathbf{d}}_{\rm out}$, one has

$$\hat{\mathbf{r}}_{\rm out} = (a\,\cos\theta, \pm\sqrt{1-a^2}, a\sin\theta). \tag{99}$$

The unit vector normal to the bend plane,

$$\hat{\mathbf{n}} = -\frac{\mathbf{L}_{\rm in}}{|\mathbf{L}_{\rm in}|}, \tag{100}$$

is known from calculations based on the particle coordinates at the entrance to the bend element. To determine a we require

$$0 = \hat{\mathbf{n}}_{\rm in} \cdot \hat{\mathbf{r}}_{\rm out} = n_x a\,\cos\theta \pm n_y\sqrt{1-a^2} + n_z a\,\sin\theta. \tag{101}$$

Solving for a,

$$a = \frac{n_y}{\sqrt{n_y^2 + n_x^2\cos^2\theta + 2n_x n_z \cos\theta\sin\theta + n_z^2\sin^2\theta}}. \tag{102}$$

The angular advance ϕ then satisfies

$$\cos\phi = \hat{\mathbf{r}}_{\rm in}\cdot\hat{\mathbf{r}}_{\rm out} = \hat{x}_{\rm in} a\cos\theta + \hat{y}_{\rm in} b. \tag{103}$$

The radial coordinate is then given by Eq. (71) which is repeated here;

$$r = \frac{\lambda}{1+\bar{\epsilon}\widetilde{h}_\theta}, \tag{104}$$

where $\widetilde{h}_\theta$ is given by Eq. (77). The output radius vector is then given by

$$\mathbf{r}_{\rm out} = r\,\hat{\mathbf{r}}_{\rm out}. \tag{105}$$

In this way the evolution has been completed using just Courant Snyder coordinates.

5 Transfer Matrix Evolution of the Muñoz-Pavic (MP) Vector

Except in the nonrelativistic limit, Muñoz and Pavic's generalized Hamilton vector $\widetilde{\mathbf{h}}$ is not conserved in any inertial coordinate frame. M and P do, however, introduce a "vector" $\widetilde{\mathbf{j}}$, defined in terms of the components of $\widetilde{\mathbf{h}}$, that *is* conserved in a (nonuniformly-) rotating frame of reference. With θ being the instantaneous angular coordinate of a particular particle being tracked, let ψ be the angle of this rotating frame at the same instant. The symbol ψ has intentionally been chosen to be reminiscent of the phase advance angle in the Courant-Snyder magnetic lattice formalism. The hope is that descriptions of motions in electric and magnetic rings will be quite similar when ψ is chosen as independent variable in both cases. In their Eq. (37), M and P define $\widetilde{\mathbf{j}}$ by

$$\widetilde{\mathbf{j}} = \widetilde{h}_\theta\widehat{\boldsymbol{\theta}} + \kappa\widetilde{h}_r\hat{\mathbf{r}}. \tag{106}$$

Which, using Eq. (77)), can be written as

$$\widetilde{\mathbf{j}}(\theta) = \begin{pmatrix}\widetilde{j}_\theta(\theta)\\ \widetilde{j}_r(\theta)\end{pmatrix} = \begin{pmatrix}\widetilde{C}\cos(\kappa\theta-\kappa\theta_0)\\ \widetilde{C}\sin(\kappa\theta-\kappa\theta_0)\end{pmatrix} = \begin{pmatrix}\widetilde{C}\cos(\kappa\theta)\cos(\kappa\theta_0)+\widetilde{C}\sin(\kappa\theta)\sin(\kappa\theta_0)\\ \widetilde{C}\sin(\kappa\theta)\cos(\kappa\theta_0)-\widetilde{C}\cos(\kappa\theta)\sin(\kappa\theta_0)\end{pmatrix}, \tag{107}$$

so that

$$\widetilde{\mathbf{j}}(0) = \begin{pmatrix}\widetilde{j}_\theta(0)\\ \widetilde{j}_r(0)\end{pmatrix} = \begin{pmatrix}\widetilde{C}\cos(\kappa\theta_0)\\ -\widetilde{C}\sin(\kappa\theta_0)\end{pmatrix}. \tag{108}$$

As discussed previously in Section 4.1, it is inconvenient for the initial conditions to be expressed in terms of the angle θ_0, which is related to a remote perihelion position. We therefore introduce the angle $\Delta\theta = \theta - \theta_0$, which vanishes at the local position and therefore measures the advance of the independent variable from this position. Propagation from this position is described by

$$\widetilde{\mathbf{j}}(\Delta\theta) = \begin{pmatrix}\widetilde{j}_\theta(\Delta\theta)\\ \widetilde{j}_r(\Delta\theta)\end{pmatrix} = \begin{pmatrix}\cos(\kappa\Delta\theta) & -\sin(\kappa\Delta\theta)\\ \sin(\kappa\Delta\theta) & \cos(\kappa\Delta\theta)\end{pmatrix}\begin{pmatrix}\widetilde{j}_\theta(0)\\ \widetilde{j}_r(0)\end{pmatrix}. \tag{109}$$

This produces the familiar transfer matrix form

$$\widetilde{\mathbf{j}}(\Delta\theta) = M(\Delta\theta)\widetilde{\mathbf{j}}(0). \tag{110}$$

(In the terminology of this report $M(\Delta\theta)$ will be referred to as an "implicit" or as a "particle specific" transfer matrix. This distinction is needed because, through κ, the elements of $M(\Delta\theta)$ depend on the

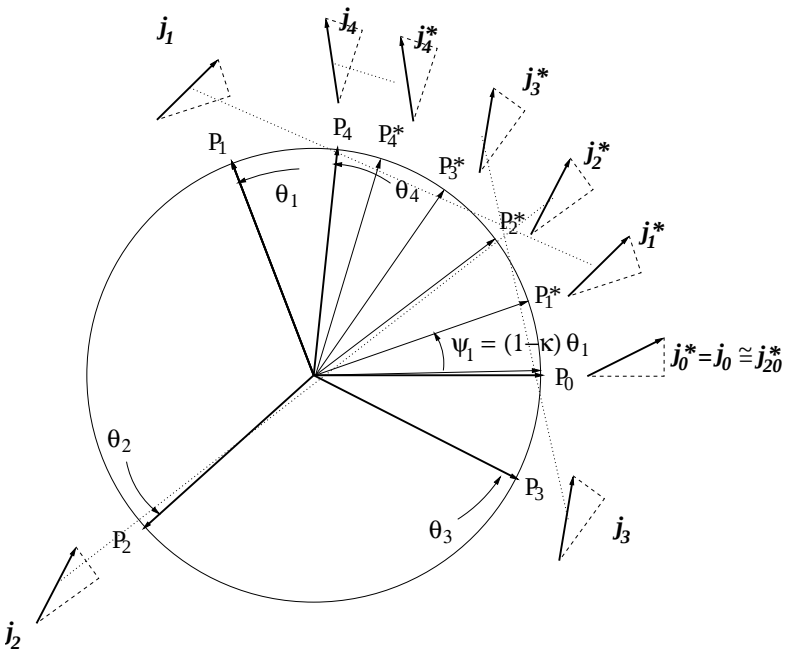

Figure 7: Graphical representation of the evolution of the "vector" $\widetilde{\mathbf{j}}$ whose magnitude is conserved. Long bold arrows point to actual positions P_i of the particle in the ring at successive intervals, and the arrows plotted there are values of $\widetilde{\mathbf{j}}$ at those instants. Faint arrows with tips at P_i^* represent orientations of the rotating frame at the matching instants, and the arrows $\widetilde{\mathbf{j}}^*$ plotted (outside the circle) there show $\widetilde{\mathbf{j}}$ viewed in the rotating frame; their orientations relative to the rotating frame axis are all the same. At the starting point $\widetilde{\mathbf{j}}_\mathbf{0}^* = \widetilde{\mathbf{j}}_\mathbf{0}$. Also $\widetilde{\mathbf{j}}_\mathbf{20}^* \approx \widetilde{\mathbf{j}}_\mathbf{0}^*$ since $\widetilde{\mathbf{j}}$ is constant in the rotating frame, and the rotating frame has returned almost to its starting position after twenty intervals. In a realistic lattice, with drift sections and quadrupoles, the global view is more complicated than this figure indicates. But, at least in principle, a non-uniformly rotating coordinate frame can be found in which the vector $\mathbf{j}^*$ is constant.

coordinates of the particular particle being tracked. Technically Eq. (110) defines a transfer map rather than a transfer matrix.) From this and/or Eq. (77) it can be seen that $\widetilde{j}_r^2 + \widetilde{j}_\theta^2 = \widetilde{\mathcal{C}}^2$ is conserved. (Our previous quotation mark qualification of $\widetilde{\mathbf{j}}$ as being less than a full-fledged vector, was because the only way a true vector can be defined in terms of the components of another vector is if the components are strictly proportional, which is not the case here. The subsequent vector analysis treatment by M and P is therefore of dubious validity, but this will not affect our treatment.)

The angular velocity of their special rotating frame is given by Muñoz and Pavic's Eq. (39) to be

$$\frac{d\psi}{dt}\,\widehat{\mathbf{L}} = (1-\kappa)\,\frac{d\theta}{dt}\,\widehat{\mathbf{L}} = (1-\kappa)\,\frac{\mathbf{L}}{\gamma m_p r^2}. \tag{111}$$

The first of these two equations shows that θ and ψ are linearly related for each particular particle. Integrating, and suppressing a constant of integration,

$$\psi = (1-\kappa)\theta. \tag{112}$$

When the particle has rotated through angle θ, rotating $\widetilde{\mathbf{j}}$ through angle $-\kappa\theta$ brings $\widetilde{\mathbf{j}}$ back to its original orientation. This shows that there is a rotating frame (labeled by *) in which the components $\widetilde{j}_\theta^*$ and $\widetilde{j}_r^*$ are conserved. This is illustrated in Figure 7, and explained in the caption.

The vector $\widetilde{\mathbf{j}}^*$ viewed in the rotating frame, is numerically advantageous in tracking a particle through a bend element since both of its components are conserved. The betatron components x and $p_x \sim x'$ need

to be written to output only occasionally, for example at the centers of selected elements. The relativistic factor γ^I can be obtained from $\widetilde{h}_\theta$ using Eq. (74). Then x is determined by energy conservation. (This will be useful as a consistency check. A different way of determining x will be established shortly.) Recapitulating the relevant equations here, and redefining $V(r)$ in Eq. (2) as $V(x)$,

$$\gamma^I = \frac{\mathcal{E}_M}{\kappa^2 m_p c^2} + \frac{k}{\kappa^2 L c^2}\,\widetilde{h}_\theta, \tag{113}$$

$$V(x) = \frac{E_0 x}{1 + x/r_0}. \tag{114}$$

With γ^I known, so also is $|\mathbf{p}|$. The radial component of $\widetilde{\mathbf{h}}$ can be obtained using

$$\widetilde{h}_r = \widetilde{\mathbf{h}}\widehat{\mathbf{r}} = \gamma^I \mathbf{v}\cdot\widehat{\mathbf{r}} \tag{115}$$

(Manipulation of this formula to avoid loss of precision caused by a cancellation to leading order in this equation is discussed in connection with Eq. (85)). The radial momentum component is therefore given by

$$p_x = m_p \widetilde{h}_r. \tag{116}$$

Before the laboratory frame betatron components can be worked out it is necessary to rotate $\widetilde{j}^*$ into the laboratory frame. To do this it is necessary to employ the laboratory angle θ. For any particular particle the turning angle advance is approximately equal to, but not exactly equal to, the design particle turning angle. The exact angle at the magnet exit can be found by solving a nonlinear equation, but this small correction can be neglected without harming the symplecticity of the tracking. To this approximation, θ will not be known exactly. Also, in spite of numerical treatment such as shown in Eq. (82), because of the subtraction of nearly equal quantities, precision is lost in determining the local betatron components. Such errors are local, however; they need not accumulate, no matter how finely an element is split (provided the policy is adopted of forbidding transformation to the laboratory and back as the evolution proceeds).

On exiting a bending element the particle may encounter a lattice element, such as a quadrupole, which causes a (tiny) deflection that depends on the position x and the momentum p, both of which are subject to the numerical loss of precision discussed in the previous paragraph. It is numerically important for this deflection to be transformed into the rotating frame before applying it to $\widetilde{\mathbf{j}}^*$. In this way fractional precision to near machine precision can be maintained. The y deflection will alter the orbit plane (represented by $\widehat{\mathbf{L}}$) slightly. Also, because the unit normal vector $\widehat{\mathbf{L}}$ is not necessarily exactly equal to $\hat{\mathbf{y}}$, each quadrupole will be slightly "skew". The resulting "cross coupling" between x and y will also alter $\widehat{\mathbf{L}}$, slightly.

Over long times the $\widetilde{\mathbf{j}}$ vector will "lap" $\widetilde{\mathbf{j}}^*$ arbitrarily many times, and small errors can cause substantial accumulating angular errors. These will cause "phase" or "tune" errors, which will not, however, alter the magnitude of $\widetilde{\mathbf{j}}$. This will guarantee symplecticity through bend elements. It will not as yet, however, guarantee overall symplecticity, as the MP-vector components will also be altered through drifts and other beam elements.

For bunched beams, over long times, synchrotron stability will cause the ratio of accumulated $\widetilde{\mathbf{j}}$ and $\widetilde{\mathbf{j}}^*$ angles to be the same for all particles.

5.1 Pseudoharmonic Description of the Motion

In general the MP plane will be close to, but not exactly identical with the horizontal lattice design plane. In this section, for simplicity in making contact with Twiss functions, these two planes will be treated as equivalent. In general, the definition of lattice functions within electric bend elements will be more complicated, but also not very important for the EDM experiment.

At this point we wish to correlate the dynamic quantities introduced so far with more familiar (to accelerator scientists) quantities such as Twiss functions, betatron phase advances, transfer maps, and

so on. The relationships are especially simple for a combined function, weak-focusing ring; this will be described before developing the full Twiss function formulation needed for separated function lattices.

junk

Then Eq. (87) yields

$$h_\theta = r_0 \frac{d^2x}{ds^2}. \tag{117}$$

In traditional Courant-Snyder (CS) formalism the betatron phase ψ and the positive-definite lattice function $\beta(s)$ are related by

$$\psi' \equiv \frac{d\psi}{ds} = \frac{1}{\beta(s)}, \tag{118}$$

Even with $\theta = s/r_0$, because $\beta(s)$ is not necessarily constant, the angles ψ and $\theta = s/r_0$, though monotonically related, are not strictly proportional. The power of the beta function formalism is primarily due to its ability to describe orbits in complicated lattices with drifts and quads.

Shortly we will have to admit that our generalization of the CS formalism to electric lattices will be limited to describing orbits *outside* bending elements. The parameter β introduced now will be applicable only *inside* bends, and it is assumed to be independent of s. Furthermore it will not match up continuously with the adjacent *outside* β functions.

As already stated, our electric lattice model admits only uniform, inverse square law bending elements (with artificial thin trim elements). Within such a bend $\beta' \equiv d\beta/ds = 0$ and horizontal"betatron" oscillations of amplitude a are described by

$$\begin{aligned} x &= a\beta^{1/2}\cos\psi, \\ x' &= -a\beta^{1/2}\sin\psi\,\psi' = -a\beta^{-1/2}\sin\psi. \end{aligned} \tag{119}$$

Differentiating once more yields

$$x'' = -a\beta^{-3/2}\cos\psi = -\beta^{-2}x. \tag{120}$$

Substituting this into Eq. (87) produces

$$x = -\frac{\beta^2}{r_0}\,h_\theta. \tag{121}$$

Just as h_r and h_θ vary "in quadrature, so also do x and x'. The ratios of their maxima are

$$\frac{h_{\theta,\max}}{h'_{\theta,\max}} = \frac{r_0}{\kappa}, \quad \text{and} \quad \frac{x_{\max}}{x'_{\max}} = \frac{h_{\theta,\max}}{h'_{\theta,\max}} = \frac{r_0}{\kappa} \overset{\text{also}}{=} \beta. \tag{122}$$

Collecting results, we have

$$\beta = \frac{r_0}{\kappa}, \quad x = -\frac{r_0}{\kappa^2}\,h_\theta = -\frac{r_0}{\kappa^2}\,j_\theta, \quad \text{and} \quad x' = h_r = \frac{1}{\kappa}\,j_r. \tag{123}$$

(As an aside one should note that these x and x' values are only Frenet-Serret laboratory coordinates if the M-P plane coincides with the horizontal laboratory frame.) To summarize, one sees that, to linearized approximation, the components of the MP-vector are, except for scale factors, identical to the betatron phase space components.

The parameter β has been used in this section only to produce familiar-looking formulas. We have now seen that this β need never have been introduced, since it is just an abbreviation for r_0/κ. It is independent of s, but through its κ factor it depends on γ, x and x', and is therefore different for different particles.

5.1.1 Separated Function Ring

In a separated function ring containing electric elements one cannot avoid distinguishing between "outside" and "inside" the electric bend elements. (For thick electric quadrupoles, sextupoles, etc. one should make a similar distinction, but we are allowing only thin multipole elements.)

In spite of our use of a β-functions within the pseudo-harmonic formalism of the previous section, a conservative attitude would be that the strong coupling between kinetic energy and position simply invalidates the traditional CS formalism, including its Twiss functions. Rather than accepting this we now try to adapt the traditional Twiss function formalism to separated function electric rings.

In a separated function ring, particles are repeatedly crossing boundaries at which the electric potential changes discontinuously. (The further complication that the true potential, though varying rapidly in fringe fields is, in fact, continuous, will be addressed later. For now we assume true discontinuity at bend boundaries.) Certainly the transverse coordinate x of any particular particle cannot change discontinuously. If we require the phase angle ψ (in a formula like Eq. (119)) to be continuous, as we do, then we will have to tolerate β-function discontinuity across boundaries. Rather than facing this prospect we will, for the time being, simply *refuse to define the β-function inside bend elements.* As a result the β-function to be defined now will be different from the β parameter of the previous section. Respecting the usual, unfortunate, accelerator tradition, we will refrain from introducing a new symbol to distinguish between these different quantities.

To use only "outside" β-functions we will have to treat the bend elements themselves as "black boxes" which transform input coordinates to output coordinates. Here it is assumed that the electric potential vanishes on the outer surfaces of both input and output bend field boundaries.

After we have succeeded in determining the β-functions on all such surfaces we will still be unable to answer the main question of storage ring physics "does a particular particle wipe out on the chamber wall". To answer this question we will have to learn how to interpolate orbits into the interior of electric bend elements. In any case the question is somewhat academic since a particle that should have been predicted to wipe out in the interior of a bend element will soon wipe out outside the bend element.

The reason for restricting discussion to "outside" regions is that the kinetic energy is constant there (except, as always, for its tiny changes in RF cavities). With this constraint satisfied, the customary CS formalism should provide its valuable global representation of orbits for which the kinetic energy changes only adiabatically.

To evolve lattice Twiss functions across finite intervals one must first obtain transfer matrices that evolve individual particle orbits across finite intervals. In the next section the transfer matrix across a thick uniform bend element will be obtained.

5.2 Implicit Transfer Matrix for an Electric Sector Bend

In tracking a particle through a uniform bend the first thing that needs to be done is to use the particle position and the potential energy discontinuity to determine the particle's inside kinetic energy. The parameter κ defined in Eq. (69) can then be determined. Unfortunately these calculations have to be done on a particle by particle basis.

Eq. (119) can be rearranged using Eqs. (123) into the form

$$\begin{pmatrix} -\frac{\kappa^2}{r_0}\, x_{\Delta\theta} \\ \kappa x'_{\Delta\theta} \end{pmatrix} = \begin{pmatrix} \cos\kappa\Delta\theta & -\sin\kappa\Delta\theta \\ \sin\kappa\Delta\theta & \cos\kappa\Delta\theta \end{pmatrix} \begin{pmatrix} -\frac{\kappa^2}{r_0}\, x_0 \\ \kappa x'_0 \end{pmatrix}. \tag{124}$$

This can be further rearranged into the form

$$\begin{pmatrix} x_{\Delta\theta} \\ x'_{\Delta\theta} \end{pmatrix} = \begin{pmatrix} \cos\kappa\Delta\theta & \frac{r_0}{\kappa}\sin\kappa\Delta\theta \\ -\frac{\kappa}{r_0}\sin\kappa\Delta\theta & \cos\kappa\Delta\theta \end{pmatrix} \begin{pmatrix} x_0 \\ x'_0 \end{pmatrix}. \tag{125}$$

For a full ring $\Delta\theta = 2\pi$ and the once-around transfer matrix is

$$\mathbf{M} = \begin{pmatrix} \cos 2\pi\kappa & \frac{r_0}{\kappa}\sin 2\pi\kappa \\ -\frac{\kappa}{r_0}\sin 2\pi\kappa & \cos 2\pi\kappa \end{pmatrix} = \begin{pmatrix} \cos 2\pi Q & \beta\sin 2\pi Q \\ -\frac{1}{\beta}\sin 2\pi Q & \cos 2\pi Q \end{pmatrix}. \tag{126}$$

The rightmost matrix is in the canonical form for a once-around matrix in terms of Twiss parameters β and tune Q at a point where $\alpha = 0$ (which is true for a ring with mirror symmetry about the origin). Matching elements confirms the earlier determination that $\beta = r_0/\kappa$, and also shows that

$$Q = \kappa. \tag{127}$$

The transfer matrix, for example through bend $\Delta\theta/2$,

$$\mathbf{B}^{(\mathbf{m=1})}_{\boldsymbol{\Delta\theta/2}} = \begin{pmatrix} \cos\kappa\Delta\theta/2 & \frac{r_0}{\kappa}\sin\kappa\Delta\theta/2 \\ -\frac{\kappa}{r_0}\sin\kappa\Delta\theta/2 & \cos\kappa\Delta\theta/2 \end{pmatrix}, \tag{128}$$

is manifestly symplectic. Curiously, in spite of the non-conservation of kinetic energy, any implication this has for the orbit evolution is implicit; i.e. it is being taken care of invisibly. Both input and output potential energies can be calculated using Eq. (114), enabling other kinematic variables to be calculated. (One can worry, for $m \neq 1$, that it is ambiguous whether to use the potential corresponding to $m = 1$ or to the actual value of m. As it happens, if both input and output points are at the same electric potential (presumably zero) their kinetic energies and other outside kinematic magnitudes are identical, irrespective of the value of m. Because of this one does not necessarily have to calculate the energy discontinuity at every interface.) The superscript $m = 1$ has been added to $\mathbf{B}^{(\mathbf{m=1})}_{\boldsymbol{\Delta\theta}}$ as a reminder that this formula is specific to the inverse square law electric field dependence. Compensating for different radial dependence will be accomplished by splitting the bend and inserting thin focusing elements. This will be discussed shortly.

5.3 Transverse Coordinate Redefinition

Even the choice of transverse coordinates is influenced by the complication caused by the particle speed variation in an electric field. In a magnetic field it is legitimate to treat all deflections by delta function impulses, and all translations as straight line segments. Such a "finite-element" separation fails in an electric field because the straight line orbit in a drift is inconsistent with the potential energy varying along the path causing the particle speed to vary. Our coordinate choice also has to resemble the Frenet coordinates of conventional accelerator formalism, while preserving analytically manageable propagation through finite longitudinal curved orbit intervals (using the MP formalism already derived).

The strategy for our choice of coordinates has already been explained. Some aspects are illustrated in Fig. 8. The Muñoz-Pavic formalism is two dimensional. The center of rotation is uniquely defined for every bend element. Along with its position and tangent vector this defines a unique orbit plane for every particle. Each particle has its own plane. The (conserved) angular momentum vector is normal to this plane. Instead of keeping track of the proton's curved, 3D orbit, we need only keep track of the proton's orbit in the 2D orbit plane.

Coordinate x is redefined (relative to MAD/UAL) such that the radial (spherical) coordinate r and x are related by

$$r = r_0 + x. \tag{129}$$

From the lower left figure in Fig. 8, the conventional accelerator radial displacement can be seen to be the projection of the radial displacement x onto the horizontal axis. This is now labelled $\bar{x}$. For most purposes the distinction between x and $\bar{x}$ will be numerically unimportant. If the "actual" projected value $\bar{x}$ is calculated, for whatever reason, the result must not be used as an intermediate value for subsequent evolution, as that could lead to unacceptable loss of precision.

To assure long term tracking stability, all bend calculations are based on the two dimensional Muñoz-Pavic (MP) formalism. Each particle j lies in its own "wobbling", particle-specific bend plane, which is specified by its angular momentum $\mathbf{L}_j$, normal to the orbit plane.

After x has evolved through a bend element, $\mathbf{L}_j$ will have to be rotated by the design bend angle, to bring it into the new local Frenet coordinate frame. This is a rotation around $\mathbf{L_0}$ of the vector $\mathbf{L}$ shown in the upper figure of Fig. 8.

(Just as in a magnetic lattice) the turning angle of particle j as it exits from a bending element will, in general, be slightly different from the turning angle of the design particle. Coordinate y (normal to the bend plane) is superfluous since the particle remains in the bend plane. The roles of the y and p_y coordinates are to be taken over by L_x and L_z.

The zero length "virtual" quadrupoles (included to compensate for deviation of field index m from $m = 1$) remain erect in the wobbling bend plane. But true physical qudrupoles, presumably erect in the laboratory, will be at least slightly displaced and slightly skew relative to the bend plane. This needs to be

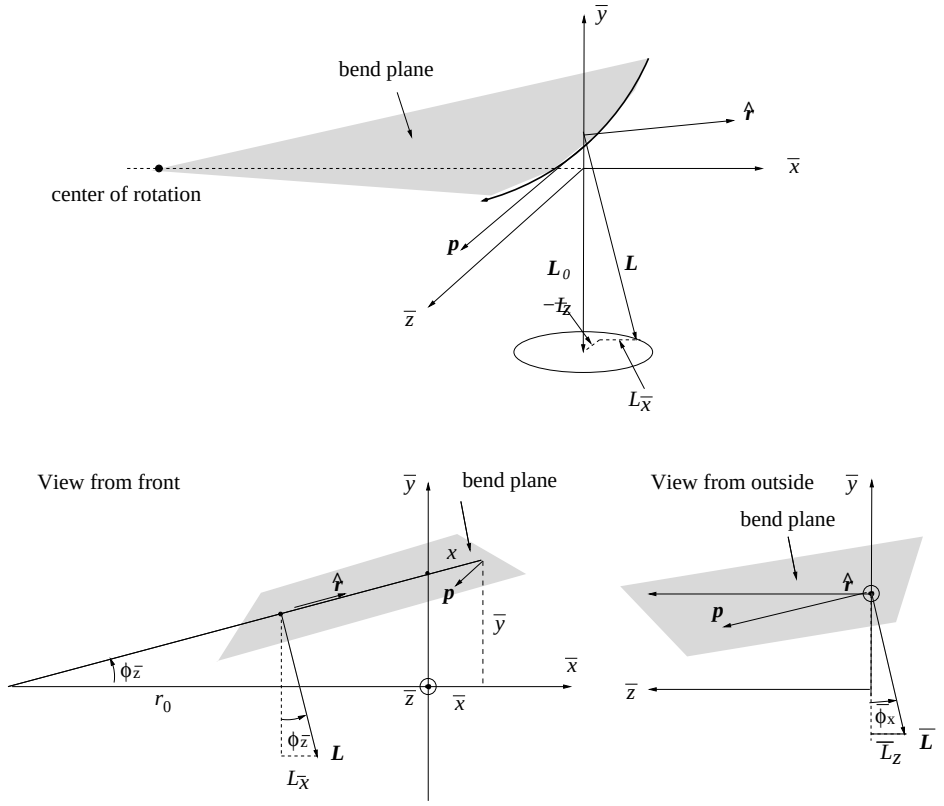

Figure 8: The wobbling 2D Muñoz-Pavic Plane $\mathcal{F}$, related to the stationary 3D laboratory frame, $\overline{\mathcal{F}}$.

accounted for at every quadrupole (or other multipole) location. Because of the possible skew component, such a quad itself rotates the bend plane slightly; this is accounted for by changing $(L_j, L_{j,x}, L_{j,y})$.

5.4 Transformation From CS to MP Coordinates

The Muñoz-Pavic formalism is two dimensional in the sense that orbits are monoplanar, but fully three dimensional in the sense that the orbit plane is arbitrary. Relative to an origin at the bend center the three dimensional geometry has been expressed in compact closed form in Section 4.4. For our accelerator application this description is unnecessarily general in that the actual particle orbits will, in fact, remain close to the horizontal plane.

An overly general formalism would not be a problem except for an issue of numerical precision. Standard accelerator formalism is based on a "paraxial" expansion about a "design orbit". In this exansion a transverse displacement δx as small as one micrometer (or even smaller) is typically significant. This displacement is some eight orders of magnitude smaller than the bend radius r_0, whose typical magnitude is, for example, 40 m. When using formulas from the fully three dimensional M-P geometry expressions such as Eq. (104). In this expression there is a potential loss of numerical precision of eight decimal places. By careful rearrangement of the formulas it may be possible to prevent such loss of precision, but the resulting code is complicated and bug-prone. To work around this problem an approximate, paraxial, nearly two dimensional geometry is appropriate.

In Section 4.4 the fully-3D geometry is described. The numerical precision in this approach is adequate for obtaining linear transfer matrices and, from them, Twiss functions and other lattice functions. The nearly two dimensional formalism is described next. This approach is needed for long term stability calculations, such as the determination of spin coherence time.

Though the moving MP frame $\mathcal{F}$ "wobbles" it actually remains quite close (angles less than one

milliradian) to the local laboratory frame $\bar{\mathcal{F}}$ for the EDM experiment. This permits the two frames to be related by something less than the full Euler angle formalism. We define $\phi_{\bar{z}}$ and $\phi_{\bar{x}}$ as rotation angles around $\bar{z}$ and $\bar{x}$ axes, respectively, to carry $\bar{\mathcal{F}}$ into $\mathcal{F}$. (In all cases the positve signs of rotation angles are fixed by right-hand rule.) Because rotations do not commute these angles are not quite unambiguous. But the angles are small enough to make the ambiguity unimportant (at least until proved otherwise.)

We define $\bar{C}_z = \cos\phi_{\bar{z}}$, $\bar{S}_z = \sin\phi_{\bar{z}}$, $\bar{C}_{x/2} = \cos(\phi_{\bar{x}}/2)$, $\bar{S}_{x/2} = \sin(\phi_{\bar{x}}/2)$. The rotation matrix M_z for the $\phi_{\bar{z}}$ rotation, defined by

$$\begin{pmatrix} x \\ y \\ z \end{pmatrix} = M_z \begin{pmatrix} \bar{x} \\ \bar{y} \\ \bar{z} \end{pmatrix}, \quad \text{is given by} \quad M_z = \begin{pmatrix} \bar{C}_z & \bar{S}_z & 0 \\ -\bar{S}_z & \bar{C}_z & 0 \\ 0 & 0 & 1 \end{pmatrix}. \tag{130}$$

The rotation matrix $M_{x/2}$ for the $\phi_{\bar{x}/2}$ rotation is

$$M_{x/2} = \begin{pmatrix} 1 & 0 & 0 \\ 0 & \bar{C}_{x/2} & \bar{S}_{x/2} \\ 0 & -\bar{S}_{x/2} & \bar{C}_{x/2} \end{pmatrix}. \tag{131}$$

The reason for introducing half angles for the x rotation has been to minimize the rotation ambiguity. We perform a half angle x-rotation, followed by a full angle z-rotation, then another half-angle x-rotation;

$$\begin{aligned} M &= \begin{pmatrix} 1 & 0 & 0 \\ 0 & \bar{C}_{x/2} & \bar{S}_{x/2} \\ 0 & -\bar{S}_{x/2} & \bar{C}_{x/2} \end{pmatrix} \begin{pmatrix} \bar{C}_z & \bar{S}_z & 0 \\ -\bar{S}_z & \bar{C}_z & 0 \\ 0 & 0 & 1 \end{pmatrix} \begin{pmatrix} 1 & 0 & 0 \\ 0 & \bar{C}_{x/2} & \bar{S}_{x/2} \\ 0 & -\bar{S}_{x/2} & \bar{C}_{x/2} \end{pmatrix} \\ &= \begin{pmatrix} \bar{C}_z & \bar{S}_z\bar{C}_{x/2} & \bar{S}_z\bar{S}_{x/2} \\ -\bar{S}_z\bar{C}_{x/2} & \bar{C}_z\bar{C}_{x/2}^2 - S_{x/2}^2 & \bar{C}_z\bar{S}_{x/2}\bar{C}_{x/2} + \bar{S}_{x/2}\bar{C}_{x/2} \\ \bar{S}_z\bar{S}_{x/2} & -\bar{C}_z\bar{S}_{x/2}\bar{C}_{x/2} - \bar{S}_{x/2}\bar{C}_{x/2} & -\bar{C}_z\bar{S}_{x/2}^2 + \bar{C}_{x/2}^2 \end{pmatrix}. \end{aligned} \tag{132}$$

Fig. 8 establishes the rotation angle $\phi_{\bar{z}}$ that orients the $\bar{\mathcal{F}}$ frame such that a particle vertically displaced by $\bar{y}$ lies in the MP plane;

$$\tan\phi_{\bar{z}} = \frac{\bar{y}/r_0}{1 + \bar{x}/r_0} \approx \frac{\bar{y}}{r_0}. \tag{133}$$

(For small angles this agrees with Eq. (96).) Rotation through angle $\bar{\phi}_{x/2}$ around the $\overline{x}$-axis, applied twice, puts $\mathbf{p}$ in the bend plane;

$$\begin{pmatrix} 1 & 0 & 0 \\ 0 & \bar{C}_{x/2} & \bar{S}_{x/2} \\ 0 & -\bar{S}_{x/2} & \bar{C}_{x/2} \end{pmatrix}^2 \begin{pmatrix} \bar{p}_x \\ \bar{p}_y \\ \bar{p}_z \end{pmatrix} = \begin{pmatrix} . \\ 0 \\ . \end{pmatrix}. \tag{134}$$

This fixes $\phi_{\bar{x}}$;

$$\tan\phi_{\bar{x}} = \frac{-\bar{y'}}{\sqrt{1 - \bar{x'}^2 - \bar{y'}^2}} \approx -\bar{y'}. \tag{135}$$

(For small angles this agrees with Eq. (96) because $\tilde{p}_{\bar{y}} \approx y'$.) These formulas are to be used only to transform from the Frenet, cylindrical coordinates, conventional in accelerator physics, to MP coordinates, or vice versa. One must be careful using these Frenet coordinates as intermediate variables for subsequent particle evolution, for example in the next section, where the Frenet variables are used to propagate through bend free regions. In such bend free regions the Frenet variables are simply laboratory variables, with y vertical, z aligned with the local beamline direction, and x outward.

5.5 Conversion of Implicit Transfer Matrices to Explicit Form

5.5.1 Transfer Matrix Determination Using Finite Differences

By using 2×2 transfer matrices we have succeeded in treating an electric bend element as a "black box" that can be represented by a transfer matrix giving the output coordinates (x_1, x_1') in terms of the input

coordinates (x_0, x_0'). Unfortunately we have "cheated" by allowing the matrix elements to be functions of individual particle kinetic energies. Concatenating maps like this is possible, at least in principle, using differential algebra. But, because of computational complexity, we are unprepared for such a program.

What we can do, however, is what was done to find transfer matrices in the pre-UAL version of the TEAPOT code. One starts by defining a set of 20 standard starting coordinates with judiciously-selected "differentially-displacements" from the closed orbit "fixed point". Here "differential" means small enough that linearized treatment yields negligible error, but large enough for round off errors to be negligible. A typical "differential" dispacement might be x1typ $= 10^{-6}$m, x2typ $= 10^{-6}$ m, deltyp $= \delta\mathcal{E}_{\rm typ}/\mathcal{E}_\prime = 10^{-6}$.

Using the implicit transfer matrix (such as Eq. (128)) one can evolve these 20 rays (or rather 21 if the closed orbit has non-vanishing initial displacement) from input to output. Using finite difference formulas, accurate first order transfer matrix elements can be obtained from the output coordinates. Less accurate, but satisfactory, second order transfer matrix elements can be obtained the same way.

The simplest way to spell this out in detail is to show the actual fortran code used to produce the standard starting coordinates. The following starting coordinates are sufficient to obtain all transfer matrix elements through second order; fewer are sufficient if only linear matrix elements are needed. The second argument of starting coordinate `trtrin(i, j)` gives the particle index, the first gives the phase space coordinate index. `orbit(i)` contains the starting fixed point and `delta` allows for an intentional energy offset.

```
C     ---  generate rays for tracking to get transfer matrix

      DO i = 1, 4
         DO j = 0, 20
            trtrin(i, j) = orbit(i)
         ENDDO
      ENDDO
      DO j = 0, 20
         trtrin(5, j) = 0.0d0
         trtrin(6, j) = delta
      ENDDO

      trtrin(1, 1) = trtrin(1, 1) + x1typ
      trtrin(1, 2) = trtrin(1, 2) - x1typ
      trtrin(2, 3) = trtrin(2, 3) + x2typ
      trtrin(2, 4) = trtrin(2, 4) - x2typ
      trtrin(3, 5) = trtrin(3, 5) + y1typ
      trtrin(3, 6) = trtrin(3, 6) - y1typ
      trtrin(4, 7) = trtrin(4, 7) + y2typ
      trtrin(4, 8) = trtrin(4, 8) - y2typ
C     --   delta ones
      trtrin(6, 9) = trtrin(6, 9) + deltyp
      trtrin(6, 10) = trtrin(6, 10) - deltyp
C     --   double ones
      trtrin(1, 11) = trtrin(1, 11) + x1typ
      trtrin(2, 11) = trtrin(2, 11) + x2typ
      trtrin(3, 12) = trtrin(3, 12) + y1typ
      trtrin(4, 12) = trtrin(4, 12) + y2typ
C     --   coupling ones
      trtrin(1, 17) = trtrin(1, 17) + x1typ
      trtrin(3, 17) = trtrin(3, 17) + y1typ
      trtrin(1, 18) = trtrin(1, 18) + x1typ
      trtrin(4, 18) = trtrin(4, 18) + y2typ
      trtrin(2, 19) = trtrin(2, 19) + x2typ
```

```
      trtrin(3, 19) = trtrin(3, 19) + y1typ
      trtrin(2, 20) = trtrin(2, 20) + x2typ
      trtrin(4, 20) = trtrin(4, 20) + y2typ
C     --   double delta ones
      trtrin(1, 13) = trtrin(1, 13) + x1typ
      trtrin(6, 13) = trtrin(6, 13) + deltyp
      trtrin(2, 14) = trtrin(2, 14) + x2typ
      trtrin(6, 14) = trtrin(6, 14) + deltyp
      trtrin(3, 15) = trtrin(3, 15) + y1typ
      trtrin(6, 15) = trtrin(6, 15) + deltyp
      trtrin(4, 16) = trtrin(4, 16) + y2typ
      trtrin(6, 16) = trtrin(6, 16) + deltyp
```

5.5.2 Post-Processing Determination of Transfer Matrices

The code used to obtain explicit transfer matrix elements is shown next. The notation should be self-explanatory, and justification for the formulas can be puzzled out.

```
C     ---  get transfer matrices using tracking output

      rx(1, 1) = (trtrout(1, 1) - trtrout(1, 2))/(2.*x1typ)
      rx(2, 1) = (trtrout(2, 1) - trtrout(2, 2))/(2.*x1typ)
      rx(1, 2) = (trtrout(1, 3) - trtrout(1, 4))/(2.*x2typ)
      rx(2, 2) = (trtrout(2, 3) - trtrout(2, 4))/(2.*x2typ)
      ry(1, 1) = (trtrout(3, 5) - trtrout(3, 6))/(2.*y1typ)
      ry(2, 1) = (trtrout(4, 5) - trtrout(4, 6))/(2.*y1typ)
      ry(1, 2) = (trtrout(3, 7) - trtrout(3, 8))/(2.*y2typ)
      ry(2, 2) = (trtrout(4, 7) - trtrout(4, 8))/(2.*y2typ)

C     --   coupled ones
      r(1, 3) = (trtrout(1, 5) - trtrout(1, 6))/(2.*y1typ)
      r(2, 3) = (trtrout(2, 5) - trtrout(2, 6))/(2.*y1typ)
      r(1, 4) = (trtrout(1, 7) - trtrout(1, 8))/(2.*y2typ)
      r(2, 4) = (trtrout(2, 7) - trtrout(2, 8))/(2.*y2typ)
      r(3, 1) = (trtrout(3, 1) - trtrout(3, 2))/(2.*x1typ)
      r(4, 1) = (trtrout(4, 1) - trtrout(4, 2))/(2.*x1typ)
      r(3, 2) = (trtrout(3, 3) - trtrout(3, 4))/(2.*x2typ)
      r(4, 2) = (trtrout(4, 3) - trtrout(4, 4))/(2.*x2typ)

C     ---  now get delta ones

      rx(1, 3) = (trtrout(1, 9) - trtrout(1, 10))/(2.*deltyp)
      rx(2, 3) = (trtrout(2, 9) - trtrout(2, 10))/(2.*deltyp)
      ry(1, 3) = (trtrout(3, 9) - trtrout(3, 10))/(2.*deltyp)
      ry(2, 3) = (trtrout(4, 9) - trtrout(4, 10))/(2.*deltyp)

C     ---  put these in one big matrix
      DO i = 1, 2
         DO j = 1, 2
            r(i, j) = rx(i, j)
            r(i + 2, j + 2) = ry(i, j)
         ENDDO
      ENDDO
```

```
      r(1, 5) = rx(1, 3)
      r(2, 5) = rx(2, 3)
      r(3, 5) = ry(1, 3)
      r(4, 5) = ry(2, 3)

C     ---  return if only first order
      IF (iorder .NE. 1) THEN
```

5.6 Determination of Twiss Functions From Transfer Matrices

5.6.1 Analysis of the Once-Around Transfer Matrix at the Origin

In this section x and y and ct subscripts will be suppressed, and only transverse evolution is to be discussed. The most general transfer matrix is a six-by-six matrix $\mathbf{M}(s_i, s_j)$, which propagates a phase space vector $\mathbf{x}(s_i)$ at s_i, to its value $\mathbf{x}(s_j)$ at s_j;

$$\mathbf{x}(s_j) = \mathbf{M}(s_i, s_j)\,\mathbf{x}(s_i). \tag{136}$$

UAL/ETEAPOT starts by assigning coordinates at the origin, $s_0 = 0$, to the particles in a standard bunch (as described earlier), and then evolves the standard bunch and records the coordinates $\mathbf{x}(s_i)$ at all points s_i. From these results the transfer matrices $\mathbf{M}(0, s_i)$ can be calculated (also as described earlier). By definition

$$\mathbf{M}(0, 0) = \mathbf{I}, \tag{137}$$

where $\mathbf{I}$ is the 6×6 identity matrix.

To extract Twiss lattice functions one needs "once-around" transfer matrices defined by

$$\widetilde{\mathbf{M}}(s_i) \equiv \mathbf{M}(s_i, s_i + \mathcal{C}_0) = \mathbf{M}(0, s_i)\,\mathbf{M}(s_i, \mathcal{C}_0). \tag{138}$$

where $\mathcal{C}_0$ is the circumference of the design orbit; the final step has been taken because knowledge of $s_i + \mathcal{C}_0$ requires tracking for more than one complete turn, but we are assuming that tracking has been done only for exactly one complete turn. Propagation from $s = \mathcal{C}_0$ to $\mathcal{C}_0 + s_i$ is the same as propagation from $s = 0$ to s_i. The Twiss parameterization of (one partitioned diagonal 2×2 block of) such a once-around, symplectic transfer matrix is

$$\widetilde{\mathbf{M}}(s_i) = \begin{pmatrix} \cos\mu + \alpha \sin\mu & \beta \sin\mu \\ -\frac{1+\alpha^2}{\beta} \sin\mu & \cos\mu - \alpha \sin\mu \end{pmatrix}. \tag{139}$$

Extraction of the α_0 and β_0, the Twiss parameters at the origin, can start from

$$\cos\mu = \frac{1}{2}\left(\widetilde{\mathbf{M}}_{11}(0) + \widetilde{\mathbf{M}}_{22}(0)\right), \tag{140}$$

which fixes $\cos\mu$. Because of sign ambiguity, this determines only $|\sin\mu|$. One also has the relations

$$\beta_0 = \left|\frac{\widetilde{\mathbf{M}}_{12}(0)}{\sin\mu}\right|. \tag{141}$$

and

$$\alpha_0 = \frac{1}{2\sin\mu}\left(\widetilde{\mathbf{M}}_{11}(0) - \widetilde{\mathbf{M}}_{22}(0)\right). \tag{142}$$

With β being positive by convention, from the 1,2 element, $\mathrm{sign}(\sin\mu)$ can be seen to be the same as $\mathrm{sign}(\widetilde{\mathbf{M}}_{12})$. With $\cos\mu$ known, this fixes $\sin\mu$. Together, these relations fix $\sin\mu$, $\cos\mu$, α_0, and β_0.

Conventionally one also introduces the third Twiss parameter

$$\gamma_0 = \frac{1 + \alpha_0^2}{\beta_0}, \tag{143}$$

which can be obtained once β_0 and α_0 have been determined.

Because of the multiple-valued nature of inverse trig functions, these relations do not determine a unique value for μ. They do, however, determine the quadrant in phase space in which the angle μ resides. For $\mathrm{sign}(\sin\mu)>0$ the angle μ resides in the first or second quadrant, in which case the fractional tune is less than 1/2; otherwise the fractional tune is greater than 1/2. For $\mathrm{sign}(\cos\mu)>0$ the angle μ resides in the first or fourth quadrant, in which case the fractional tune is below 1/4 or above 3/4. These considerations fix the fractional parts of the tunes.

An "aliasing" or "integer-tune" ambiguity remains, however, which cannot, even in principle, be obtained from the once-around matrix. Only if both transverse tunes are less than 1 (which is hardly ever the case) would the tunes be equal to the fractional tunes that have been determined. In general, to obtain the integer tunes, it is necessary to analyse the turn by turn data at sufficiently closely-space intermediate points in the lattice.

5.6.2 Evolving the Twiss Functions Around the Ring

To find the Twiss parameters at an arbitrary location s_i in the ring requires the once-around transfer matrix $\widetilde{\mathbf{M}}(s_i)$. This can obtained most compactly by multiplying the equation

$$\mathbf{M}(0, s_j) = \mathbf{M}(s_i, s_j)\,\mathbf{M}(0, s_i) \tag{144}$$

on the right by $\mathbf{M}^{-1}(0, s_i)$ to produce

$$\mathbf{M}(s_i, s_j) = \mathbf{M}(0, s_j)\,\mathbf{M}^{-1}(0, s_i). \tag{145}$$

Substituting this with $s_j = \mathcal{C}_0$ into Eq. (138) produces

$$\widetilde{\mathbf{M}}(s_i) = \mathbf{M}(0, s_i)\,\widetilde{\mathbf{M}}(0)\,\mathbf{M}^{-1}(0, s_i). \tag{146}$$

Aside on matrix inversion :
There are multiple ways of performing the matrix inversion required to use Eq. (146). One is to use a numerical matrix inversion code, commercial or open source. A procedure that checks the symplecticity of the transfer matrices involved uses an algebraic property of a symplectic matrix. Assuming that $\widetilde{\mathbf{M}}$ is, in fact, symplectic, one has

$$\widetilde{\mathbf{M}}^{-1} = -\mathbf{S}\,\widetilde{\mathbf{M}}^{T}\mathbf{S}, \tag{147}$$

where $\widetilde{\mathbf{M}}^{T}$ signifies matrix transposition and the matrix $\mathbf{S}$ is given by

$$\mathbf{S} = \begin{pmatrix} 0 & 1 & 0 & 0 & 0 & 0 \\ -1 & 0 & 0 & 0 & 0 & 0 \\ 0 & 0 & 0 & 1 & 0 & 0 \\ 0 & 0 & -1 & 0 & 0 & 0 \\ 0 & 0 & 0 & 0 & 0 & 1 \\ 0 & 0 & 0 & 0 & -1 & 0 \end{pmatrix}. \tag{148}$$

End of aside.

Having obtained $\widetilde{\mathbf{M}}(s_i)$, the procedure described in the previous subsection can then be used to obtain $\alpha(s_i)$ and $\beta(s_i)$. But the integer tune ambiguity can, again, not be resolved. To resolve this ambiguity both x and y phases have to be tracked continuously through the lattice, requiring that they advance continuously and monotonically. (Later, at least in principle, the same ambiguity will have to be faced for longitudinal motion. But the integer longitudinal tune is almost always zero, so the problem will not appear in the longitudinal case.)

UAL/ETEAPOT requires the lattice description to be in the form of an `.sxf` file. To be "legal" the granularity of such a file has to be fine enough that no phase can advance by more than a quarter integer through any element in the file. Before working out the α and β function evolution, ETEAPOT first works out the total phase advances from the origin to every node specified by the `.sxf` file (or, if some elements are sliced more finely, by every node after slicing).

There is an alternative way of finding the betatron phase advances. It starts with a Twiss parameterization of $\mathbf{M}(0, s)$ from the origin to an arbitrary position s in the lattice;

$$\mathbf{M}(0, s) = \begin{pmatrix} \sqrt{\frac{\beta(s)}{\beta_0}}\Big(\cos\psi(s) + \alpha_0 \sin\psi(s)\Big) & \sqrt{\beta_0\beta(s)}\,\sin\psi(s) \\ \cdot & \sqrt{\frac{\beta_0}{\beta(s)}}\Big(\cos\psi(s) - \alpha(s)\sin\psi(s)\Big) \end{pmatrix}. \tag{149}$$

The 2,1 element is quite complicated; it is not shown here since it will not be needed for the following analysis. Dividing the 1,1 element by the 1,2 element produces

$$\frac{\mathbf{M}_{1,1}(0,s)}{\mathbf{M}_{1,2}(0,s)} = \frac{\sqrt{\frac{\beta(s)}{\beta_0}}\Big(\cos\psi(s) + \alpha_0 \sin\psi(s)\Big)}{\sqrt{\beta_0\beta(s)}\,\sin\psi(s)} = \frac{\cot\psi(s) + \alpha_0}{\beta_0}. \tag{150}$$

Rearranging this equation produces

$$\psi(s) = \tan^{-1}\,\frac{\mathbf{M}_{1,2}(0,s)}{\beta_0\mathbf{M}_{1,1}(0,s) - \alpha_0\mathbf{M}_{1,2}(0,s)}. \tag{151}$$

Like all inverse trigonometric formulas, this equation has multiple solutions. But, with the `.sxf` granularity being required to be fine enough, one can (in principle) sequentially obtain unique phases. With $\psi(s)$ starting from $\psi(0) = 0$, as s increases from s_i to s_{i+1} there is a unique solution of Eq. (151), $\psi(s_i) >= \psi(s_{i-1})$ such that the function $\psi(s)$ increases monotonically, as required. Because the interval from $s_{i=1}$ to s_i is non-zero, ψ will, superficially, advance discontinuously; the correct solution is the least discontinuous. The same calculation has to be done for both the x and y betatron sectors. Unfortunately, even though, theoretically, the phase advances monotonically, numerical errors can cause Eq. (151) to give local phase decrease. This can cause Eq. (151) to give occasionally erratic results.

A more robust procedure is to use the equation[3]

$$\psi(s_0 + \ell) = \psi(s_0) + \int_{s_0}^{s_0+\ell} \frac{ds'}{\beta(s')}, \tag{152}$$

along with the equation[3] governing evolution of the beta function through a drift section;

$$\beta(s) = \beta_0 - 2\alpha_0\, s + \gamma_0\, s^2, \tag{153}$$

which describes the evolution of β in drift regions. For sufficiently fine slices the denominator in Eq. (152) is positive definite; the integral is then readily performed numerically. Exact for the phase evolution through drifts, the same formula gives a good approximation in all lattice elements, and becomes exact in the thin-slice limit.

5.6.3 Beta Function Comparisons

Figure 9 compares β_x evaluations for the "benchmark" lattice `E_BM_Z_sl4.sxf`. This is the lattice closest to "cylindrical" with lumped quadrupoles just barely strong enough to move the lattice away from the boundary between vertical stability and vertical instability. The upper figure beta functions are evaluated by ETEAPOT, the lower by the linearized (Wollnik) formulas re-derived in Appendix 8.1. There is agreement to excellent accuracy on tune Q_x (which has been confirmed both by counting cycles, by analytic evaluation, and by the average $\langle\beta_x\rangle$. Perfect agreement cannot be expected since the two approaches make slightly different approximations.

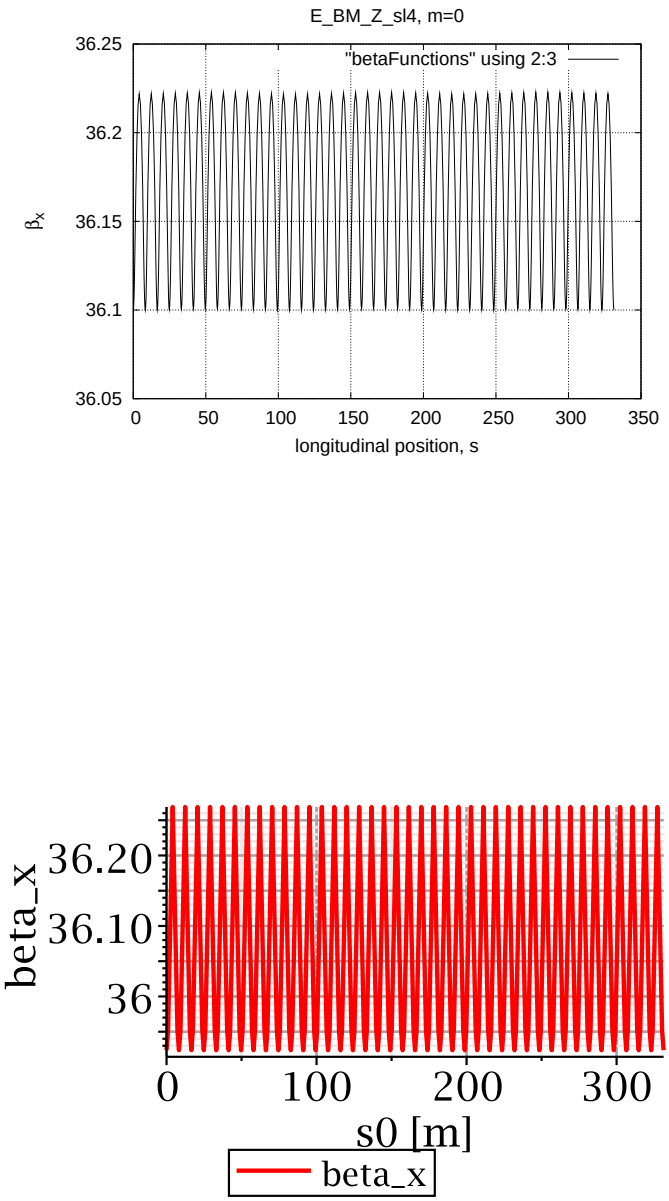

Figure 9: The upper figure shows β_x as calculated by ETEAPOT. The lower figure shows, for the same benchmark lattice "E_BM_Z_sl4", β_x as calculated by the linearized (Wollnik) formulas defined in Appendix 8.1. As explained in the text, the apparent "disagreement" results from the slightly different definitions of β.

6 UAL/ETEAPOT Simulation Code

6.1 Revolution Period

For modeling longitudinal dynamics it is critical to obtain the revolution period $T_{\mathrm{rev.}}$ to good accuracy for every particle. From Eqs. (61), (74), (77), and (81) one has

$$\frac{dt}{d\theta} = \frac{\mathcal{E}_M \lambda^2}{L\kappa^2 c^2} \frac{1}{\Big(1+\epsilon\cos\kappa(\theta-\theta_0)\Big)^2} + \frac{m_p k\widetilde{\mathcal{C}}\lambda^2}{\kappa^2 L^2 c^2} \frac{\cos\kappa(\theta-\theta_0)}{\Big(1+\epsilon\cos\kappa(\theta-\theta_0)\Big)^2} \tag{154}$$

Both integrals can be evaluated in closed form to obtain t as a function of θ. However the evaluation is numerically treacherous.

For the study of longitudinal dynamics and synchrotron oscillations what is needed is the deviation of the time of flight from the time of flight of the design particle. This is a very small difference of two large numbers. Eq. (154) can be recast as

$$t - t_0 = A\int \frac{d\Delta\theta}{(1+\epsilon\cos\kappa\Delta\theta)^2} - A_0\int d\Delta\theta + B\tilde{\mathcal{C}}\int \frac{\cos\kappa\Delta\theta\, d\Delta\theta}{(1+\epsilon\cos\kappa\Delta\theta)^2}. \tag{155}$$

Here $\Delta\theta = \theta - \theta_0$, the factors A and B (both of which deviate little from constancy and can never become "small") replace the other factors in Eq. (154), and A_0 is the values of A on the design orbit. All of the factors A, B, A_0, ϵ, and κ are constant on any particular orbit being followed, and all have values very close to their values on the design orbit. The only variable factor is $\Delta\theta$. The first two terms cancel approximately, which makes the evaluation of the first term critical. The third term requires no special treatment since the $\tilde{\mathcal{C}}$ factor is already differentially small. The cancellation tendency can be ameliorated by adding and subtracting a term $A_0\int d\Delta\theta = A_0\Delta\theta$ to produce

$$t - t_0 = \epsilon\int \frac{(-2A + B/\tilde{\epsilon})\cos\kappa\Delta\theta - A\epsilon\cos^2\kappa\Delta\theta}{(1+\epsilon\cos\kappa\Delta\theta)^2}\, d\Delta\theta + (A - A_0)\Delta\theta. \tag{156}$$

Here $\tilde{\mathcal{C}} = \epsilon/\tilde{\epsilon}$ has been obtained using Eq. (81). In Eq. (156) all terms are differentially small and the small differences of large numbers have been moved outside the integrals. For the proton EDM experiment, since $|\epsilon|$ never exceeds 1/1000, the integrand can be expanded in powers of ϵ before integrating. A typical leading term in these integrals is $\Delta\theta$ multiplied by a constant factor. Currently ETEAPOT includes this term as well as terms with extra powers of ϵ up to ϵ^5 and *does not* check automatically that this last term is, itself, negligible.

A subtle feature of the time of flight evaluation is that the ellipticity ϵ vanishes on perfectly circular orbits (of which the design orbit is one). This causes the angle θ_0, which is the angle to perigee, to be indeterminate because perigee is indeterminate on a circular orbit. Eq. (81), the second of Eqs. (72) and Eq. (79) force ϵ to be non-negative. And yet the major and minor axes can switch from prolate to oblate when an arbitrarily small kink is applied to an orbit for which ϵ is close enough to zero. When this happens the angle θ_0 advances discontinuously through $\pi/2$. When this happens the angle θ also advances discontinuously through the same angle. But these changes do not affect the integrals in Eq. (156) which depend only on $\theta - \theta_0$.

6.2 Lumped Correction for Field Index Deviation

Analytic propagation formulas have been given for $1/r^2$ radial dependence of the electric field. The actual radial dependence will deviate from this, with m, the deviant field index, having been defined in Eq. (1). $E \sim 1/r^{1+m}$, so $m = 1$ for the Coulomb's law field dependence. For this, the "spherical" case, the orbit equations have been solved in closed form in Section 4.1.

The ETEAPOT strategy, even for $m \neq 1$, is to treat sector bends as *thick* elements with orbits given by the analytic $m = 1$ formulas. The $m \neq 1$ case is handled by inserting zero thickness "kicks" of appropriate strength. As usual with TEAPOT, this approximation becomes arbitrarily good in the thin

slicing limit. Though the idealized model differs from the physical apparatus, the orbit description within the idealized model is exact, and hence symplectic. For too coarse slicing, though the orbit deviates from the true orbit, it remains "exact". One blames the inaccuracy on the fact that the lattice model deviates from the true lattice, not on the fact that the equations are being solved approximately. By varying the slicing one can judge from the limiting behavior what degree of slicing is appropriate.

Just as in a nonuniform magnetic field, a deviant field index m introduces horizontal and vertical focusing terms of equal magnitude, $|K_1| = |m|/r_0^2$, but of opposite sign, into the focusing equations. See Eqs. (212) and (224).

$$\begin{aligned} K_{x,1}^{(m)} &= \left(\frac{1}{r_0^2} + \frac{1}{\gamma_0^2 r_0^2}\right) - \frac{m}{r_0^2}, \\ K_{y,1}^{(m)} &= \frac{m}{r_0^2}. \end{aligned} \tag{157}$$

Note that for $m = 0$ (the "cylindrical" case) there is no vertical focusing; with the electric field being independent of y for cylindrical electrodes, this is obviously correct. The subscript "1" indicates "quadrupole" order. The large parentheses segregate the geometric focusing (which is independent of m) from the gradient focusing (which vanishes for $1/r$ field variation). These formulas agree with Wollnik's equations in his section 4.3.2. Re-writing these equations for our spherical $m = 1$ case;

$$\begin{aligned} K_{x,1}^{\text{sph.}} &= \left(\frac{1}{r_0^2} + \frac{1}{\gamma_0^2 r_0^2}\right) - \frac{1}{r_0^2}, \\ K_{y,1}^{\text{sph.}} &= \frac{1}{r_0^2}. \end{aligned} \tag{158}$$

(With our sign convention, positive K-value corresponds to *focusing*. Hence, for example, there is already some vertical *focusing* in our Coulomb case.) These are the focusing terms we have accounted for so far; Eqs. (157) are the extra terms we want. We have to make up the differences;

$$\begin{aligned} \Delta K_{x,1}^{(m)} &= K_{x,1}^{(m)} - K_{x,1}^{\text{sph.}} = \frac{-m+1}{r_0^2}, \\ \Delta K_{y,1}^{(m)} &= K_{y,1}^{(m)} - K_{y,1}^{\text{sph.}} = \frac{m-1}{r_0^2}. \end{aligned} \tag{159}$$

These are the coefficients of the distributed focusing we have to apply to "convert" the Coulomb formulas to model the actual m value. For example, suppose the actual electrodes are saddle-shaped, with $m = -1$ to make $E(r)$ be independent of r. This gives substantial vertical defocusing. Yet the Coulomb field provides vertical focusing. The strengths of the quads we insert artificially are therefore the sum of two terms; one cancels the Coulomb defocusing handled by the MP formalism; the other superimposes focusing proportional to m.

The artificial quadrupoles have zero length, but their length-strength product has to be matched to the "field integral" corresponding to length L_{bend} of the bending slice being compensated.

Before continuing with the treatment for $m \neq 0$ it is important to remember the discontinuous increments to $\mathcal{E}$ as a particle enters or leaves a bending element. The discontinuity is equal (in magnitude) to the change in potential energy. When correcting the focusing by artificial quadrupoles we have to decide whether the artificial quadrupoles are "inside" or "outside", since the actual deflections will be different in the two cases. Since the difference is quadratic in transverse displacement, the difference would be called a "sextupole" effect. By treating the artificial quad as "inside", which we do, we avoid introducing an artificial sextupole effect.

Whatever criteria for slicing quadrupoles that have been used in the past, the same criteria apply here. The default slicing in ETEAPOT treats a thick bend as a half bend, a single kick at the center, and then another half bend. For example, with $m = -1.3$, the central quad is vertically defocusing with inverse focal length $q = 1/f = 2.3\ell/r_0^2$, where ℓ is the arc length through the bend.

Numerically, with $r_0 = 40\,\text{m}$ and ℓ equal to, say, $16\,\text{m}$ the ratio of focal length to element length is $(40/16)^2/2.3 \approx 2.7$. With element length small compared to focal length, this suggests that the

compensation will be fairly good even with no finer slicing. The entire EDM ring, with its 8 full cells, would then be represented by 16 half-bends. In practice one will slice more finely.

The transfer matrices for the thin effective quadrupole are

$$\mathbf{K}_{\mathbf{x}}^{(\mathbf{m})}(\Delta\theta) = \begin{pmatrix} 1 & 0 \\ (m-1)\Delta\theta/r_0 & 1 \end{pmatrix},$$
$$\mathbf{K}_{\mathbf{y}}^{(\mathbf{m})}(\Delta\theta) = \begin{pmatrix} 1 & 0 \\ (-m+1)\Delta\theta/r_0 & 1 \end{pmatrix}, \tag{160}$$

For $m = 1$ these kick matrices reduce to identity matrices.

6.3 Bend/Kick/Bend Orbit Evolution

Bend/Kick/Bend evolution through bend angle $\Delta\theta$ in an element with field index m is then described by the matrix

$$\mathbf{M}_{\boldsymbol{\Delta\theta}}^{(\mathbf{m})} = \mathbf{B}_{\boldsymbol{\Delta\theta/2}}^{(\mathbf{1})}\mathbf{K}^{(\mathbf{m})}(\Delta\theta)\mathbf{B}_{\boldsymbol{\Delta\theta/2}}^{(\mathbf{1})} \tag{161}$$

The $\mathbf{B}$ matrices depend implicitly on γ^I (via κ). Substituting from Eqs. (128) and (160), the horizontal transfer matrix is

$$\mathbf{M}_{\mathbf{x},\boldsymbol{\Delta\theta}}^{(\mathbf{m})} =$$
$$\begin{pmatrix} \cos\kappa\Delta\theta/2 & \frac{r_0}{\kappa}\sin\kappa\Delta\theta/2 \\ -\frac{\kappa}{r_0}\sin\kappa\Delta\theta/2 & \cos\kappa\Delta\theta/2 \end{pmatrix}\begin{pmatrix} 1 & 0 \\ (m-1)\Delta\theta/r_0 & 1 \end{pmatrix}\begin{pmatrix} \cos\kappa\Delta\theta/2 & \frac{r_0}{\kappa}\sin\kappa\Delta\theta/2 \\ -\frac{\kappa}{r_0}\sin\kappa\Delta\theta/2 & \cos\kappa\Delta\theta/2 \end{pmatrix}. \tag{162}$$

A complication that needs to be remembered is that the coefficient κ, defined in Eq. (69), is a function of $\mathcal{E}$, which can be different for different particles.

The vertical transfer matrix is

$$\mathbf{M}_{\mathbf{y},\boldsymbol{\Delta\theta}}^{(\mathbf{m})} = \begin{pmatrix} 1 & r_0\Delta\theta/2 \\ 0 & 1 \end{pmatrix}\begin{pmatrix} 1 & 0 \\ (-m+1)\Delta\theta/r_0 & 1 \end{pmatrix}\begin{pmatrix} 1 & r_0\Delta\theta/2 \\ 0 & 1 \end{pmatrix}. \tag{163}$$

For a true drift section of length ℓ (as contrasted with the effective drift section associated with a sliced bend element) the horizontal and vertical transfer matrices are identical;

$$\mathbf{M}_{\text{drift}} = \begin{pmatrix} 1 & \ell \\ 0 & 1 \end{pmatrix}. \tag{164}$$

6.4 Coding Strategies

Subtraction of one "large" quantity from another can cause large loss of numerical accuracy and must not, therefore, be allowed. Therefore, when propagating a particle through a bend (or any other) element, only dynamic quantities that are "small" can be allowed to vary. Here small means, for displacements, small compared to r_0 and, for angles, small compared to 1. For long term tracking, manifest symplecticity has to be preserved at every step. The ETEAPOT lattice model makes this possible by permitting only pure rotations (in phase space), which are evaluated exactly, and thin element kicks. Time of flight calculations have to be accurate, but need not be exact. Polymorphic, truncated power series formulas can only be symplectic to the highest expansion order retained.

For determination of Twiss functions and other lattice functions, transfer maps are needed and, within UAL, this requires that only polymorphic coding operations be used. (This is not fundamental; it only reflects design constraints in the UAL code architecture.) "UAL Optics calculator" code is to be cloned from magnetic code and then modified appropriately for electric lattice.

For ETEAPOT the six phase space coordinates are to be redefined as shown in Table 1 and in Fig. 8. In the table the original magnetic, coordinate definitions, identical in MAD and UAL, are shown in the block of columns labelled MAD/ UAL/ TEAPOT. These coordinates, specifying deviations from a design orbit lying in a single horizontal plane, are now being assigned overhead bars. $x \to \bar{x}$, $p_x \to \bar{p}_x$, $y \to \bar{y}$,

and so on. This frees up unbarred symbols for ongoing use in ETEAPOT. Unlike the coordinates about to be introduced, these original coordinates are symplectic in the sense that they preserve the form of Hamilton's equations. But absence of symplecticity in this sense is not essential for numerical tracking.

ETEAPOT re-definitions are shown in columns 4, 5, and 6, and redefinitions needed for the Muñoz-Pavic formalism are in the final three columns.

For truncated power series formulation it is essential to have indexed coordinates. These are indicated in the first column of the table. The conceptual definitions of these components, shown in the second column, are the six phase space coordinate offsets from the design orbit (approximately) as they were first introduced in the TRANSPORT code of Karl Brown. Minor variations involve displacement by one of the indices, rescaling of the momenta, and redefinition of the longitudinal coordinates. Entries in the column labeled "linearized", are somewhat closer to the original Karl Brown definitions.

One challenge for ETEAPOT has been to introduce coordinates in terms of which the transverse dynamics can be described by the exact Muñoz/Pavic formulation, which is two dimensional, while retaining the ability to determine the corresponding Frenet coordinates. A significant step in achieving this has been to cannibalize the y and p_y coordinates, using those slots instead for the angular momentum components L_z and $-L_x$, both of which, like y and p_y, are zero on the design orbit.

Such a fundamental change might be expected to make all existing code obsolete. But, for reasons to be explained in this section, the coordinate definitions in the "ETEAPOT" columns permit much of the existing TEAPOT code to survive unchanged. Here the minimum requirement for being satisfactory is that the linearized transfer matrices and lattice functions conform with conventional, magnetic lattice definitions. It is the numerical values of the entries in the columns labeled "scaled" that are stored in the computer as the indexed coordinates used as truncated power series variables.

The most basic coordinate redefinition is that x, instead of being the rectangular (actually cylindrical) radial Frenet displacement from the design orbit, is newly defined to be the radial displacement in spherical coordinates; i.e. $r = r_0 + x$. Mathematically this is a serious redefinition, but numerically, with r_0 being, say, forty meters, and x and y not exceeding, say, one centimeter, the distinction between cylindrical and spherical coordinates is numerically negligible.

With x thus redefined, and with L_z and L_x rescaled as shown in the column labeled "ETEAPOT, coord. scaled", the linearized and rescaled values of L_z and L_x are numerically the same as the scaled values of y and p_y. This is spelled out more fully in the next section. Working out the relations between the new coordinates and Frenet coordinates in higher than linear order is quite complicated. But it is the linear maps, along with their off-momentum dependence, that are most essential for accelerator design. Also, if high order maps turn out to be needed for long term evolution (which has rarely, if ever, been particularly useful in practical accelerator technology) high order transformation to conventional coordinates will only be needed for comparison with high order maps produced by other programs. (Incidentally, a nonlinear map, is not necessarily "correct" to whatever order it is expressed; it is only guaranteed to agree, to its stated order, with the underlying formulas from which it has been obtained, and they may be wrong in any order.)

Table 1: Transfer-matrix-preserving redefinitions of the phase space coordinates. Note that the total energy displacement $\Delta\mathcal{E}/(p_0c)$ is conserved everywhere except in RF cavities.

	MAD/	UAL/	TEAPOT	ETEAPOT, drift/kick			Muñoz-	Pavic	bend/kick
coord.	coord.	coord.	coord.	coord.	coord.	coord.	coord.	coord.	coord.
indexed	concept.	scaled	linear.	concept.	scaled	linear.	concept.	scaled	linear.
p[0]	$\bar{x}$	$\bar{x}$	$\bar{x}$	x	$x = r_0 - r$	$\approx \bar{x}$	h_θ	$-\beta^2 h_\theta/r_0$	$\approx \bar{x}$
p[1]	$\bar{p}_x$	$\bar{p}_x/p_0$	$\bar{x}' \approx \bar{\theta}_x$	p_r	p_r/p_0	$\approx \bar{p}_x/p_0$	h_r	h_r	$\approx \bar{p}_x/p_0$
p[2]	$\bar{y}$	$\bar{y}$	$\bar{y}$	$\bar{L}_x$	$r_0\bar{L}_x/\bar{L}$	$\approx \bar{y}$	$\bar{L}_x$	$r_0\bar{L}_x/\bar{L}$	$\approx \bar{y}$
p[3]	$\bar{p}_y$	$\bar{p}_y/p_0$	$\bar{y}' \approx \bar{\theta}_y$	$\bar{L}_z$	$-\bar{L}_z/\bar{L}$	$\approx \bar{p}_y/p_0$	$\bar{L}_z$	$-\bar{L}_z/\bar{L}$	$\approx \bar{p}_y/p_0$
p[4]	Δt	$-\Delta z/v_0$		Δt	$-\Delta z/v_0$		Δt	$-\Delta z/v_0$	
p[5]	$\Delta\mathcal{E}$	$\Delta\gamma m_p c/p_0$		$\Delta\mathcal{E}$	$\Delta\mathcal{E}/(p_0c)$		$\Delta\mathcal{E}$	$\Delta\mathcal{E}/(p_0c)$	

6.5 Propagation Through Bend-Free Regions

At every entrance into a bend element it is necessary to transform to MP variables from laboratory variables, and at every exit from a bend element it is necessary to transform back to MP variables.

6.6 Treatment of Coupling Between Energy and Position

As explained previously, the original TEAPOT strategy was to use drift/kick evolution, with coarsest possible slicing of bend elements. All orbit deflections are applied via delta function impulses and propagation through finite intervals, with magnetic field set to zero, is described by straight lines. While slicing electric bend regions similarly, one wishes to treat all deflections by delta function impulses and the intervening spaces as drifts. But the particle speed is, in fact, changing continuously through the drift regions. At a minimum this complicates the calculation of time-of-flight and of spin evolution. For *transverse* coordinates, the error is small and the fractional error decreases more strongly than linearly with slice thickness. This could make it legitimate, should it be needed, to use existing TEAPOT formalism for modeling transverse evolution through the artificial drift regions established when bend elements are sliced. Such a treatment is unnecessary, however, since propagation through electric sector bends can be treated by the transfer matrices given by Eqs. (162) and (163).

Neither longitudinal phase space nor spin evolution can be accurately modeled by a pure drift/kick formalism. Time of flight errors occur both because the straight line paths lengths are seriously shorter than the more nearly elliptical paths (a defect from which TEAPOT has always suffered, and which has often led to finer slicing than would otherwise have been needed) and because the particle speed is not constant. Both of these errors can be eliminated by applying analytic MP formulas to calculate the evolution through bends. The orbit then consists of elliptical segments separated by kinks. The time of flight is calculated for the elliptical segments. The time of flight through a kink vanishes.

Spin evolution is to be handled the same way.

The exact treatment of orbits in inverse square law electric field, as described in Section 4, is the only way we know how to simultaneosly preserve symplecticity through thick elements, provide closed form analytic expressions for handling synchrobetatron coupling, and obtain an analytic formula for time of flight. Here we attempt to integrate this formulation into a simple, possibly only approximate treatment, adequate for obtaining traditional accelerator quantities like dispersion, chromaticity, and synchrotron oscillation parameters. This treatment is largely motivated by the desire to retain the existing TEAPOT formalism to the extent possible.

The redefinition of coordinates `p[0]` through `p[3]` has already been discussed. Looking next at the last row of Table 1, one sees that changing from magnetic to electric definitions only requires care in the interpretation of `p[5]`, and does not require any actual change in its definition. In magnetic lattices one can say, all with equal validity, that speed, magnitude of momentum, kinetic energy, and total energy are conserved everywhere except in RF cavities. `p[5]`, whether defined as fractional deviation of total energy or (sometimes) as fractional change of total momentum is therefore conserved in magnetic lattices, except in RF cavities. In electric lattices `p[5]` is similarly conserved, but only as long as its definition as fractional total energy $\Delta\mathcal{E}/(p_0c)$ is scrupulously adhered to. Hardly anything could be easier during particle tracking than refusing to change `p[5]` except in RF cavities.

Problems remain, however. One problem, easily handled, is that a particle's "stiffness" is proportional to its momentum rather than to its total energy. Knowing the radial position x, the potential energy $eV(x)$ is directly calculable. Then, with the total energy $\mathcal{E}$ known, the kinetic energy $K = \mathcal{E} - eV(x) - m_pc^2$ can be inferred by conservation of energy. The momentum p, and from it the stiffness, can then be obtained. These calculations have to be performed before the kick produced by a lattice quadrupole or other multipole element can be worked out and applied. This makes it necessary to account for the kinetic energy discontinuities suffered by every particle at every bend edge, in order to account for the dependence on external kinetic energy of the kicks applied by lattice elements other than bends. Curiously enough though, since all such external elements will be in regions of zero potential energy, the momentum magnitude for any one particle will be the same at all external elements (except, as usual, for the effect of RF cavities).

Within bends the off-energy effects are more complicated. As included in Eqs. (162) and (163), the transfer matrices through bends depend on the total energy $\mathcal{E}$ which is different for different particles and, with RF cavities present, different at different times for the same particle. Fortunately $\mathcal{E}$ is constant within bends. But the value of $\mathcal{E}$ can vary erratically, even for the same particle, as it depends on the value of x at the entrance point. So the κ parameter contained in the transfer matrices through bends has to be calculated on every turn for every particle at every bend.

Time of flight represents a more serious problem. By splitting bends into short enough intervals the time of flight can be calculated to arbitrary precision. This approach would not be essentially different from the Runge-Kutta, numerical differential equation solution approach. For some purposes this may be adequate but it contradicts the TEAPOT style, both because of excessive computational time and the hazard of numerical instability.

It is therefore necessary to obtain time of flight using Eq. (154), or rather the integrated version of that equation. Since this has not yet been done, it is not known whether this can be accomplished within the polymorphic operation constraint. If not some approximation to those integrals will have to be used.

6.7 Minimal, Geometricized Migration from TEAPOT to ETEAPOT

With the exception of ELSEPARATOR elements, lattice elements in TEAPOT are implicitly assumed to be magnetic. But, in linear lattice theory, element parameters are *geometric*—element lengths, bend angles, and (for quadrupoles) focal lengths. Electric elements can be similarly geometricized. For element lengths it is irrelevant whether the elements are magnetic or electric. Similarly, when quadrupole strengths are entered as (inverse) focal lengths, whether the quadrupole is magnetic or electric does not affect the lattice functions. Bend elements are not so simple, particularly for weak focusing rings, such as the proton EDM ring. (For strong focusing lattices the small geometric focusing is overwhelmed by the alternating gradient focusing, making electric and magnetic elements essentially equivalent.)

Even in a uniform magnetic field there is a small geometric focusing effect. (It is what provides the "1" in the $Q_x^2 + Q_y^2 = 1$ relation for the tunes in a weak focusing magnetic lattice.) This relation is not valid for electric lattice because there is a further "dynamic focusing" effect that accompanies the change of mechanical energy as a particle moves between regions of different electric potential. In TEAPOT the geometric focusing is introduced by inserting an artificial lens at the center of bend elements. This element focuses in the horizontal plane but not in the vertical plane. In the code the name for the inverse focal length of this artificial element is `btw01`.

To a first approximation, the dynamic focusing effect in an electric bend can be modeled by just changing the value of `btw01`. This is what is done in a preliminary (1 January, 2011) version of ETEAPOT. Rather than calculating the correct `btw01` analytically we have adjusted it empirically to match the horizontal tune calculated using formulas from Appendix 8.1.

In a decoupled lattice (which we assume, for now, to be the) case, changing `btw01` will not affect the vertical tune Q_y. This corresponds to the fact that there is vertical focusing in neither magnetic nor electric bend elements, as long as they are erect.

For more delicate quantities, orbit path lengths, dispersion and so on, more accurate formulas have to be used.

7 Multipole Expansion of Field Deviation

7.1 Impulsive Deflections Caused by Thin Electric Elements

With x horizontal, y vertical and s longitudinal, a transverse electric field takes the form $\mathbf{E} = (E_x, E_y, 0)$. The change $d\mathbf{p}$ in momentum, as charge e passes infinitesimal longitudinal distance ds in this field satisfies

$$d\mathbf{p} = \frac{ds}{v_s}\,(eE_x\hat{\mathbf{x}} + eE_y\hat{\mathbf{y}}). \tag{165}$$

As one consequence, $p_s = m\gamma v_s$ is conserved. Furthermore, in the limit of zero element thickness, with no potential drop across the thin element (at least in our idealized model) and no discontinuity in transverse particle position, the magnitude of momentum is conserved, just as in a magnetic multipole. The relativistic factor γ is therefore also conserved. Substitution into Eq. (165) produces

$$d\mathbf{v}_\perp = \frac{ds}{m_p\gamma v_s}\,e\mathbf{E} = \frac{ds}{p_s/e}\,\mathbf{E}. \tag{166}$$

Since $\mathbf{E}$ is, itself, transverse, this gives changes only in $\mathbf{v}_\perp$. But, corresponding to the constancy of γ, v_s will also change.

In spite of the uncertain self-consistency of these assumptions, and in the same spirit as the thin magnetic multipole model, as well as accepting Eq. (166), we require constancy of p, just as for magnetic lattices. This will assure conservation of both energy and symplecticity. With p_s being conserved, Eq. (166) can be extended to a finite interval Δs as a quite accurate approximation,

$$\frac{\Delta\mathbf{v}_\perp}{c} = \frac{\mathbf{E}}{p_s c/e}\,\Delta s. \tag{167}$$

The denominator factor p_s is approximately, but not exactly, equal to the total momentum. Using the actual value of p_s represents an improvement over the paraxial approximation. The modified longitudinal velocity can be obtained from the relation

$$\frac{v_s}{c} = \sqrt{1 - \frac{v_\perp^2}{c^2} - \frac{1}{\gamma^2}}. \tag{168}$$

In the thin element approach, Δs is to be replaced by an actual element length or, for improved accuracy, the length of one of the segments into which the element has been sliced. [4]

7.2 Multipole Expansion of Transverse Electric Field

The radial electric field component E_x for a power law field can be obtained (for $y = 0$) from Eq. (237);

$$\begin{aligned} E_x(y=0) &= -E_0\left(1 + \frac{x}{r_0}\right)^{-(1+m)} \\ &\approx -E_0\left(1 - (1+m)\,\frac{x}{r_0} + \frac{(1+m)(2+m)}{2!}\left(\frac{x}{r_0}\right)^2 + \cdots\right). \end{aligned} \tag{169}$$

By analogy with a standard treatment of magnetic multipoles, this formula can be correlated with a (complex) multipole expansion formula;

$$E_x + iE_y = -E_0\sum_{n=0}^{M}(b_n^E + ia_n^E)\big(x + iy\big)^n. \tag{170}$$

[4] It can be mentioned here, and repeated later, that slicing an electric element that causes finite bending into thin elements separated by drifts (as is valid in magnetic bending elements) would surely lead to incorrect focusing, because of incorrect thick element evolution in a changing electric potential.

The b_n^E are referred to as "erect" coefficients, the a_n^E as "skew". The (unconventional) overall negative sign is included so that, for the proton EDM lattice, both E_0 and (leading coefficient) b_0^E are positive.

For magnetic rings it is conventional to introduce a "$B\rho$" normalization factor, using the result that central momentum and central radius are related by $p_0/e = B_0\rho_0$. This has the effect of "geometricizing" the description so that the absolute momentum cancels out of the description. Then, for an element of length ℓ, coefficients $\tilde{b}_n = \ell b_n/(B_0\rho_0)$ are introduced. For $n = 0, 1, \ldots$, $\tilde{b}_0, \tilde{b}_1$ represent (at least approximately) bend angle, inverse focal length and so on.

For an electrostatic ring the analogous normalization factor is $p_0/e = v_0 E_0 \rho_0$ and, for an element of length ℓ, coefficients $\tilde{b}_n^E$ are defined by

$$\tilde{b}_n^E = \frac{b_n^E}{p_0/e}\,\ell. \tag{171}$$

Skew coefficients $\tilde{a}_n^E$ are defined analogously.

The factors ℓ included in the definitions of the $\tilde{b}_n^E$ are introduced to prepare for allowing the element length to become arbitrarily short while the fields increase to hold constant the deflections they cause. The quantities $\tilde{E}_x$, $\tilde{E}_y$, $\tilde{a}_n^E$ and $\tilde{b}_n^E$ will then be referred to as "field integrals".

Having previously blurred the distinction between cylindrical and spherical coordinates, we have now introduced the locally Cartesian (Frenet) coordinates customarily used for paraxial accelerator treatments. (Also recall the further complication that the coordinate $(1-\xi) = r_0/r$, represents yet another coordinate definition.)

Real and imaginary coefficients R_n and I_n of the final factor of Eq. (170) are defined by

$$(x+iy)^n = R_n + iI_n. \tag{172}$$

A few of their values are given in Table 2.

Table 2: Deflections caused by electrical elements and notations for their strengths. With v_0 being the central velocity, $x' = p_x/p_0$ and $y' = p_y/p_0$, for small deflections the $\tilde{b}_n^E$ and $\tilde{a}_n^E$ coefficients are related to conventional geometric parameters, such as bend angle and focal length, shown in columns 5 and 6. They cause the deflections shown in the last two columns.

	n	R_n	I_n	$\tilde{b}_n^E$	$\tilde{a}_n^E$	$\Delta x'$	$\Delta y'$
Horz. bend	0	1	0	$\Delta\theta^x$	0	$-\Delta\theta^x$	0
Vert. bend				0	$\Delta\theta^y$	0	$\Delta\theta^y$
Erect quad	1	x	y	$q = 1/f$	0	$-qx$	qy
Skew quad				0	$q^s = 1/f^s$	$q^s y$	$q^s x$
Erect sext	2	$x^2 - y^2$	$2xy$	$S/2$	0	$-S(x^2-y^2)/2$	$S2xy/2$
Skew sext				0	$S^s/2$	$S^s 2xy/2$	$S^s(x^2-y^2)/2$
Erect oct	3	$x^3 - 3xy^2$	$3x^2y - y^3$	$O/6$	0	$-O(x^3-3xy^2)/6$	$O(3x^2y-y^3)/6$
Skew oct				0	$O^s/6$	$O^s(3x^2y-y^3)/6$	$O^s(x^3-3xy^2)/6$

As defined, the multipole series has been normalized to the main centripetal electric field, $-E_0\hat{\mathbf{r}}$. However this leading term in the expansion will, in practice, invariably be treated separately by an exact, thick element method. This will assure that the focusing associated with changes in electric potential are treated adequately. Only *deviations* from the dominant bend field, and explicit electrostatic quadrupoles and sextupoles will be represented by multipole expansions.

In spite of the inappropriateness mentioned earlier, of retaining the leading term, as an example, let us consider the expansion for the $m = 1$, inverse square law, case. From Eq. (169), for an element of length ℓ, equating the first few terms of the two expansions yields

$$\begin{aligned}\frac{E_x(y=0)\ell}{-E_0} &= \ell\left(1 - 2\,\frac{x}{r_0} + 3\left(\frac{x}{r_0}\right)^2 + \cdots\right)\\ &= v_0 E_0 r_0\big(\tilde{b}_0^E + \tilde{b}_1^E x + \tilde{b}_2^E x^2\big).\end{aligned} \tag{173}$$

Equating coefficients we have (still for $m = 1$)

$$\tilde{b}_0^E = \frac{\ell}{v_0 E_0 r_0}, \quad \tilde{b}_1^E = \frac{-2\ell}{v_0 E_0 r_0^2}, \quad \tilde{b}_2^E = \frac{3\ell}{v_0 E_0 r_0^3}, \quad \cdots. \tag{174}$$

We can also promote this result to give the y dependence using expansion (170);

$$\begin{aligned} E_x + iE_y &= b_0^E + b_1^E\big(x+iy\big) + b_2^E\big(x+iy\big)^2 + \cdots \\ &= b_0^E + b_1^E x + b_2^E(x^2-y^2) + \cdots + i\Big(b_1^E y + b_2^E 2xy + \cdots\Big). \end{aligned} \tag{175}$$

What makes a procedure known to be valid for magnetic fields also valid for electric fields is that the electric and magnetic fields satisfy the same Maxwell equation. Separating into real and imaginary parts,

$$\begin{aligned} E_x(x,y) &= -E_0\bigg(1 - 2\,\frac{x}{r_0} + 3\,\frac{x^2-y^2}{r_0^2} + \cdots\bigg), \\ E_y(x,y) &= -E_0\bigg(-2\,\frac{y}{r_0} + 3\frac{2xy}{r_0^2} + \cdots\bigg). \end{aligned} \tag{176}$$

7.3 Integrable Thick Element Field With Lumped Deviations

7.3.1 Rationale

The only field shape for which the orbit equation can be solved in closed form is the inverse square law field. In our parameterization m is the index deviation from the logarithmic potential, $1/r$ field dependence. That is to say $1/r^2 = 1/r^{(1+m)}$, meaning that $m = 1$ for the inverse square law field. But (as will be established later) the inverse square law field variation is by no means optimal for the radial field of an accelerator. This means that the convenient field for orbit following is inconvenient for accelerator performance, and vice versa.

Actually the term "inconvenient" just used is too mild. For reliable orbit and spin tracking over storage times that may be measured in hours, it may be that analytically exact tracking *has to be* employed. One alternatives is to solve the evolution differential equations numerically using, for example, Runge-Kutta differential equation solvers. This suffers from one disadvantage and one fatal flaw. The disadvantage results from the computation time required for tracking through elements sliced thin enough to achieve the required Runge-Kutta accuracy. The fatal flaw is that, even with absurdly great computer power available, there is a mathematical theorem due to Zhong and Marsden[15], and described by Sanz-Serna and Calvo[16], stating that approximate numerical orbitry cannot simultaneously conserve energy and symplecticity. Another possible alternative is the use of high order nonlinear maps.

Yet our requirements are even more strigent in that we need to preserve energy and symplecticity for both orbits and spins. Rather than simply give up at this point, our approach is to design an accelerator lattice for which the motion *is* analytically solveable. As we have seen, this forces us to use the inverse square law field, which has been stated to be unacceptable (for reasons not yet explained.) (As mathematicians) the only escape from this dilemma is to allow ourselves to use infinitesimally thin elements. As physicists we know that it will be impossible to make such elements; but as physicists we can pretend we have such elements and design a lattice using them. After succeeding in this, using realizeable elements we actually build a lattice, which, to the best of our judgement, seems to be equivalent to the idealized model in all ways we consider important. For predicting the performance of our realizable ring we use the analytical description of our idealized ring. Instead of "approximate tracking in an exact lattice" we are then performing "exact tracking in an approximate lattice".

We cannot claim, as mathematicians, there there is anything guaranteed to be successful in this approach. But, as physicists, it seems like a sensible thing to try. Furthermore, once the actual ring is built, we can test empirically whether beam evolution is correctly described.

This "exact" tracking approach was first employed for long term tracking of the SSC (the never-constructed Superconducting SuperCollider) using the code TEAPOT (Thin Element Accelerator Program for Optics and Tracking) due to Schachinger and Talman[17]. Radical, at the time, was dispensing with transfer matrices. But the method was otherwise a fairly minor refinement of so-called "kick codes" that were beginning to be popular for symplecticity preservation. By now TEAPOT has evolved into UAL/TEAPOT, Here UAL stands for "Universal Accelerator Libraries" which is a C++ code based, object oriented environment of which TEAPOT is just one of numerous mutually consistent evolution

modules. The sorts of empirical tests mentioned in the previous paragraph have, at least so far, and for magnetic lattices, proved to describe realistic accelerator performance quite faithfully. A quite careful comparison of TEAPOT and high order, truncated power series evolution of orbits in the SSC is described by Yan et al.[18].

7.3.2 Implementation

To illustrate the implementation of this approach, let us suppose, based on practical accelerator considerations, that the ideal electric field profile is inverse power law, with field variation $1/r^{(1+m)}$ where delta has some value, such as $m = 0$, that is different from the $m = 1$, inverse square law choice.

The two electric field dependencies are

$$\mathbf{E_m} = -E_0 \, \frac{r_0^{1+m}}{r^{1+m}} \, \hat{\mathbf{r}}, \quad \text{and} \quad \mathbf{E_2} = -E_0 \, \frac{r_0^2}{r^2} \, \hat{\mathbf{r}}. \tag{177}$$

With $r = r_0 + x$, expanded in powers of x, the difference of these fields is given by

$$\frac{E_m - E_2}{-E_0} = (1-m) \, \frac{x}{r_0} + \Big(-2 + \frac{3}{2} \, m + \frac{1}{2} \, m^2 \Big) \, \frac{x^2}{r_0^2} + \cdots . \tag{178}$$

As in Eq. (176), this result can be promoted to include also the y dependence as well as giving the $E_y(x, y)$ field component;

$$\begin{aligned} \frac{E_{m,x} - E_{2,x}}{-E_0} \, (x, y) &= (1-m) \, \frac{x}{r_0} + \Big(-2 + \frac{3}{2} \, m + \frac{1}{2} \, m^2 \Big) \, \frac{x^2 - y^2}{r_0^2} + \cdots , \\ \frac{E_{m,y} - E_{2,y}}{-E_0} \, (x, y) &= (1-m) \, \frac{y}{r_0} + \Big(-2 + \frac{3}{2} \, m + \frac{1}{2} \, m^2 \Big) \, \frac{2xy}{r_0^2} + \cdots . \end{aligned} \tag{179}$$

Because this is a pure multipole field, which produces no net angular deflection, it can, with good accuracy be lumped, longitudinally, into one or more thin elements. Thick element tracking from thin element to thin element will be performed using analytic formulas and tracking through the thin elements will be performed as indicated in Table 2.

The lattice so defined is therefore subject to "exact" tracking. Again the term "exact" is being used with a sense that some may object to. The quadrupole focusing due to the change in potential corresponding to the r-independent electric field is being properly included, but the sextupole effect due to the r-variable electric field is not being properly included.

It might be thought that, with another iteration, the linear terms of Eq. (179) could be removed by another subtraction, to more correctly model nonlinear orbit evolution. But this will only work if sufficiently accurate, analytic evolution formulas through thick quadrupoles can be found.

8 Explicit Transfer Matrices

For describing electric lattices it is useful to introduce the concept of "implicit transfer matrices"; they might more properly be referred to as "transfer maps", because their components are functions of particle-specific kinematic quantities, such as kinetic energy and angular momentum. This discussion is especially useful in the inverse square law case; because the implicit transfer matrices are so simple it is computationally inexpensive to evaluate the implicit transfer matrix elements separately for each particle that is being tracked. As a result, for the inverse square law case, with only this added complication of needing to calculate the transfer matrix elements for each particle, the "linearized" treatment is, in fact, exact.

8.1 Wollnik Transfer Matrix Formalism

Transfer matrices for power law electric fields have been worked out in Section 3.0.5. Here, largely for checking purposes, transfer matrices are worked out using the Wollnik formalism[12]. His formalism is

general in the senses that lenses can be either focusing or defocusing and can describe combined function elements or pure quadrupoles, either electric or magnetic. For notational simplicity, we will specialize to electrostatic, horizontally focusing, combined function elements and vertically focusing pure quadrupoles. These choices correspond to the primary building blocks needed for the proton EDM experiment.

Early on (but no longer) it was assumed that all bending would occur in the regions between curved sections of coaxial vertical cylinders. These elements, which provide horizontal focusing but no vertical focusing, are described first. At both ends of these element are pure, vertically focusing (and therefore horizontally defocusing) quadrupoles. These are described in Section 8.1.8.

For calculating particle orbits and lattice functions it is convenient to exploit existing accelerator codes, such as MAD or UAL, that assume magnetic bending and focusing. To accomplish this one can introduce effective bend angle $\Delta\theta^{(E)}_{\text{eff.}}$, effective quadupole coefficient $K^{(E)}_{1,\text{eff.}}$ and so on. For a code such as MAD-8, treated as a "black box", this will not work, because, for that code, horizontal and vertical focusing is necessarily equal and opposite. We don't pursue remedying this by "hacking" into the code this, or by seeking other codes. We have, however, incorporated these features into an updated UAL/ETEAPOT.

The linearized equations of horizontal motion in a pure magnetic focusing element are

$$\frac{d^2x}{dz^2} = -K_1 x, \quad \text{and} \quad \frac{d^2y}{dz^2} = K_1 y. \tag{180}$$

Regrettably the notation here is not universal. The signs have been chosen to conform to the MAD lattice description conventions. Positive K_1 indicates that the bending field deflection increases with increasing x, which results in horizontal focusing. These same formulas will be applied to focusing in gently curving sector elements, but then extra "geometric" focusing terms have to be applied to account for the fact that x and y, rather than being purely Cartesian variables, are coordinates in a gradually rotating frame.

In an electrostatic field the horizontal and vertical focusing strengths are not, in general, equal and opposite. For example, with proton EDM cylindrical electrodes, there is horizontal focusing but no vertical focusing. Also the lack of constancy of particle speed in an electric field leads to "inertial" focusing effects.

8.1.1 Notation

To call attention to one complication accompanying the introduction of electric elements, we define here two fractional energy offset variables: "fractional rigidity offset" δ_R and "fractional total energy offset" δ. For magnetic lattices the latter quantity will also be referred to as $\delta_{MAD/UAL}$ as it is the longitudinal phase space coordinate definition used by MAD and UAL (and now also by ETEAPOT). Its definition is

$$\delta = \frac{\mathcal{E} - \mathcal{E}_0}{p_0 c}, \tag{181}$$

where p_0 is the design momentum, $\mathcal{E} = \gamma m_p c^2 + eV(\mathbf{x})$ is the total energy and γ is the conventional relativistic parameter. The "mechanical energy" is defined to be $\gamma m_p c^2$. For magnetic elements, because γ is conserved, this definition is applicable either inside or outside bend elements. For electric elements (for which it is $\mathcal{E}$ that is conserved) γ varies discontinuously as a particle moves between regions of different electric potential.

It has been agreed that, for comparing differently derived results, it is parameter values *outside* electric elements that should be compared (even if the ring is a single annular ring for which particles are *never* outside. To avoid confusion, quantities will frequently be specified with superscript "O" for "outside" or "I" for "inside".

The defining equation for fractional rigidity offset is

$$R = R_0(1 + \delta_R), \tag{182}$$

where R_0 is the radius of the design circular orbit (in a particular element) and R is the radius of the orbit (locally circular) of the offset particle in the same local field. By this definition δ_R is identical to

(or at least very close to) Wollnik's[12] Δ, which he defines in his Section 4.1.1.2. (For a uniform electric or any magnetic field the "at least very close to" qualification is unnecessary. For a non-uniform electric field one has to follow Wollnik's definitions more carefully than we have done, to declare that Eq. (182) is equivalent to Wollnik's first formula in Section 4.1.1.2.)

ETEAPOT uses δ defined above as the sixth phase space component of a particle being tracked through a lattice. However, as mentioned above, and can be seen in Section 3.0.6, δ cannot be used to differentiate between orbits of different radii inside a bend element having electric field proportional to $1/r$; this is because the dependence of radius on mechanical energy is singular. Regrettably the original pEDM bend field varied as $1/r$. This is no longer true, but it remains necessary to keep track of γ^O (or the parameters from which it can be calculated) in order to specify its value once the particle is outside in a drift region. Outside electrical field regions,

$$\delta = \frac{(\gamma^O - \gamma_0) m_p c^2}{p_0 c}. \tag{183}$$

In drifts (or magnets) this is identical to Eq. (181).

By design the electric potential is *everywhere* zero on the design orbit. Element errors will cause the central closed orbit to deviate somewhat from the design orbit. Except for this $\gamma^O = \gamma^I$ on the central closed orbit.

8.1.2 Horizontal Focusing, Separated Function Quadrupoles

The formalism will be established first for horizontally focusing, separated function, quadrupoles, (to be indicated by superscript "hfsf"). Following Wollnik[12], (though not in detail) it is convenient to introduce positive real quantities $k_x^{\rm hfsf}$ and $k_y^{\rm hfsf}$ in terms of which the equations of motion are

$$x'' + {k_x^{\rm hfsf}}^2\, x = 0, \quad y'' + (ik_y^{\rm hfsf})^2\, y = 0, \tag{184}$$

Even for an electrostatic quadrupole, because the electric field vanishes exactly on the design orbit. Other than accounting for the particle rigidity, it is not necessary to account for inertial focusing effects because, to lowest order, the particle rigidity is independent of transverse deviations.

For a pure quadrupole $k_x^{\rm hfsf} = k_y^{\rm hfsf} = k^{\rm hfsf} \geq 0$. In the thin lens limit, for a lens of length L,

$$q_x^{\rm hfsf} = \frac{1}{f_x^{\rm hfsf}} = k^{\rm hfsf} \sin k^{\rm hfsf} L, \quad q_y^{\rm hfsf} = \frac{1}{f_y^{\rm hfsf}} = -k^{\rm hfsf} \sin k^{\rm hfsf} L. \tag{185}$$

The general solutions of Eqs. (184) are

$$\begin{aligned} x(z) &= c_1\, \cos k^{\rm hfsf} z + d_1\, \sin k^{\rm hfsf} z \\ y(z) &= c_2\, \cos ik^{\rm hfsf} z - id_2\, \sin ik^{\rm hfsf} z = c_2\, \cosh k^{\rm hfsf} z + d_2\, \sinh k^{\rm hfsf} z. \end{aligned} \tag{186}$$

Expressed in terms of transfer matrices

$$\begin{pmatrix} x \\ x' \\ \Delta \end{pmatrix} = \begin{pmatrix} c_x & s_x & \cdot \\ -s_x {k^{\rm hfsf}}^2 & c_x & \cdot \\ \cdot & \cdot & 1 \end{pmatrix} \begin{pmatrix} x_0 \\ x'_0 \\ \Delta_0 \end{pmatrix}, \tag{187}$$

$$\begin{pmatrix} y \\ y' \end{pmatrix} = \begin{pmatrix} c_y & s_y \\ s_y {k^{\rm hfsf}}^2 & c_y \end{pmatrix} \begin{pmatrix} y_0 \\ y'_0 \end{pmatrix}, \tag{188}$$

where

$$c_x = \cos k^{\rm hfsf} z, \quad s_x = \frac{\sin k^{\rm hfsf} z}{k^{\rm hfsf}}, \quad c_y = \cosh k^{\rm hfsf} z, \quad s_y = \frac{\sinh k^{\rm hfsf} z}{k^{\rm hfsf}}. \tag{189}$$

The third rows and columns of the horizontal matrix, and the longitudinal offset coordinate Δ will be derived later.

For small z the 1,2 elements reduce to the immediate drift length z and the $2,1$ components reduce to the inverse focal length ascribable to length z. For a vertically focusing quad the sines and cosines are replaced by sinh and cosh functions, and the sign of the 2,1 element is reversed.

8.1.3 Chromatic Deflection

The (assumed to be positive) curvature of a proton with momentum p_0 in a radial electric field E_0 is given by

$$\frac{1}{r_0} = \frac{eE_0}{\beta_0 p_0 c} \overset{\text{also}}{=} \frac{eE_0}{\beta_0^2 \gamma_0 m_p c^2}. \tag{190}$$

For inward (in the $-x$ direction) acceleration, the radial electric field component E_r will be negative. Expanding as a function of horizontal displacement x,

$$E_r(x, y = 0) = -E_0 \left(1 + \frac{K_{x,1} r_0}{1!}\, x + \frac{K_{x,2} r_0}{2!}\, x^2 + \frac{K_{x,3} r_0}{3!}\, x^3 + \dots \right). \tag{191}$$

In a particle tracking program a general particle has momentum $p_0 + \Delta p$. The horizontal orbit equation of Eq. (184) can be augmented to account for this deviation. Assuming, for now, that $x = 0$;

$$\left.\frac{d^2x}{dz^2}\right|_{x=0} = \frac{d}{dz}\,\frac{dx}{dz} = \frac{d}{dz}\,\frac{p_x}{p_z} = \frac{1}{p_z}\,\frac{dp_x}{dz} \approx -\frac{eE_0}{pv}. \tag{192}$$

where the constancy, in a radial electric field, of the longitudinal momentum component p_z has been assumed. The longitudinal deviation variable δ used in MAD and UAL is defined by

$$\delta = \frac{\Delta \mathcal{E}_{\text{mech.}}}{p_0 c} = \frac{m_p c^2 \Delta\gamma}{p_0 c}. \tag{193}$$

Here $\mathcal{E}_{\text{mech.}} = \gamma m_p c^2$ stands for the "mechanical energy", which is the total energy minus the potential energy. One then finds

$$\Delta(pv) = m_p \Delta(\gamma v^2) = m_p c^2 \Delta\left(\gamma - \frac{1}{\gamma}\right) = \left(1 + \frac{1}{\gamma_0^2}\right) \frac{p_0 v_0}{\beta_0}\, \delta, \tag{194}$$

and

$$pv \approx p_0 v_0 \left(1 + \left(1 + \frac{1}{\gamma_0^2}\right) \frac{1}{\beta_0}\, \delta. \right) \tag{195}$$

Substitution into Eq. (192) yields

$$\left.\frac{d^2x}{dz^2}\right|_{x=0} = -\frac{1}{r_0} + \frac{1}{r_0} \left(1 + \frac{1}{\gamma_0^2}\right) \frac{1}{\beta_0}\, \delta. \tag{196}$$

This is the equation of motion for x treated as a Cartesian coordinate. It includes the design bending force. But we are only looking for the radial acceleration ascribable to the offset δ. We therefore suppress the first term to obtain the "dispersive" contribution

$$\left.\frac{d^2x}{dz^2}\right|_{\text{disp.}} = \frac{1}{r_0} \left(1 + \frac{1}{\gamma_0^2}\right) \frac{1}{\beta_0}\, \delta \equiv \frac{\Delta}{r_0}. \tag{197}$$

As defined here, the fractional rigidity deviation Δ relates the radius of curvature r of a deviant particle to the radius of curvature r_0 of an on-momentum particle, both in the same uniform field;

$$r = r_0\,(1 + \Delta). \tag{198}$$

Δ is therefore related to the MAD/UAL momentum deviation factor δ by[5]

$$\Delta = \left(1 + \frac{1}{\gamma_0^2}\right) \frac{1}{\beta_0}\, \delta \quad \left(= 2.744\, \delta \quad \text{for the proton EDM experiment.} \right) \tag{199}$$

[5]For comparison with Wollnik's Eq. (4.58c) one should note that Wollnik's $\delta_K = (K - K_0)/K_0$ is a fractional kinetic energy, while our MAD/UAL $\delta = (E - E_0)/p_0 c$. The numerators are the same but our denominator is bigger by $p_0 c/K_0 = 3.01$.

8.1.4 Thin Element Representation of Electrostatic Bend/Lens

Unlike in a magnetic field, the speed of a particle is *not* preserved in an electrostatic element. Depending on transverse displacement, a proton slows down or speeds up as it enters the element. We wish, nevertheless, to treat the electrostatic bend/lens element as a thin element (even if the element is "thin" only by virtue of being one of the many slices of an element that is actually "thick".) In this approximation the input, output, and central values of x are all the same for any single slice. (Of course x can change in the drift section between slices and even change gradually over many slices of a thick element.)

In the "hard edge" approximation" it has to be assumed that acceleration changes the speed discontinuously at the input face and, in the thin element limit, restores the speed discontinuously at the output. While the particle is between the plates of a thick element the magnitude of the particle's momentum depends on its transverse displacement (x, y), (or, to good approximation for weak vertical focusing, just x.) The particle's deflection angle needs to be compensated accordingly for this "inertial" effect.

In the interior of a thick element, as the particle passes from one slice to the next, the particle has no possibility of returning to its external speed. But this does not matter, as its speed stays close to its current internal value on entering the next slice. (In the limit of infinitesimal slice thickness the speed changes continuously.) When entering the first slice of an actually thick element, or when exiting the last slice, the effect of the actual fringe field has to be taken into account. As with magnetic pole-face rotation focusing, there is a focusing effect of non-normal entry. For now we assume normal entry. Adapting standard terminology, we refer to the electrostatic device as a "sector bend".

In a magnetic field the particle "rigidity" can be taken to be its momentum p. In an electric field, a consistent definition of rigidity is pv/c or, equivalently, $p^2c/(\gamma m_c^2)$. The magnetic and electric rigidities become equal in the ultrarelativistic limit. In passing from outside to inside, both numerator and denominator change values, which is something of a nuisance.

For a particle with charge e,

$$m_p c^2 \gamma_{\rm inside} \approx m_p c^2 \gamma_{\rm outside} + eE_{\rm nom.}\, x. \tag{200}$$

(A proton with x positive will have less kinetic energy than with x negative; because the electric field has to be centripetal, so $E_{\rm nom.}$ is negative.)

We are assuming balanced electrode voltages, so the energy of a proton on the design orbit is unchanged upon entry. This simplifies the description of the design orbit. (If balanced voltages are experimentally inconvenient, small changes in the formulas will be required.) By incorporating the inertial effect into the focusing strength coefficients, the kinetic energy of each proton can ultimately be treated as a constant of motion everywhere. But, for now, the equations will have the proton kinetic energy correctly tracking the electric potential. For convenience we rearrange Eq. (200) to

$$\frac{\gamma_{\rm inside}}{\gamma m_p c^2} \approx 1 + \frac{eE_{\rm nom.}\, x}{\gamma m_p c^2} \tag{201}$$

where here, and from now on, we suppress the "outside" subscript, and use $\gamma m_p c^2$. The total momentum inside satisfies

$$\begin{aligned} p_{\rm inside}^2 c^2 &= ((\gamma m_p c^2) + eE_{\rm nom.} x)^2 - m_p^2 c^4 \\ &\approx p^2 c^2 + 2eE_{\rm nom.}(\gamma m_p c^2)\, x. \end{aligned} \tag{202}$$

To this approximation

$$\frac{p_{\rm inside}^2}{p^2} = 1 + \frac{2eE_{\rm nom.}(\gamma m_p c^2)\, x}{p^2 c^2} \tag{203}$$

Combining equations, evaluating the ratio on-momentum, and remembering that $E_{\rm nom.}$ is negative, we obtain

$$\begin{aligned} \frac{(p^2/\gamma m_c^2)_{\rm inside}}{p^2/(\gamma m_p c^2)} &\approx \frac{1 + \frac{2eE_{\rm nom.}(\gamma m_p c^2)}{p^2 c^2}\, x}{1 + \frac{eE_{\rm nom.}}{(\gamma m_p c^2)}\, x} \\ &\approx 1 + \frac{eE_{\rm nom.}}{\beta^2 \gamma m_p c^2}\,(2 - \beta^2)\, x \approx 1 - \left(\frac{1}{r_0} + \frac{1}{\gamma_0^2 r_0}\right) x \end{aligned} \tag{204}$$

Positive x implies reduced rigidity, which is correct for electrodes providing centripetal force. The presence of the final term shows that the particle deflection depends on x even if the radial electric field is independent of x. This formula provides the fractional change in rigidity ascribable to the displacement x.

Letting $X = x_0 + x$ (with x_0 representing the design orbit and x the betatron offset from the design orbit) for on-momentum motion close to the design orbit

$$\frac{d^2x_0}{dz^2} = -\frac{1}{r_0}, \quad \text{and} \quad \frac{d^2(x_0+x)}{dz^2} = -\frac{1+x/r_0}{r_0}. \tag{205}$$

This is Newton's equation with "acceleration" on the left hand side and "force" on the right hand side and with "mass" effectively set equal to 1. If the "mass" actually depends on x the right hand side of the equation has to be modified proportionally;

$$\frac{d^2(x_0+x)}{dz^2} = -\frac{1+x/r_0}{r_0}\,\frac{1}{1-(\frac{1}{r_0}+\frac{1}{\gamma_0^2 r_0})\,x} \approx -\frac{1}{r_0} - \frac{x}{r_0^2} - \Big(\frac{1}{r_0^2}+\frac{1}{\gamma_0^2 r_0^2}\Big)\,x. \tag{206}$$

A betatron restoring force ascribable to inertia can therefore be defined by

$$\frac{d^2x}{dz^2}\Big|_{\text{inertial}} = -\left(\frac{1}{r_0^2}+\frac{1}{\gamma_0^2 r_0^2}\right)x = -K_x^{\text{inertial}}x. \tag{207}$$

In practice, the radial electic field may intentionally be designed to have a component varying proportional to x. This will cause what will be referred to as a "multipole effect", with the field being predominanly "quadrupole". In what follows the formalism will be rearranged to subsume the inertial effect into the quadrupole strength parameter. Summing the inertial effect and the field effect, the focusing effect of an element can be represented by an (effective) quadrupole coefficient $K_{1,\text{eff.}}^{(E)}$. If needed, calculation of an effective sextupole coefficient $K_{2,\text{eff.}}^{(E)}$ will have to be worked out as well.

8.1.5 Matching to Conventional Magnetic Formalism

In TRANSPORT notation, the magnetic field in the horizontal plane containing the design orbit is expressed as a series

$$B_y(x, y=0) = B_{y0}\left(1 - n\,\frac{x}{r_0} + \beta\frac{x^2}{r_0^2} + \gamma\frac{x^3}{r_0^3} + \ldots,\right) \tag{208}$$

where the "field index" n is (therefore) defined by

$$n = -\frac{r_0}{B_{y0}}\,\frac{\partial B_y}{\partial x}\bigg|_{x=0}, \tag{209}$$

where r_0 is the design orbit radius. Consider a sector bend magnet of (arc) length L. The curvature $1/r_0$ and the bend angle $\Delta\theta^{(M)}$ of a proton of momentum p_0 are given by

$$\frac{1}{r_0} = \frac{cB_{y0}}{p_0 c/e}, \quad \text{and} \quad \Delta\theta^{(M)} = -\frac{L}{r_0} = -\frac{cB_{y0}L}{p_0 c/e}. \tag{210}$$

In MAD notation the same x-dependence is parameterized as

$$B_y(x, y=0) = B_{y0}\left(1 + \frac{K_1 r_0}{1!}\,x + \frac{K_2 r_0}{2!}\,x^2 + \frac{K_3 r_0}{3!}\,x^3 + \ldots\right). \tag{211}$$

Matching formulas we have, for example,

$$K_1 = -\frac{n}{r_0^2}, \quad K_2 = \frac{2\beta}{r_0^3}. \tag{212}$$

In thin element approximation the bend angle is

$$\Delta\theta^{(M)}(x, y=0) = \frac{cB_{y0}L}{pc/e}\left(1 + \frac{K_1 r_0}{1!}\,x + \frac{K_2 r_0}{2!}\,x^2 + \frac{K_3 r_0}{3!}\,x^3 + \dots\right). \tag{213}$$

For counter-clockwise (from above) orbit rotation, to make $\Delta\theta^{(M)}$ be negative requires $B_y < 0$.

Repeating Eq. (191), and specializing to the *logarithmic potential* electric field, the corresponding expansion for electric field in the horizontal plane is

$$\begin{aligned} E_r(x, y=0) &= -E_0\left(1 + \frac{K_{x,1} r_0}{1!}\,x + \frac{K_{x,2} r_0}{2!}\,x^2 + \frac{K_{x,3} r_0}{3!}\,x^3 + \dots\right) \\ &= -E_0\left(1 - \frac{x}{r_0} + \frac{K_{x,2} r_0}{2!}\,x^2 + \frac{K_{x,3} r_0}{3!}\,x^3 + \dots\right). \end{aligned} \tag{214}$$

We could define effective parameters by matching electric and magnetic coefficients. For example $K_{x,1} = K_1^{\text{multipole}} = -1/r_0^2$. However, this would be incorrect, or at least misleading, in three different ways: for elements with non-zero bending it would fail to include a geometric focusing effect; it would not yet include the inertial effect discussed in Section 8.1.4, and it suggests that vertical and horizontal focal lengths are exactly equal but opposite, which is not true in general.

The geometric effect comes from our careless treatment of x both as a Cartesian coordinate and as a radial deviation $x = r - r_0$. In a uniform fiels (e.g. a cyclotron) a radially deflected particle returns to its starting point after one revolution, in spite of there being neither multipole nor inertial focusing. We ascribe this restoring action to a geometric restoring coefficient given by $K_{x,1}^{\text{geometric}} = 1/r_0^2$. (That this is the appropriate coefficient will be confirmed shortly, when the horizontal tune is determined.) To incorporate the inertial and geometric effects, as well as distinguishing horizontal and vertical, using Eq. (207), one can define effective on-momentum focusing coefficients,

$$\begin{aligned} K_{x,1}^{(E,\text{eff.})} &= K_{x,1}^{\text{multipole}} + K_{x,1}^{\text{inertial}} + K_{x,1}^{\text{geometric}} \\ &= -\frac{1}{r_0^2} + \left(\frac{1}{r_0^2} + \frac{1}{\gamma_0^2 r_0^2}\right) + \frac{1}{r_0^2} \\ &= \frac{1}{r_0^2} + \frac{1}{\gamma_0^2 r_0^2}, \end{aligned} \tag{215}$$

$$K_{y,1}^{(E,\text{eff.})} = 0. \tag{216}$$

These equations agree with Wollnik's equations in his section 4.3.2, with his $n_1 = 0$.

Using the coefficients $K_{x,1}^{(E,\text{eff.})}$ and $K_{y,1}^{(E,\text{eff.})}$ in a formula or program intended for magnetic elements will include (in first approximation) the optical effects caused by the electric field. In the original TEAPOT code, and in the current UAL/TEAPOT code, the $K_1^{\text{geometric}}$ focusing term is already included in the treatment of bend magnets. So, for that code, it is only the K_1^{inertia} term that needs to be added. Similar alterations need to be made in sextupole and higher orders.

Even with $K_1 = 0$ there is a focusing effect. There is a similar horizontal focusing effect in a uniform magnetic field. A particle launched at a small angle returns to the starting point after one turn. This implies a horizontal tune equal to 1. This is said to represent "geometric" focusing, which accounts for the "geom." superscript in Eq. (215). From lattice theory, in a magnet with no vertical focusing (i.e. a cyclotron) the horizontal tune is $Q_x = \sqrt{1-n} = 1$, where n is the coefficient in Eq. (208). One infers that the second term in the last of Eqs. (215) is the geometric effect of the electric field bending the design orbit in a circle. The third term $1/(r_0^2\gamma_0^2)$ is due to the variation of particle rigidity with radial position in the electric field case.

8.1.6 Lattice Properties of a Uniform Ring

The simplest possible electrostatic ring would consist of coaxial cylindrical electrodes. Using Eqs. (215), with z now replaced by (arc length) s the betatron equations in such a ring are

$$\begin{aligned} \frac{d^2x}{ds^2} &= -\frac{1}{r_0^2} - \frac{1}{\gamma_0^2 r_0^2}, \\ \frac{d^2y}{ds^2} &= 0. \end{aligned} \tag{217}$$

Expressed in pseudo-harmonic form, the cosine-like x motion for a particle with betatron amplitude a_x is

$$x(s) = a_x\sqrt{\beta_x}\cos\big(\psi_x(s)\big) = a_x\sqrt{\beta_x}\cos\frac{s}{\beta_x}, \tag{218}$$

where

$$\psi_x(s) = \int_0^s \frac{ds'}{\beta_x(s')} = \frac{s}{\beta_x}, \tag{219}$$

where, obviously, $\beta_x(s)$ is independent of s, which makes the integral trivial. Similarly for y. Eqs. (217) could just as well have been solved directly to give

$$\begin{aligned} x(s) &= A_x\cos\left(\sqrt{\frac{\gamma_0^2+1}{\gamma_0^2 r_0^2}}\,s\right), \\ y(s) &= A_y. \end{aligned} \tag{220}$$

Matching x arguments gives

$$\beta_x = \frac{1}{\sqrt{1+1/\gamma_0^2}}\,r_0, \quad \Big(\overset{\text{e.g.}}{=} 0.78\times 30 = 23\,\text{m}\Big). \tag{221}$$

The phase advance per turn μ_x and the tune $Q_x = \mu_x/(2\pi)$ are obtained by matching x arguments to give

$$Q_x = \frac{\mu_x}{2\pi} = \frac{r_0}{\beta_x} = \sqrt{1+\frac{1}{\gamma_0^2}} \quad \Big(\overset{\text{pEDM}}{=} 1.281\Big), \tag{222}$$

and $Q_y = 0$.

8.1.7 Explicit Transfer Matrix With Geometric and Inertial Effects and Dispersion

We now adapt the formalism to include combined function and dispersion effects in a horizontally focusing, combined function electrostatic element. We generalize Eqs. (180) to incorporate Eqs. (197) and (215), even allowing a (presumably small, or preferably zero) multipole focusing coefficient K_1,

$$x'' + {k_x^{\text{hfcf}}}^2\,x - \frac{\Delta}{r_0} = 0, \quad \text{where} \quad {k_x^{\text{hfcf}}}^2 = K_1 + \frac{1}{r_0^2}\Big(1+\frac{1}{\gamma_0^2}\Big), \tag{223}$$

$$y'' + {k_y^{\text{hfcf}}}^2\,y = 0, \quad \text{where} \quad {k_y^{\text{hfcf}}}^2 = -K_1. \tag{224}$$

For the vertical focusing we will be assuming, K_1 will be negative, but certainly with magnitude small enough for ${k_x^{\text{hfcf}}}^2$ to be positive. In other words, there will be net focusing in both planes.

The longitudinal rigidity offset parameter Δ was defined in Eq. (198). Equations that are very nearly equivalent to these are derived in the Wollnik book[12]. The very different notation, especially concerning the definition of Δ, plus several minor misprints, makes it quite difficult to compare the formulas in detail however. Here we are following Wollnik's section 4.3.2[12], though varying his notation somewhat.

The general solutions of Eqs. (223) and (224) are

$$x(z) = c_1\ \cos k_x^{\rm hfcf} z + d_1\ \sin k_x^{\rm hfcf} z - \frac{\Delta}{{k_x^{\rm hfcf}}^2 r_0}, \tag{225}$$

$$y(z) = c_2\ \cos k_y^{\rm hfcf} z + d_2\ \sin k_y^{\rm hfcf} z. \tag{226}$$

Eliminating c_1, d_1, c_2, d_2, in favor of initial conditions $x_0, x_0', \Delta_0, y_0, y_0'$, at $z = 0$, one obtains

$$\begin{pmatrix} x \\ x' \\ \Delta \end{pmatrix} = \begin{pmatrix} c_x & s_x & d_x \\ -s_x {k_x^{\rm hfcf}}^2 & c_x & s_x/r_0 \\ 0 & 0 & 1 \end{pmatrix} \begin{pmatrix} x_0 \\ x_0' \\ \Delta_0 \end{pmatrix}, \tag{227}$$

$$\begin{pmatrix} y \\ y' \end{pmatrix} = \begin{pmatrix} c_y & s_y \\ -s_y {k_y^{\rm hfcf}}^2 & c_y \end{pmatrix} \begin{pmatrix} y_0 \\ y_0' \end{pmatrix}, \tag{228}$$

where

$$c_x = \cos k_x^{\rm hfcf} z, \quad s_x = \frac{\sin k_x^{\rm hfcf} z}{k_x^{\rm hfcf}}, \quad d_x = \frac{\cos k_x^{\rm hfcf} z - 1}{r_0 {k_x^{\rm hfcf}}^2},$$
$$c_y = \cos k_y^{\rm hfcf} z, \quad s_y = \frac{\sin k_y^{\rm hfcf} z}{k_y^{\rm hfcf}}. \tag{229}$$

For small z the 1,2 elements reduce to the immediate drift length z and the $2,1$ components reduce to the inverse focal length ascribable to length z.

8.1.8 Vertical Focusing Quadrupoles

It is assumed vertical focusing will occur primarily in electrostatic, separated function quadrupoles, (indicated by superscript "vfsf"). Following Wollnik[12], (though not in detail) it is convenient to introduce positive real quantities $k_x^{\rm vfsf}$ and $k_y^{\rm vfsf}$ in terms of which the equations of motion are

$$x'' + (ik_x^{\rm vfsf})^2\, x = 0, \quad y'' + {k_y^{\rm vfsf}}^2\, y = 0, \tag{230}$$

For a pure quadrupole $k_x^{\rm vfsf} = k_y^{\rm vfsf} = k^{\rm vfsf} \geq 0$. In the thin lens limit, for a lens of length L,

$$q_x^{\rm vfsf} = \frac{1}{f_x^{\rm vfsf}} = -k^{\rm vfsf} \sin(k^{\rm vfsf} L), \quad q_y^{\rm vfsf} = \frac{1}{f_y^{\rm vfsf}} = k^{\rm vfsf} \sin(k^{\rm vfsf} L). \tag{231}$$

The general solutions of Eqs. (230) are

$$x(z) = c_1\ \cos ik^{\rm vfsf} z - id_1\ \sin ik^{\rm vfsf} z = c_1\ \cosh k^{\rm vfsf} z + d_1\ \sinh k^{\rm vfsf} z,$$
$$y(z) = c_2\ \cos k^{\rm vfsf} z + d_2\ \sin k^{\rm vfsf} z. \tag{232}$$

Expressed in terms of transfer matrices

$$\begin{pmatrix} x \\ x' \\ \Delta \end{pmatrix} = \begin{pmatrix} c_x & s_x & 0 \\ s_x {k^{\rm vfsf}}^2 & c_x & 0 \\ 0 & 0 & 1 \end{pmatrix} \begin{pmatrix} x_0 \\ x_0' \\ \Delta_0 \end{pmatrix}, \tag{233}$$

$$\begin{pmatrix} y \\ y' \end{pmatrix} = \begin{pmatrix} c_y & s_y \\ -s_y {k^{\rm vfsf}}^2 & c_y \end{pmatrix} \begin{pmatrix} y_0 \\ y_0' \end{pmatrix}, \tag{234}$$

where

$$c_x = \cosh k^{\rm vfsf} z, \quad s_x = \frac{\sinh k^{\rm vfsf} z}{k^{\rm vfsf}}, \quad c_y = \cos k^{\rm vfsf} z, \quad s_y = \frac{\sin k^{\rm vfsf} z}{k^{\rm vfsf}}. \tag{235}$$

For small z the 1,2 elements reduce to the immediate drift length z and the $2,1$ components reduce to the inverse focal length ascribable to length z. For a vertically focusing quad the sines and cosines are replaced by sinh and cosh functions, and the sign of the 2,1 element is reversed.

9 Particle-by-Particle Evolution by Implicit Transfer Matrices

9.1 Variable Index Electric Sector Bends

The Muñoz and Pavic, Hamilaton vector approach described in Section 4, though valuable for exact particle tracking through an inverse square law electric field, is less naturally matched to developing the Courant-Snyder, Twiss function description conventional in accelerator theory. A more conventional approach is developed in this section.

To produce weak vertical focusing the radial electric field has to fall off as $1/r^{1+m}$, where $0 < m$. The $m = 0$ case is singular, and leads to a logarithmic potential.[6] Introducing design radius r_0 and central field $-E_0$ the electric field for y=0 is

$$\mathbf{E}(r,0) = -E_0 \frac{r_0^{1+m}}{r^{1+m}} \hat{\mathbf{r}}, \tag{237}$$

and the electric potential $V(r)$, adjusted to vanish at $r = r_0$, is

$$V(r) = -\frac{E_0 r_0}{m}\left(\frac{r_0^m}{r^m} - 1\right). \tag{238}$$

The independent (longitudinal) coordinate s is to be replaced by the angular coordinate θ

$$\theta = \frac{s}{r_0}. \tag{239}$$

Following treatments of relativistic Kepler orbits such as [1], we change dependent variable from $x(s) = r - r_0$ (with independendent variable s) to a (dimensionless) dependent variable $\xi(\theta)$ (with independent variable θ);

$$\xi = \frac{x}{r} = \frac{x}{r_0 + x} = 1 - \frac{r_0}{r}, \quad \text{and} \quad \frac{d\xi}{d\theta} = \frac{r_0}{r^2}\frac{dr}{d\theta}, \quad \text{or} \quad \xi' = \frac{r_0^2}{r^2}\, x'. \tag{240}$$

Note that ξ is proportional to x for small x and that, notationally, $x' \equiv dx/ds$ and $\xi' = d\xi/d\theta$. The present discussion is limited to planar orbits, in which case the definition of x by $r = r_0 + x$ is the usual Frenet-Serret definition. For 3D motion this definition is not quite exact but realistic vertical amplitudes will always be small enough that the effect on x of projection onto the horizontal plane will be neglected. The identity

$$\frac{r_0}{r} = 1 - \xi \tag{241}$$

will be prominent in subsequent formulas. Inverse relations are

$$x = \frac{r_0 \xi}{1 - \xi}, \quad \text{and} \quad x' = \frac{r_0 d\xi/ds}{(1-\xi)^2} = \frac{\xi'}{(1-\xi)^2}. \tag{242}$$

With ξ regarded as a function of θ and x as a function of s, the abbreviations $\xi' = d\xi/d\theta$ and $x' = dx/ds$ have been used, leading to $x' = \xi'/(1-\xi)^2$. Adapting Eq. (17) for non-integer field index

$$\left(\mathcal{E} - \frac{eE_0 r_0}{m} + \frac{eE_0 r_0}{m}(1-\xi)^m\right)^2 = \frac{L_y^2 c^2}{r_0^2}\left(\frac{d\xi}{d\theta}\right)^2 + \frac{L_y^2 c^2}{r_0^2}(1-\xi)^2 + p_y^2 c^2 + m_p^2 c^4. \tag{243}$$

[6] Integrating this field from $r = 1$ to $r = 1 + \Delta$ one reconstructs the potential from the electric field—call it $\tilde{V}$. Its value at $r = 1 + \Delta$ is

$$\tilde{V}(1+\Delta) = \frac{(1+\Delta)^{-m} - 1}{m} = \ln(1-\Delta) + O(m). \tag{236}$$

The logarithmic potential can be seen to be a degenerate form required for $m = 0$, where $E \propto 1/r$. The electric field corresponding to this potential is $E \propto 1/r^{1+m}$. This shows how $\tilde{V}$ approaches the logarithmic potential in the limit of small m.

Differentiating this equation with respect to θ, and simplifying,

$$\begin{aligned}\frac{d^2\xi}{d\theta^2} &= 1-\xi-\left(\mathcal{E}\,\frac{eE_0r_0^3}{L_y^2c^2}-\frac{e^2E_0^2r_0^4}{L_y^2c^2}\,\frac{1}{m}\right)\frac{1}{(1-\xi)^{1-m}}-\frac{e^2E_0^2r_0^4}{L_y^2c^2}\,\frac{1/m}{(1-\xi)^{1-2m}}\\ &= 1-\xi-\left(\frac{\mathcal{E}/e}{L_yc/(er_0)}\frac{E_0r_0}{L_yc/(er_0)}-\Big(\frac{E_0r_0}{L_yc/(er_0)}\Big)^2\,\frac{1}{m}\right)\frac{1}{(1-\xi)^{1-m}}-\Big(\frac{E_0r_0}{L_yc/(er_0)}\Big)^2\,\frac{1/m}{(1-\xi)^{1-2m}}\\ &= 1-\xi-\left(\frac{\mathcal{E}}{\mathcal{E}_0}\,\frac{L_0^2}{L_y^2}-\frac{L_0^2}{L_y^2}\,\frac{\beta_0^2}{m}\right)\frac{1}{(1-\xi)^{1-m}}-\frac{L_0^2}{L_y^2}\,\frac{\beta_0^2}{m}\,\frac{1}{(1-\xi)^{1-2m}}.\end{aligned}\tag{244}$$

This equation can be reduced to quadratures but, certainly for non-integer values of m, the subsequent integral cannot be performed analytically.

9.2 Specialization to $m = 1$ Planar Orbits

The formulas of Section 9.1 simplify spectacularly for $m = 1$. For example, the electric potential (defined to vanish for $x = 0$) is given by

$$V(\xi) = E_0r_0\xi.\tag{245}$$

9.2.1 Orbits

To obtain the orbit equation we can start from Eq. (244), specialized to the spherical electrode geometry shown in Fig. 5. When the field index m was first introduced it was visualized as being a small number, just large enough (and positive) to produce some vertical focusing. But the subsequent analysis did not rely on m being small. Eq. (244) becomes especially simple for motion in the $y = 0$ plane with m =1;

$$\frac{d^2\xi}{d\theta^2} = 1-\frac{L_0^2}{L_y^2}\,\frac{\mathcal{E}}{\mathcal{E}_0}-\left(1-\frac{L_0^2}{L_y^2}\,\beta_0^2\right)\xi \equiv -Q_x^2(\xi-\xi_{\rm co}).\tag{246}$$

The last form introduces the abbreviations Q_x and $\xi_{\rm co}$. The identification of closed orbit and the representation of transverse displacements as the sum of a "betatron" part and an "off-energy" part proceeds as for the $1/r$ electric field dependence analysed in Section 3.0.1. For our application the coefficient Q_x^2 is positive, which means there is horizontal focusing with horizontal tune Q_x given by

$$\boxed{Q_x = \sqrt{1-\frac{L_0^2}{L_y^2}\,\beta_0^2}.}\tag{247}$$

The off-energy central orbit is given by

$$\boxed{\xi_{\rm co} = \frac{1}{Q_x^2}\left(1-\frac{L_0^2}{L_y^2}\,\frac{\mathcal{E}}{\mathcal{E}_0}\right),\quad \xi'_{\rm co} = 0.}\tag{248}$$

With L_y and $\mathcal{E}$ allowed to vary, the parameters Q and $x_{\rm co}$ have to be regarded as locally, rather than globally, defined. It is important to notice though, that the parameters entering the definitions of both Q_x and $\xi_{\rm co}$ are invariants of any given particle's motion. The quantities E_0 and β_0 are obviously invariant because they are properies of the on-energy central orbit. The quantities $\mathcal{E}$ and L_y^2 are invariant by conservation of energy and angular momentum, but they are, in general, different for different particles.

9.2.2 Particle-Specific Transfer Matrices

In practice there will be drift regions, quadrupoles and other apparatus in the ring, not to mention artificial thin quadrupoles inserted within the bend to compensate for actual field index differing from $m = 1$. Eq. (246) will be applied only within individual sector bend elements. But the simplest possible application of the formulas has a single element bending through 2π—which is to say, making up the

whole accelerator. The x motion described by linearized treatment is only sinusoidal for small amplitudes. But, since the denominator is a periodic function of θ, $x(\theta)$ has the same period. For the frozen spin value $\beta_x = 0.59838$, with orbits close enough to circular that $L \approx L_0$, $Q_x = 0.8012$. (Notice that the parameter Q and the Muñoz parameter κ are identical parameters.)

Our equations, being fully relativistic, are valid in the nonrelativistic limit $\beta_0 \to 0$. In the nonrelativistic limit the orbits are simply Keplerian planetary orbits, which are known to form closed ellipses, corresponding to $Q_x = 1$. So one can say that the shift of Q_x away from 1 is a relativistic effect.[7] An orbit having initial vertical displacement or slope leaves the horizontal (design) plane. It nevertheless lies in a single plane, and its evolution is the same as if it were in the design plane. It follows that the vertical and horizontal tunes are equal;

$$Q = Q_y = Q_x = \sqrt{1-\beta_0^2}. \tag{249}$$

For propagating the radial displacement $\Delta\xi = \xi - \xi_{\rm co}$, one introduces cosine-like trajectory $C_\xi(\theta)$ satisfying $C_\xi(0) = 1$, $C'_\xi(0) = 0$ and sine-like trajectory $S_\xi(\theta)$ satisfying $S_\xi(0) = 0$, $S'_\xi(0) = 1$. They are given by

$$\begin{aligned} C_\xi(\theta) &= \cos(Q\theta) \\ C'_\xi(\theta) &= -Q\,\sin(Q\theta) \\ S_\xi(\theta) &= \frac{\sin(Q\theta)}{Q} \\ S'_\xi(\theta) &= \cos(Q\theta). \end{aligned} \tag{250}$$

For describing evolution of (ξ, ξ') from its initial values $(\xi_{\rm in}, \xi'_{\rm in})$ at $\theta = 0$ to its values at θ one can use the "transfer matrix" defined by

$$\mathbf{M}_\xi\,(\theta) = \begin{pmatrix} C_\xi(\theta) & S_\xi(\theta) \\ C'_\xi(\theta) & S'_\xi(\theta) \end{pmatrix} = \begin{pmatrix} C & S/Q \\ -SQ & C \end{pmatrix}, \tag{251}$$

where $C \equiv \cos(Q\theta)$ and $S \equiv \sin(Q\theta)$, to give

$$\begin{pmatrix} \xi(\theta) \\ \xi'(\theta) \end{pmatrix} = \begin{pmatrix} \xi_{\rm co} \\ 0 \end{pmatrix} + \mathbf{M}_\xi(\theta) \begin{pmatrix} \xi_{\rm in} - \xi_{\rm co} \\ \xi'_{\rm in} \end{pmatrix}. \tag{252}$$

or

$$\begin{aligned} \xi(\theta) &= \xi_{\rm co} + C\,(\xi_{\rm in} - \xi_{\rm co}) + (S/Q)\,\xi'_{\rm in}, \\ \xi'(\theta) &= \qquad -SQ(\xi_{\rm in} - \xi_{\rm co}) + C\xi'_{\rm in}. \end{aligned} \tag{253}$$

(The subscript ξ on $\mathbf{M}_\xi$ and its components is to serve as a reminder that this matrix is particle-specific, and is therefore not a transfer matrix in the conventional, linearized, particle-independent, sense. In spite of appearing superficially to be linearized, $\mathbf{M}_\xi$ describes nonlinear motion, and is exact for all amplitudes.) Eq. (253) can be written more compactly as

$$\begin{pmatrix} \xi(\theta) - \xi_{\rm co} \\ \xi'(\theta) \end{pmatrix} = \mathbf{M}_\xi \begin{pmatrix} \xi_{\rm in} - \xi_{\rm co} \\ \xi'_{\rm in} \end{pmatrix} = \begin{pmatrix} C & S/Q \\ -SQ & C \end{pmatrix} \begin{pmatrix} \xi_{\rm in} - \xi_{\rm co} \\ \xi'_{\rm in} \end{pmatrix}. \tag{254}$$

[7] As a curiosity, one can evaluate the corresponding tune shift of the orbit of planet Mercury around the sun. We pretend the orbit is circular (when in fact its eccentricity is $\epsilon = 0.21$, yielding, for fixed total energy, $(L/L_0)^2 \approx 1/(1-\epsilon^2) \approx 1.04$.) Mercury's mean orbital velocity is 47.87 km/s so $\beta_0 = 1.596 \times 10^{-4}$ and $Q_x \approx 1 - \beta_0^2/2 = 1.27 \times 10^{-8}$; this represents a *negative* fractional *advance* of the perihelion each turn. (Our electrostatic formulation amounts to accounting for the relativistic increase in inertial mass with no corresponding increase in gravitational attraction.) Since its orbital period of 0.241 years, Mercury completes 100/0.241=415 revolutions in 100 years. Meanwhile, its Einsteinian general relativistic perihelion advance is 43 arc-sec. Expressed as a fractional deviation per revolution, this is $43/(360\times3600\times415) = 7.99\times10^{-8}$. It appears, therefore, that the perihelion advance is reduced by about 16% by the special relativistic inertial increase. This seems to be in the same ballpark as a calculation by Engelke and Chandler[20], (who use quite complicated assumptions) except possibly for the sign, and modulo confusing issues I have not tried to unravel.

9.2.3 Propagation Through a Sector Bend

Starting from known coordinates $(x_{\rm in}, x'_{\rm in-})$ just preceding the entrance to a sector bend, where the electric potential vanishes, one also presumably knows $\mathcal{E}$ and, therefore,

$$p^2_{\rm in-} = \mathcal{E}^2/c^2 - m_p^2c^2, \quad p^2_{z,\rm in-} = \frac{p^2_{\rm in-}}{1+x'^2_{\rm in-}}, \quad p_{x,\rm in} = x'_{\rm in-}\sqrt{p^2_{z,\rm in-}}. \tag{255}$$

(In our hard edge approximation) just past the entrance, x, $\mathcal{E}$, and p_x are unchanged, but the other dynamic variables have changed. In particular, using conservation of p_x,

$$p^2_{\rm in+} = \Big(\frac{\mathcal{E}}{c} - \frac{E_0 r_0\, x_{\rm in}/c}{r_0 + x_{\rm in}}\Big)^2 - m_p^2c^2, \quad p^2_{z,\rm in+} = p^2_{\rm in+} - p^2_{x,\rm in}, \quad x'_{\rm in+} = \frac{p_{x,\rm in}}{\sqrt{p^2_{z,\rm in+}}}. \tag{256}$$

This has determined $x'_{\rm in+}$. The last expression has been arranged to give not just the magnitude, but also the sign of $x'_{\rm in+}$. The argument of the square root can never change sign. Notice that this calculation has included the (very small, because of near-normal incidence) "refractive" bending at the interface. Using Eq. (240), initial coordinates $(\xi_{\rm in}, \xi'_{\rm in})$, just inside the sector bend can be obtained;

$$\xi_{\rm in} = \frac{x_{\rm in-}}{r_0 + x_{\rm in-}}, \quad \xi'_{\rm in} = \frac{r_0^2 x'_{\rm in+}}{(r_0 + x_{\rm in-})^2}. \tag{257}$$

Note also that L_y, which is proportional to $(r_0 + x)p_z$ changes according to

$$\frac{L^2_{y,\rm in+}}{L^2_{y,\rm in-}} = \frac{p^2_{z,\rm in+}}{p^2_{z,\rm in-}}, \tag{258}$$

with both numerator and denominator known from earlier formulas. From Eqs. (247) and (248) it can be seen that L_y is the only varying parameter in the definitions of Q and $x_{\rm co}$; (not counting changes in $\mathcal{E}$ occurring in RF cavities). Q and $x_{\rm co}$ can be updated accordingly. With the updated version of $x_{\rm co}$ one can determine $\xi_{\rm in} - x_{\rm co}$ which is needed as an input for the bend element transfer matrix.

From the known bend angle $\Delta\theta$, cosine and sine factors C and S can be calculated, and all elements of transfer matrix $\mathbf{M}_\xi$ determined. Then, using Eq. (254), one obtains the components $(\xi_{\rm out}, \xi'_{\rm out})$ just before the exit from the sector bend.

To get out of the bend element the steps taken at the input have to be reversed. Since $x_{\rm co}$ is current the current values of $(\xi_{\rm out}, \xi'_{\rm out-})$ can be used to obtain

$$x_{\rm out} = \frac{r_0\xi_{\rm out}}{1-\xi_{\rm out}} \quad x'_{\rm out-} = \frac{\xi'_{\rm out-}}{(1-\xi_{\rm out})^2}. \tag{259}$$

We then get

$$p^2_{\rm out-} = \Big(\frac{\mathcal{E}}{c} - \frac{E_0 r_0\, x_{\rm out}/c}{r_0 + x_{\rm out}}\Big)^2 - m_p^2c^2, \quad p^2_{z,\rm out-} = \frac{p^2_{\rm out-}}{1+x'^2_{\rm out-}}, \quad p_{x,\rm out} = x'_{\rm out-}\sqrt{p^2_{z,\rm out-}}. \tag{260}$$

Finally the coordinates just outside the exit are given by

$$p^2_{\rm out+} = \Big(\frac{\mathcal{E}}{c}\Big)^2 - m_p^2c^2, \quad p^2_{z,\rm out+} = p^2_{\rm out+} - p^2_{x,\rm out}, \quad x'_{\rm out+} = p_{x,\rm out}/\sqrt{p^2_{\rm out+}}. \tag{261}$$

9.2.4 Compensating for $m \neq 0$ Electric Field Index

This section can be skipped if the primary interest is in the time of flight calculation through bend elements. These formulas are not actually implemented in ETEAPOT. The practical EDM lattice will not necessarily have spherical electrodes, causing the field index to deviate from $m = 0$. In ETEAPOT such

fields are modeled by regular interpolation of zero length "effective quadrupoles". It is not necessary to switch from (ξ, ξ') to (x, x') coordinates to propagate through these effective quadrupoles.

Sector bends with m-values other than 1 can be modelled using element combinations represented by transfer matrices,

$$\mathbf{M}_{1/2}\mathbf{M}_q\mathbf{M}_{1/2} = \begin{pmatrix} C_{1/2} & S_{1/2}/Q \\ -S_{1/2}Q & C_{1/2} \end{pmatrix} \begin{pmatrix} 1 & 0 \\ -\tilde{q} & 1 \end{pmatrix} \begin{pmatrix} C_{1/2} & S_{1/2}/Q \\ -S_{1/2}Q & C_{1/2} \end{pmatrix}. \tag{262}$$

or

$$\mathbf{M}_{q/2}\mathbf{M}\mathbf{M}_{q/2} = \begin{pmatrix} 1 & 0 \\ -\tilde{q}/2 & 1 \end{pmatrix} \begin{pmatrix} C & S/Q \\ -SQ & C \end{pmatrix} \begin{pmatrix} 1 & 0 \\ -\tilde{q}/2 & 1 \end{pmatrix}, \tag{263}$$

where $\tilde{q} \equiv qr_0(1-\xi)$. Both approaches are made inconvenient by the $1-\xi$ factor in $\tilde{q}$. One approach is to simply replace $1-\xi$ by 1 in the form (262), recognizing that this amounts to neglecting a "sextupole" effect, which becomes progressively more negligible with finer slicing. With this approach it is natural to also forego updating L_y. Then a transfer map for the entire sector can be obtained by simple matrix multiplication.

A more accurate approach is to use form (263), updating $\tilde{q}$ each time before applying the quad matrix transformations, and updating L_y and the elements of $\mathbf{M}$ before applying it. Though complicating the code significantly, these operations do not increase the computation time very much.

9.2.5 Propagation Through Drift Regions

In (ξ, ξ') coordinates propagation through a drift of length d is quite complicated. Commonly the drift will have been immediately preceeded by a quadrupole, in which case the emergent values of (x, x') are obtained as described above. Then, after a drift of length d,

$$x_d = x + dx', \quad x'_d = x'. \tag{264}$$

The angular momentum also has to be updated.

$$L_{yd} = L_y \frac{r_0 + x_d}{r_0 + x}. \tag{265}$$

9.2.6 Propagation Through Thin Multipoles

This section can also be skipped while concentrating on time of flight. Propagation through a thin quad of strength (inverse focal length) q is described in this section. Propagation through higher order thin multipoles can be performed similarly. With postive q corresponding to horizontal *focusing*, propagation through a thin multipole is described by

$$\begin{pmatrix} x \\ x' \end{pmatrix} \to \begin{pmatrix} x \\ x' - qx \end{pmatrix} \tag{266}$$

As well as changing p_x and p_z, the quadrupole deflection also has the indirect effect of altering L_y;

$$p_z c \to \frac{pc}{\sqrt{1 + x'^2}}, \quad p_x c \to x' p_z c, \quad L_y c \to p_z c(r0 + x); \tag{267}$$

This is the evolution appropriate for quadrupoles in straight sections.

For quadrupoles in the interior of bends it is easier to work with (ξ, ξ') coordinates. Expressed in terms of ξ and ξ', using Eqs. (240) and (242),

$$\begin{pmatrix} \xi \\ \xi' \end{pmatrix} \to \begin{pmatrix} \xi \\ (1-\xi)^2 \left(\frac{\xi'}{(1-\xi)^2} - q\frac{r_0\xi}{1-\xi} \right) = \xi' - qr_0(1-\xi)\xi \end{pmatrix}. \tag{268}$$

To avoid converting from ξ to x, and then back to ξ coordinates, one can simply assign the "strength" of the quad (in dimensionless units) to be $\tilde{q} = qr_0(1-\xi)$, producing ξ-deflection $qr_0(1-\xi)\xi$. Propagation through the thin quadrupole is then represented by the transfer matrix

$$\mathbf{M}_q = \begin{pmatrix} 1 & 0 \\ -qr_0(1-\xi) & 1 \end{pmatrix}. \tag{269}$$

The quadrupole deflection also has the indirect effect of altering L_y. The alteration

$$L_y \to L_y \frac{\cos(x' + \Delta x'/2)}{\cos x'} = L_y \frac{\cos\Big((\xi' + \Delta\xi')/\big(2(1-\xi)^2\big)\Big)}{\cos\big(\xi'/(1-\xi)^2\big)}, \tag{270}$$

accounts for the change of p_r (half way through the quad) from $p\cos x'$ to $p\cos(x' + \Delta x'/2)$ with radial coordinate r unchanged. (The error in treating x' as an angle, rather than as the tangent of an angle introduces a quadratically-small error.)

There is no change in $\mathcal{E}$ at a quadrupole. The change in L_y causes changes in Q_x and $\xi_{\rm co}$ according to Eqs. (247) and (248). Since $\mathbf{M}_Q$ depends on neither Q_x nor $\xi_{\rm co}$, the order of application of $\mathbf{M}_Q$ and the updating of L_y does not matter.

For the proton EDM experiment, with $\beta_0 \approx 0.6$, the change in L_y at quadrupoles is probably insignificant. But for the electron EDM experiment, with $\beta_0 \approx 1$, the parameters are very sensitive to L_y and the effects of these changes will have to be studied carefully. Superficially the factor Q_x is hypersensitive to L_y. But it will be seen below that orbits depend primarily on $\sin(Q_x\Delta\theta)/Q_x \approx \Delta\theta$, which is very small, especially after bend-slicing has reduced the bend angle $\Delta\theta$ to be small. In this limit the orbits are essentially straight lines.

9.2.7 ξ Evolution and Convergence Estimates

Using Eq. (240), initial conditions (ξ_0, ξ_0') has been expressed in terms of initial x conditions;

$$\xi = \frac{x}{r_0 + x}, \quad \xi' = \frac{r_0^2 x'}{(r_0 + x)^2}. \tag{271}$$

The evolution of x is obtained using Eq. (253), whose upper equation yields

$$\xi = \xi_{\rm co} + (\xi_{\rm in} - \xi_{\rm co})\,\cos Q\theta + \frac{\xi'_{\rm in}}{Q}\,\sin Q\theta. \tag{272}$$

This formula will be substituted into Eq. (286), which will then be integrated to give the time of flight. Then

$$x(\theta) = \frac{r_0\xi(\theta)}{1-\xi(\theta)}, \quad \text{and} \quad r(\theta) = r_0 + x(\theta). \tag{273}$$

For the proton EDM experiment the value of radius r_0 will be, say, 40 m. An initial value $x_0 = 1$ m would be unrealistically large. It is better therefore to use centimeter units. Then $r_0 = 4000$ cm, and the initial displacement of a cosine-like trajectory is 1 cm. With the electrode spacing being 3 cm, this unit-amplitude, cosine-like trajectory happens to have something like a maximal amplitude. Dropping terms of one higher order, for example from quadrupole order to sextupole order, therefore amounts to making an error of about one part in 4000. An error of this magnitude is likely to be unimportant unless some resonance causes its repeated effect to accumulate constructively over many turns.

9.3 Time of Flight Calculation

The treatment of orbits has been based entirely on positions, slopes and momenta, with no need for velocities. To calculate time of flight, velocity is required. These calculations will proceed in parallel with the orbit calculations but they are described separately here to emphasize the essentially different influences on $\mathbf{r}(\theta)$ and $ct(\theta)$. With all quadrupoles and multipoles treated as thin in ETEAPOT, the only difficulty comes in calculating the time of flight through electric bend elements in which the particle speed depends on position.

9.3.1 Kinematic Variables Within Electric Bend Elements

For the $m = 1$, inverse square law case being emphasized, the electric field and electric potential are given by Eqs. (237) and (238);

$$\begin{aligned} \mathbf{E}(\xi) &= -E_0 \left(1-\xi\right)^2 \hat{\mathbf{r}}, \\ V(\xi) &= E_0 r_0 \xi. \end{aligned} \tag{274}$$

The latter equation, with Eq. (272), permits the potential energy to be expressed in terms of θ and initial conditions.

$$V(\theta) = E_0 r_0 \left(\xi_{\rm co} + (\xi_{\rm in} - \xi_{\rm co})\, \cos Q\theta + \frac{\xi'_{\rm in}}{Q}\, \sin Q\theta.\right) \tag{275}$$

Then $\gamma(\theta)$ is obtained from

$$\gamma(\theta) = \frac{\mathcal{E}}{m_p c^2} - \frac{E_0 r_0}{m_p c^2/e} \left(\xi_{\rm co} + (\xi_{\rm in} - \xi_{\rm co})\, \cos Q\theta + \frac{\xi'_{\rm in}}{Q}\, \sin Q\theta\right). \tag{276}$$

From this formula one can obtain $\beta(\theta)$ using

$$\beta(\theta) = \sqrt{1 - 1/\gamma^2}. \tag{277}$$

From the y-component of Eq. (8) we also have, for motion in the horizontal plane,

$$\frac{d\theta}{dt} = \frac{-L_y}{m_p r^2 \gamma}. \tag{278}$$

Note that, with right-handed Frenet coordinates, and clockwise orbit (which we are now assume) L_y is negative. This accounts for the negative sign in Eq. (278). The right hand side of this equation can now be expressed in terms of θ, invariants and initial conditions.

Warning: Note that the sign of θ and the sign of L_y are correlated in Eq. (278). The negative sign $(-L_y)$ is specific to clockwise orbits, with θ increasing along the orbit. This seeming inconsistency is built into the ETEAPOT code as of June 1, 2014. This sign ambiguity causes the tracked time of flight variable ct to also be ambiguous. The appropriate RF phase is then, similarly, ambiguous.

9.3.2 Time of Flight Through Bends

A formula for the time of flight has already been given in Eq. (154). Since this form is integrable, it gives the exact flight time in closed analytic form. However it has the disadvantage that the angle θ_0 (which is the angle to "perihelion") because it is multiple-valued, is hard to determine unambiguously, especially because perihelion is indeterminate for circular orbits. The most important circular orbit is the design central orbit and, depending on elements encountered in the ring, the local angle to perihelion can vary erratically.

It is useful, therefore, to have an alternate, highly accurate, though not necessarily exact, form, to accompany the Muńoz form developed earlier. From Eq. (278) the time of flight dt, expressed as a distance $d(ct)$ is given by

$$\frac{dct}{d\theta} = \frac{m_p c^2 r^2}{-L_y c}\, \gamma = \frac{1}{-L_y c/e}\, \frac{r_0^2}{(1-\xi)^2}\, (\mathcal{E}/e - E_0 r_0 \xi). \tag{279}$$

where

$$\boxed{\xi = \xi_{\rm co} + (\xi_{\rm in} - \xi_{\rm co})\, \cos Q\theta + \frac{\xi'_{\rm in}}{Q}\, \sin Q\theta.} \tag{280}$$

Note that the non-invariant factor, r^2, has been replaced using Eq. (241) and that the parameters Q and $\xi_{\rm co}$, though invariant, are particle-dependent as in Eqs. (247) and (248). (The proliferation of "/e" factors

is for convenience in converting electron-volts to MKS energy units.) Formula (279) can be checked on the design orbit where $\xi = 0$, using $L_0 c = -m_p c^2 \gamma_0 \beta_0 r_0$;

$$\frac{dct_0}{d\theta} = \frac{1}{\gamma_0 \beta_0 r_0 m_p c^2/e}\, r_0^2\, (\gamma_0 m_p c^2/e) = \frac{r_0}{\beta_0}, \tag{281}$$

which is correct. The time of flight through an element with angle $\Delta\theta$ is given by

$$ct = \int_0^{\Delta\theta} \frac{r_0^2(\mathcal{E}/e - E_0 r_0 \xi)}{-L_y c/e}\, \frac{1}{(1-\xi)^2}\, d\theta, \tag{282}$$

(where, for clockwise motion, $-L_y$ is positive). Over the corresponding sector the time of flight of the design particle is

$$ct_0 = \int_0^{\Delta\theta} \frac{r_0}{\beta_0} d\theta. \tag{283}$$

The increment in time relative to the design particle is

$$ct - ct_0 = \int_0^{\Delta\theta} \left(\frac{r_0^2(\mathcal{E}/e - E_0 r_0 \xi)}{-L_y c/e}\, \frac{1}{(1-\xi)^2}\, - \frac{r_0}{\beta_0} \right) d\theta, \tag{284}$$

The integrand can be expanded in a series in ξ;

$$\frac{r_0^2(\mathcal{E}/e - E_0 r_0 \xi)}{-L_y c/e}\, \frac{1}{(1-\xi)^2}\, - \frac{r_0}{\beta_0} = A_0 + A_1 \xi + A_2 \xi^2 + A_3 \xi^3 + \ldots, \tag{285}$$

where

$$\begin{aligned} A_0 &= -\frac{r_0^2 \mathcal{E}/e}{L_y c/e} - \frac{r_0}{\beta_0}, \quad A_1 = -\frac{2 r_0^2 \mathcal{E}/e}{L_y c/e} + \frac{r_0^3 E_0}{L_y c/e}, \quad A_2 = -\frac{3 r_0^2 \mathcal{E}/e}{L_y c/e} + \frac{2 r_0^3 E_0}{L_y c/e}, \\ A_3 &= -\frac{4 r_0^2 \mathcal{E}/e}{L_y c/e} + \frac{3 r_0^3 E_0}{L_y c/e}, \quad A_4 = -\frac{5 r_0^2 \mathcal{E}/e}{L_y c/e} + \frac{4 r_0^3 E_0}{L_y c/e}, \quad A_5 = -\frac{6 r_0^2 \mathcal{E}/e}{L_y c/e} + \frac{5 r_0^3 E_0}{L_y c/e}, \ldots. \end{aligned} \tag{286}$$

All the required integrals (over the range from 0 to $\Delta\theta$, which is the bend angle) are elementary—the integrands are integer powers of $\sin Q\theta$ or $\cos Q\theta$, and the series in Eq. (285) is rapidly convergent. It is important to remember that quantities, in this case L_y, which are discontinuous in the transition from just outside to just inside a bend element, have to be updated to the value *inside* before evaluating these A_i coefficients.

Because ξ^2 is necessarily positive while ξ can have either sign, the "quadratic" term proportional to ξ^2 may compete with the preceding "linear" term proportional to ξ, which can have either sign and will tend to cancel on the average. As has been stated repeatedly, since the coefficients are particle-dependent, this formula has to be performed individually for every particle at every bend,

9.3.3 Time of Flight Through Straight Sections

Different particles also have different flight times through drift sections or multipole elements of length ℓ. The path length excess is approximately

$$c(t - t_0)_{\text{path}} = \frac{x'^2 \ell^2 + y'^2 \ell^2}{2\ell\beta_0} = \frac{(x'^2 + y'^2)\ell}{2\beta_0}, \tag{287}$$

and the off-speed correction is

$$c(t - t_0)_{\text{vel.}} = \ell \left(\frac{1}{\beta} - \frac{1}{\beta_0} \right). \tag{288}$$

The total effect is

$$c(t - t_0)_{\text{straight}} = \frac{\ell}{\beta_0} \left(\frac{\beta_0}{\beta} - 1 + \frac{x'^2 + y'^2}{2} \right), \tag{289}$$

or, more directly,

$$c(t - t_0)_{\text{straight}} = \frac{\ell \sqrt{1 + x'^2}}{pc/\mathcal{E}} - \frac{\ell}{\beta_0}. \tag{290}$$

9.3.4 Time of Flight in Bends Due to Vertical Oscillation

For bends only the projection of the orbit onto the horizontal plane has been found so far. It remains to evaluate the time of flight ascribable to vertical betatron motion. We assume there is no direct coupling between x and y. We also neglect the effect of the small speed variations accompanying horizontal oscillations. Also neglecting the small bending in sufficiently-finely sliced bend elements, we treat them as straight. With these approximations the bend element is treated as a drift as far as vertical oscillations are concerned. The off-velocity effect has already been included in the horizontal calculation. Copying from Eq. (289),

$$c(t - t_0)_{\text{vert.}} = \frac{\ell\, y'^2}{2\beta_0}. \tag{291}$$

10 Spin Tracking in ETEAPOT

10.1 Approximations

- To leading approximation all spin precession occurs in central force, inverse square law, "Kepler force" regions. With this assumption the orbit through a bend element of any individual particle lies in a single fixed plane.
- Each individual particle's spin vector can be decomposed into a (conserved) component $\tilde{s}_\perp$, normal to the bend plane, and a (precessing) 2-component vector $\tilde{\mathbf{s}}_\parallel$, lying in the bend plane.
- Initially hard edge bends are assumed. Even after this approximation is dropped it will be assumed that the paths through the entrance and exit fringe fields continue to lie in the same plane as in the bend interior.
- As always in ETEAPOT, field deviations from "Spherical" will be modeled by artificial quadrupoles.
- Quadrupoles, whether real or artificial (and all multipoles) will be treated as thin. Spin evolution through multipoles will be modeled by successive rotations. All such rotations will be concatenated explicitly into a single (near-identity) precession matrix. This will circumvent the problem of large, approximately canceling precessions and avoid spurious non-commutative geometric precessions.
- Quadrupoles too thick to be validly treated as thin, will be sliced, with regions between the sliced thin quadrupoles treated as drifts.
- Bend frame spin components are $(\tilde{s}_x, \tilde{s}_y, \tilde{s}_z)$, laboratory frame spin components are (s_x, s_y, s_z).

10.2 Spin Coordinates

10.2.1 Bend Coordinates

For studying spin evolution in a frozen spin storage ring we use the coordinate system shown in Figure 10. The local frame of reference is the Frenet frame aligned with the orbit of the individual particle being tracked, with $\mathbf{e_1}$ pointing in the centrifugal (outward) direction, $\mathbf{e_3}$ pointing in the tangential direction and $\mathbf{e_2}$ pointing out of the page.

The figure shows the angle $\tilde{\alpha}$ which is the angle in the bend plane between the projection of the spin vector onto the bend plane and $\mathbf{e_3}$, tangent to the particle orbit. Spin precession is most naturally described by using, as spin coordinates, the angle $\tilde{\alpha}$ and $\tilde{s}_y$, the vertical component of spin in the bend frame. Though the spin vector has three components, only two are independent; the angle $\tilde{\alpha}$ fixes the direction of $\tilde{\mathbf{s}}_\parallel$ in the bend plane. The spin precesses about the $\tilde{y}$-axis in the bend plane. The bend frame spin coordinates are

$$\begin{pmatrix} \tilde{s}_x \\ \tilde{s}_y \\ \tilde{s}_z \end{pmatrix} = \begin{pmatrix} -\tilde{s}_\parallel \sin\tilde{\alpha} \\ \tilde{s}_\perp \\ \tilde{s}_\parallel \cos\tilde{\alpha} \end{pmatrix}. \tag{292}$$

Only two coordinates are necessary because the magnitude of $\tilde{\mathbf{s}}$ is equal to 1;

$$\tilde{s}_\parallel^2 + \tilde{s}_\perp^2 = 1. \tag{293}$$

(Note that $\tilde{\mathbf{s}}_\parallel$ is the 2D vector component of the spin vector in the bend plane, *not* the component of the spin vector parallel to the velocity.) These coordinates are ideal for evolving the spins through ring elements which cause horizontal bends.

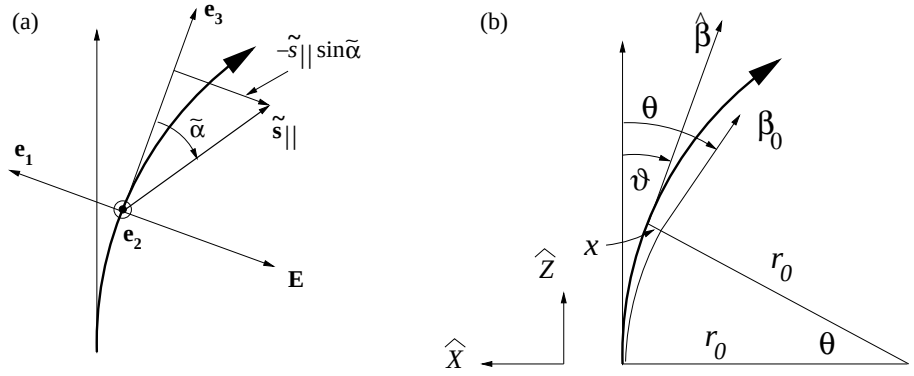

Figure 10: (a) In the bend plane the spin vector $\mathbf{s}$ has precessed through angle $\tilde{\alpha}$ away from its nominal direction along the proton's velocity. (Remember that different particles have different bend planes.) (b) Projection of figure (a) onto the laboratory horizontal plane. The projected longitudinal axis is shown coinciding with the laboratory longitudinal axis, even if this is not exactly valid. x is the deviation of the (bold face) particle orbit from the (pale face) design orbit. If the bend plane coincides with the design bend plane (as is always approximately the case) $\hat{\boldsymbol{\beta}}_0$ and $\hat{\mathbf{z}}$ are identical. θ is the reference particle deviation angle from longitudinal and ϑ is the tracked particle deviation angle from longitudinal. On the average θ and ϑ are the same, but betatron oscillations cause them to differ on a turn by turn basis, and also to make the instantaneous bend plane not quite horizontal.

10.2.2 Transformation From Lab Frame to Bend Frame (and Back Again)

From the particle tracking one has the laboratory frame vectors $\mathbf{r}$, $\mathbf{p}$, and hence $\mathbf{L} = \mathbf{r} \times \mathbf{p}$, just past the bend entrance, and one also has the spin vector $\mathbf{s}$;

$$\begin{aligned}
\mathbf{r} &= r_x\hat{\mathbf{x}} + r_y\hat{\mathbf{y}} + r_z\hat{\mathbf{z}}, \\
\mathbf{p} &= p_x\hat{\mathbf{x}} + p_y\hat{\mathbf{y}} + p_z\hat{\mathbf{z}}, \\
\mathbf{L} &= L_x\hat{\mathbf{x}} + L_y\hat{\mathbf{y}} + L_z\hat{\mathbf{z}}, \\
\mathbf{s} &= s_x\hat{\mathbf{x}} + s_y\hat{\mathbf{y}} + s_z\hat{\mathbf{z}}.
\end{aligned} \tag{294}$$

Any spin precession in the interior of a bend element occurs in the bend plane. To exploit this reduction from 3D to 2D it is first necessary to obtain the spin components in an orthonormal frame having its "y" axis perpendicular to the plane and its "z" coordinate tangential to the orbit. The purpose of this section is to document this transformation. In the (always excellent) paraxial approximation, this transformation will be close to identity.

We can establish an orthonormal, right-handed basis triad with axis 3 parallel to $\mathbf{p}$ and axis 2 parallel to $-\mathbf{L}$ (where the negative sign is appropriate for clockwise orbits);

$$\begin{aligned}
\mathbf{e_3} &= \frac{p_x}{p}\,\hat{\mathbf{x}} + \frac{p_y}{p}\,\hat{\mathbf{y}} + \frac{p_z}{p}\,\hat{\mathbf{z}}, \\
\mathbf{e_2} &= \frac{\mathbf{r}\times\mathbf{p}}{-L}, \\
\mathbf{e_1} &= \mathbf{e_2}\times\mathbf{e_3}.
\end{aligned} \tag{295}$$

These equations can be re-expressed formally, with all coefficients known, as

$$\begin{aligned}
\mathbf{e_1} &= a_{11}\hat{\mathbf{x}} + a_{12}\hat{\mathbf{y}} + a_{13}\hat{\mathbf{z}} \\
\mathbf{e_2} &= a_{21}\hat{\mathbf{x}} + a_{22}\hat{\mathbf{y}} + a_{23}\hat{\mathbf{z}} \\
\mathbf{e_3} &= a_{31}\hat{\mathbf{x}} + a_{32}\hat{\mathbf{y}} + a_{33}\hat{\mathbf{z}}.
\end{aligned} \tag{296}$$

The vector $\mathbf{s}$ can be expanded as

$$\begin{aligned}\mathbf{s} &= \tilde{s}_1\mathbf{e_1} + \tilde{s}_2\mathbf{e_2} + \tilde{s}_3\mathbf{e_3} \\ &= \tilde{s}_1(a_{11}\hat{\mathbf{x}} + a_{12}\hat{\mathbf{y}} + a_{13}\hat{\mathbf{z}}) + \ldots \\ &= (a_{11}\tilde{s}_1 + a_{21}\tilde{s}_2 + a_{31}\tilde{s}_3)\,\hat{\mathbf{x}} + \ldots . \end{aligned} \tag{297}$$

The final relation can be expressed in matrix form as

$$\begin{pmatrix} s_x \\ s_y \\ s_z \end{pmatrix} = \mathbf{R} \begin{pmatrix} \tilde{s}_1 \\ \tilde{s}_2 \\ \tilde{s}_3 \end{pmatrix}, \tag{298}$$

where $\mathbf{R}$ is an orthogonal matrix,

$$\mathbf{R} = \begin{pmatrix} a_{11} & a_{21} & a_{31} \\ a_{12} & a_{22} & a_{32} \\ a_{13} & a_{23} & a_{33} \end{pmatrix}. \tag{299}$$

(Aside: the magnitude $|\mathrm{det}\mathbf{R}|$ of the determinant of $\mathbf{R}$ is necessarily 1, but the actual value is ± 1. This sign correlates with the clockwise/counterclockwise orbit ambiguity.)

Because $\mathbf{R}$ is orthogonal, $\mathbf{R}^{-1} = \mathbf{R}^T$ and Eq. (298) can be inverted to give

$$\begin{pmatrix} \tilde{s}_1 \\ \tilde{s}_2 \\ \tilde{s}_3 \end{pmatrix} = \begin{pmatrix} a_{11} & a_{12} & a_{13} \\ a_{21} & a_{22} & a_{23} \\ a_{31} & a_{32} & a_{33} \end{pmatrix} \begin{pmatrix} s_x \\ s_y \\ s_z \end{pmatrix}. \tag{300}$$

This yields the spin components in the bend frame. Their propagation through the bend is described below. At the exit of the bend element the laboratory-frame components can be worked out using a similar formula.

After the bend plane spin components have been updated at the output edge of the bend element it is necessary to transform the resulting spin vector back to the (local) laboratory frame. This entails repeating the preceeding formulas starting with Eqs (294), but with $\mathbf{r}$, $\mathbf{p}$ and $\mathbf{L}$ having been evaluated (in local laboratory coordinates) just inside the output face of the bend element.

10.2.3 Non-Bend Elements

Some elements (especially quadrupoles) can cause vertical deflections which alter s_y. Being proportional to transverse displacements these deflections are very small and can have either polarity. Nevertheless it is necessary to keep track of their effects.

On an element by element basis, when a particle has just entered an element that bends (for example) in a plane rolled counter-clockwise by angle ϕ about the z-axis, it is first necessary to transform its laboratory frame coordinates (s_x, s_y, s_z) into bend frame coordinates $(\tilde{s}_x, \tilde{s}_y, \tilde{s}_z)$ using

$$\begin{pmatrix} \tilde{s}_x \\ \tilde{s}_y \\ \tilde{s}_z \end{pmatrix} = \begin{pmatrix} \cos\phi & -\sin\phi & 0 \\ \sin\phi & \cos\phi & 0 \\ 0 & 0 & 1 \end{pmatrix} \begin{pmatrix} s_x \\ s_y \\ s_z \end{pmatrix} \tag{301}$$

(As it stands, this equation is over-simplified since (in the presence of vertical betatron oscillation) the normal to the bend plane can have a (tiny) component along the longitudinal axis. This complication is temporarily being ignored.) The roll angle ϕ has been chosen so that the element causes pure precession through some calculable angle $\widetilde{\Delta\alpha}$ about some known axis. With the particle speed known, $\widetilde{\Delta\alpha}$ is determined unambiguously by the (known) magnitude of the angular deflection in the multipole element. The plane of deflection is also available from the particle tracking through the element. Expressing the spin precession also by a 3×3 matrix, and transforming back to the erect laboratory frame, one obtains the new cartesian components,

$$\begin{pmatrix} s_x \\ s_y \\ s_z \end{pmatrix}_{\text{after}} = \begin{pmatrix} \cos\phi & \sin\phi & 0 \\ -\sin\phi & \cos\phi & 0 \\ 0 & 0 & 1 \end{pmatrix} \begin{pmatrix} \cos\widetilde{\Delta\alpha} & 0 & -\sin\widetilde{\Delta\alpha} \\ 0 & 1 & 0 \\ \sin\widetilde{\Delta\alpha} & 0 & \cos\widetilde{\Delta\alpha} \end{pmatrix} \begin{pmatrix} \cos\phi & -\sin\phi & 0 \\ \sin\phi & \cos\phi & 0 \\ 0 & 0 & 1 \end{pmatrix} \begin{pmatrix} s_x \\ s_y \\ s_z \end{pmatrix}_{\text{before}} \tag{302}$$

As mentioned earlier, matrix products like these are to be explicitly concatenated, outside ETEAPOT, with all elements expressed as (rapidly convergent) truncated expansions in products of (small) angles and (small) precession angle $\widetilde{\Delta\alpha}$. The resultant matrix (coded into ETEAPOT) differs from the identity matrix only by differentially-small, rapidly-convergent elements.

10.3 Spin Evolution Through Muñoz-Pavic Bends

10.3.1 Analytic Formulas for Spin Precession

We introduce, at least temporarily, the term "Muñoz-Pavic Bend" to characterize a bend having field index $m = 1$, which is the case being treated in our 2D formalism. In this case (and only in this case) the orbit stays in a single plane. Also, in this frame any precession of the spin is purely around an axis normal to the plane. Obtaining the initial values of the spin components in this frame was described in the previous section.

In the bend plane the orbit lies in a single plane. Superficially this may suggest we are accounting only for horizontal betatron oscillations and neglecting vertical betatron oscillations. In fact, however, the ETEAPOT treatment accounts for arbitrary betatron and synchrotron motion by assigning different "wobbling planes" to each individual particle. Even allowing for vertical betatron motion these frames are all very nearly parallel to the global horizontal design frame of the ring. For the 2D evolution through electric bend elements in ETEAPOT, any betatron oscillations actually present for a particular particle are folded into the determination of its particle-specific orbit plane, and the initial coordinates in this plane.

As shown in Figure 10, the initial spin vector is

$$\tilde{\mathbf{s}} = -\tilde{s}_{\parallel} \sin\tilde{\alpha}\,\hat{\mathbf{x}} + \tilde{s}_y\hat{\mathbf{y}} + \tilde{s}_{\parallel}\cos\tilde{\alpha}\,\hat{\mathbf{z}}. \tag{303}$$

Here $\tilde{s}_y\hat{\mathbf{y}}$ is the out-of-plane component of $\tilde{\mathbf{s}}$, $\tilde{s}_{\parallel}$ is the magnitude of the in-plane projection of $\tilde{\mathbf{s}}$, and $\tilde{\alpha}$ is the angle between the projection of $\tilde{\mathbf{s}}$ onto the plane and the tangent vector to the orbit.

Jackson's[14] Eq. (11.171) gives the rate of change in an electric field $\mathbf{E}$, of the longitudinal spin component as

$$\frac{d}{dt}(\hat{\beta}\cdot\mathbf{s}) = -\frac{e}{m_p c}(\mathbf{s}_{\perp,\mathbf{J}}\cdot\mathbf{E})\left(\frac{g\beta}{2}-\frac{1}{\beta}\right). \tag{304}$$

(Note that Jackson's $\mathbf{s}_{\perp,J}$ is the component perpendicular to the tangent to the orbit *not* to the orbit plane.) Substituting from Eq. (303) the equation becomes

$$\frac{d}{dt}(\tilde{s}_{\parallel}\cos\tilde{\alpha}) = -\frac{e}{m_p c}(\tilde{s}_{\parallel}\sin\tilde{\alpha}\,E)\left(\frac{g\beta}{2}-\frac{1}{\beta}\right). \tag{305}$$

With the orbit confined to a plane, any precession occurs about the normal to the plane, conserving $\tilde{s}_y$. Since the magnitude of $\tilde{\mathbf{s}}$ is conserved it follows that the magnitude $\tilde{s}_{\parallel}$ is also conserved. This allows $\tilde{s}_{\parallel}$ to be treated as constant in Eq. (305). Then Eq. (305) reduces to

$$\frac{d\tilde{\alpha}}{dt} = \frac{eE}{m_p c}\left(\frac{g\beta}{2}-\frac{1}{\beta}\right). \tag{306}$$

This is undoubtedly a fairly good approximate equation in any more-or-less constant electric field, but it is *exact only for the* $m = 1$ *Keplerian electric field*, which is the only field in which arbitrary orbits stay in a fixed plane. In fact, the derivation is not quite valid even for our $m = 1$ case. Though the design orbit is circular, the betatron orbits are slightly elliptic. This violates our assumption that orbit and electric field are orthogonal. Neglecting this amounts to dropping a term from the RHS of Eq. (304) that is down by four orders of magnitude. Furthermore this term would average to zero except for a possible non-zero commutation precession which would be expected to be down by another four orders of magnitude.

Meanwhile the velocity vector itself has precessed by angle ϑ relative to a direction fixed in the laboratory. Note that this angle ϑ, the angle of the individual particle's orbit is approximately, but not exactly equal to the angle θ of the design orbit.

In the ETEAPOT treatment each particle in an electric bend element evolves in its own plane. $\tilde{\mathbf{s}}_{\|}$ is the component in this plane of the total spin vector. At every entrance to an electic bend $\tilde{\mathbf{s}}_{\|}$ has to be calculated from the known laboratory frame description of $\mathbf{s}$, which also has to be updated as the particle exits the bend. (Ideally, in an EDM storage ring experiment any out-of-plane component of $\mathbf{s}$ would be evidence of non-vanishing electric dipole moment.)

The precession rate of ϑ is governed by the equation

$$\frac{d\vartheta}{dt} = \frac{d}{dt}\left(\frac{s}{r}\right) = \frac{eE}{p}. \tag{307}$$

where the curvature is $1/r = eE/(vp)$ and (just in this equation) s temporarily stands for arc length along the orbit. Dividing Eq. (306) by Eq. (307) and using $pc = m_p c^2 \gamma\beta$,

$$\boxed{\frac{d\tilde{\alpha}}{d\theta} = \left(\frac{g}{2} - 1\right)\gamma - \frac{g/2}{\gamma}.} \tag{308}$$

In this step we have also surrepticiously made the replacement $\vartheta \to \theta$. Even though these angles are not the same, over arbitrarily long times they advance at the same rate. In any case the error in equating ϑ to θ becomes progressively more valid in the fine-slicing limit, as the orbit is more nearly approximated by straight line segments. Explicitly the bend frame precession advance is the sum of two definite integrals

$$\widetilde{\Delta\alpha} = \left(\frac{g}{2} - 1\right) I_\gamma - \frac{g}{2} I_{\gamma i}, \tag{309}$$

where

$$I_\gamma = \int_0^\theta \gamma(\theta')d\theta', \quad \text{and} \quad I_{\gamma i} = \int_0^\theta \frac{d\theta'}{\gamma(\theta')}. \tag{310}$$

To account for fringe fields two more terms, $\widetilde{\Delta\alpha}^{\rm FF,in}$ and $\widetilde{\Delta\alpha}^{\rm FF,out}$, will later be added directly to the right hand side of Eq. (309).

10.3.2 Non-Perturbative Evaluation of the Spin Precession

Eq. (308) is susceptible to solution by an approach just like that used in the time of flight determination, starting from Eq. (280). The main step is to express γ as a function of θ' using relation (276)

$$\begin{aligned}\gamma(\theta') &= \frac{\mathcal{E}/e}{m_p c^2/e} - \frac{E_0 r_0}{m_p c^2/e}\left(\xi_{\rm co} + (\xi_{\rm in} - \xi_{\rm co})\cos Q\theta' + \frac{\xi'_{\rm in}}{Q}\sin Q\theta'\right) \\ &\equiv a + b\cos Q\theta' + c\sin Q\theta'.\end{aligned} \tag{311}$$

After this replacement, θ' is the only variable factor on the RHS of Eq. (308). All of the integrals can be evaluated in closed form. The more complicated integral is given by

$$I_{\gamma i}(\theta)Q = Q\int_0^\theta \frac{d\theta'}{a + b\cos Q\theta' + c\sin Q\theta'}. \tag{312}$$

A prescription for evaluating such integrals is given, for example, in Dwight[23], formula 456.2. Define $r = \sqrt{b^2 + c^2}$, $\sin\psi = b/r$, and $\cos\psi = \pm c/r$. (In the code one must use ψ =arctan2$(b, \pm c)$ to obtain ψ, to handle the $r = 0$ possibility.) The reason for the introduction of thr $\pm$ option is explained below; until then assume the + option has been chosen. The indefinite integral is transformed to

$$\int \frac{d(Q\theta' + \psi)}{a + r\sin(Q\theta' + \psi)}. \tag{313}$$

Then, defining $x' = Q\theta' + \psi$, one obtains

$$I_{\gamma i}(\theta)Q = \int_\psi^{\psi + Q\theta} \frac{dx'}{a + r\sin x'}. \tag{314}$$

The form of this integral, as given in Dwight 436.00, depends on the relative magnitudes or a and r. In our storage ring application the oscillating part of γ is always miniscule compared to its nominal value. As a result $|a| >> |r|$ and the result is

$$I_{\gamma i}(\theta)Q = \left[\frac{2}{\sqrt{a^2-r^2}}\arctan\Big(\frac{a\tan x'/2+r}{\sqrt{a^2-r^2}}\Big)\right]_{\psi}^{\psi+Q\theta}. \tag{315}$$

In this case the denominator of the arctan argument cannot vanish. Also, practical bend element bend angles satisfy $\theta << \pi/2$ and the arctan evaluation is unambiguous. For realistically short bend elements the $\widetilde{\Delta\alpha}$ increment cannot exceed a few percent.

Another hazard to be faced is the possibility for the upper and lower limits in Eq. (315) to be on opposite sides of a discontinuity in the tan function. This was the motivation for introducing the $\pm$ option. Switching the initial choice from $+$ to $-$ is equivalent to switching the sign of ψ. The $\psi = 0$ possibility can be ignored since, in that case, there would be no possibility of upper and lower limits straddling the discontinuity. Switching the sign of ψ therefore gives two independent choices of upper and lower limits in Eq. (315) and, therefore, two evaluations of the definite integral, of which at most one is incorrect. It is not hard to decide which determination to discard. It has already been stated that the $\widetilde{\Delta\alpha}$ increment cannot exceed a few percent. Numerically this test has proved to be sufficient in numerous cases. But, as a further check, a perturbative evaluation, not subject to the arc tangent ambiguity, is described in the next section. The perturbative evaluation always agrees with the (correct) non-perturbative evaluation to 1/10 percent accuracy.

It has been stated that practical bend elements bend at most through a few degrees. The ETEAPOT code has no such constraint, however. The `sxf` file could, for example, represent a single inverse square law electric field of total bend angle arbitrarily larger than 2π. Though impractical for a storage ring, the resulting evolution can be (and has been) checked against celestial mechanics evaluations, such as those of Muñoz. The precautions described in the previous paragraph have to be altered for this case.

It is important not to apply any magnitude test to the accumulated precession angle $\tilde{\alpha}$, because its magnitude can become arbitrarily large over long times.

10.3.3 Perturbative Treatment Relative to the Magic Condition

In an EDM storage ring, the design γ value is set equal to the "magic" value γ_0. This suggests using the difference $\gamma - \gamma_0$ as independent variable for purposes of energy expansions. In practice this is likely to lead to confusion when, intentionally or unintentionally, the design value γ_D is not quite equal to γ_0. If a "magic" (in its physics sense) value is hard-coded then it becomes "magic" (in the computer science sense); which is something to be avoided. To avoid this we define, instead, with "D" standing for "design",

$$\Delta\gamma = \gamma - \gamma_D, \tag{316}$$

planning, usually, to identify γ_D with γ_0. Any particular particle being tracked will typically have a γ value different from both the magic value γ_0 and the design value γ_D. With $\gamma_D = \gamma_0$, one can check that $d\tilde{\alpha}/d\theta$ vanishes at the magic condition $\gamma = \gamma_0$;

$$\Big(\frac{g}{2}-1\Big)\gamma_D - \frac{g/2}{\gamma_D} = 0. \tag{317}$$

where $a \equiv G = 1.7928474$, $g = 2G+2 = 5.5856948$. The "magic" relativistic factor is $\gamma_0 = \sqrt{g/(g-2)} = 1.2481073$. Exploiting this relation, substituting from Eq. (316), and expanding in powers of $\Delta\gamma$,

$$\begin{aligned}\frac{d\tilde{\alpha}}{d\theta} &= \Big(\frac{g}{2}-1\Big)(\gamma_d+\Delta\gamma) - \frac{g/(2\gamma_d)}{1+\delta\gamma/\gamma_d} \\ &= \Big(\frac{g}{2}-1\Big)\Delta\gamma + \frac{g}{2\gamma_D}\Big(\frac{\Delta\gamma}{\gamma_D} - \frac{\Delta\gamma^2}{\gamma_D^2} + \frac{\Delta\gamma^3}{\gamma_D^3} - \dots\Big).\end{aligned} \tag{318}$$

The infinite series in Eq. (318) would be slowly convergent except for the fact that, typically, in an storage ring, $\Delta\gamma/\gamma_0 < 10^{-3}$. So the expansion can be applied to an arbitrary accelerator and not just a frozen spin accelerator. Furthermore, at little computational cost, the series can be truncated with no numerical test nor defined tolerance, just by retaining a conservatively large number of terms.

Repeating Eq. (271) here for convenience, from initial displacements $(x_{\rm in}, x'_{\rm in})$ one introduces intermediate variables,

$$\xi_{\rm in} = \frac{x_{\rm in}}{r_0 + x_{\rm in}}, \quad \xi'_{\rm in} = \frac{r_0^2 x'_{\rm in}}{(r_0 + x_{\rm in})^2}. \tag{319}$$

In terms of these variables, neglecting the $\xi_{\rm co}$ offset, and using Eqs. (276) and (250), evolution through a Muñoz-Pavic bend from $\theta = 0$ to θ can be approximated by

$$\begin{aligned}\frac{\Delta\gamma(\theta)}{\gamma_D} &= \frac{\mathcal{E}}{m_p c^2 \gamma_D} - 1 - \frac{eE_0 r_0}{m_p c^2 \gamma_D}\left(\cos(Q\theta)\,\xi_{\rm in} + \frac{\sin(Q\theta)}{Q}\,\xi'_{\rm in}\right) \\ &= \frac{\Delta\gamma}{\gamma_D} + \frac{eE_0 r_0 \xi_{\rm in}}{m_p c^2 \gamma_D} - \frac{eE_0 r_0}{m_p c^2 \gamma_D}\left(\cos(Q\theta)\,\xi_{\rm in} + \frac{\sin(Q\theta)}{Q}\,\xi'_{\rm in}\right)\end{aligned} \tag{320}$$

Substituting from Eq. (319) into Eq. (318) one finds, to a lowest approximation, and continuing to assume $\gamma_D = \gamma_0$,

$$\begin{aligned}\frac{d\tilde{\alpha}}{d\theta} &\approx \left(\frac{g}{2} - 1\right)\Delta\gamma + \frac{g}{2\gamma_D}\left(\frac{\Delta\gamma}{\gamma_D}\right) \\ &= \left(\frac{g}{2} - 1\right)\Delta\gamma + \frac{g}{2\gamma_D}\left(\frac{\Delta\gamma}{\gamma_D} + \frac{eE_0 r_0 \xi_{\rm in}}{m_p c^2 \gamma_D} - \frac{eE_0 r_0}{m_p c^2 \gamma_D}\left(\cos(Q\theta)\,\xi_{\rm in} + \frac{\sin(Q\theta)}{Q}\,\xi'_{\rm in}\right)\right) \\ &= \left(\frac{g}{2} - 1\right)\Delta\gamma + \frac{g}{2\gamma_D}\left(\frac{\Delta\gamma}{\gamma_D} + \frac{eE_0 r_0}{m_p c^2 \gamma_D}\left(\left(1 - \cos(Q\theta)\right)\xi_{\rm in} - \frac{\sin(Q\theta)}{Q}\,\xi'_{\rm in}\right)\right).\end{aligned} \tag{321}$$

This can be trivially integrated to give $\widetilde{\Delta\alpha}$. The total energy $\mathcal{E}$, is a constant of the motion (not counting RF cavities). If needed, higher order terms can be included similarly.

The phase advance over any single Muñoz-Pavic bend will normally be very small compared to 2π and the oscillating factor can have either sign. In fact the phase advances may sometimes be sufficiently small across individual bends to legitimize approximating $\cos Q\theta \approx 1$ and $\sin(Q\theta) \approx Q\theta$ to give a quick "ball park" estimate of the spin precession.

The way vertical betatron oscillations are treated in ETEAPOT, is to regard the Muñoz-Pavic plane as being slightly tilted. This is why the result in Eq. (321) has been expressed as $\widetilde{\Delta\alpha}$. As explained previously, small spin orientation corrections are required at entrance to and exit from bend elements, to consistently integrate the 3D and 2D descriptions.

10.4 Spin Evolution Through Fringe Fields

So far in ETEAPOT, as a particle enters or exits a bend element, its potential energy has been treated as changing discontinuously with its kinetic energy changing correspondingly. We now have to treat this region more carefully. Instead of treating the potential as discontinuous, we now assume the change occurs over a longitudinal distance $\Delta z^{\rm FF}$ which, for estimation purposes, we take equal to the separation distance (symbol *gap*) between the electrodes; $\Delta z = gap$. (For the "protonium" model introduced later, the drift lengths are taken to be almost zero and fringe field spin precession is negligible.) The fringe field region is assumed to be short enough to be treated as "thin". That is, any change in the particle's radial offset occuring in range Δz is to be neglected and the integrated deflection applied at the center (i.e. the edge of the bend). As a result the curve $x(z)$ is continuous, but its slope dx/dz is discontinuous. Entrance transitions from outside a bend to inside are described first.

Inside the bending element the increase in potential energy from orbit centerline to radial position x is $e\Delta V(x)$. As synchroton oscillations move the particle radially in and out, the sign of $\Delta V(x)$, just inside the bend edge oscillates between negative and positive values, and the sign of the deviation from

the magic velocity oscillates correspondingly. This will tend to average away the spin run-out occurring in the fringe field region over times long compared to the synchrotron period. In the long run it is the deviation from zero of this average that has to be determined. This can be by pure numerical tracking or theoretically or, most likely, by a theoretical averaging based on numerical tracking data.

Once one is able to determine the spin decoherence the task will shift to designing sextupole distributions capable of increasing the spin coherence time SCT. Our approach will be to study the effectiveness of such schemes before attempting to improve the precision of our fringe field treatment.

The deflection angle $\theta^{(FF)}$ of the design orbit in the fringe field at one such edge is approximately

$$\theta^{(FF)} \approx \frac{1}{2}\,\frac{\Delta z^{\rm FF}}{r_0} \quad \Big(\stackrel{\rm e.g.}{=} 0.5 \times 0.03/40 = 0.375 \times 10^{-3} \Big); \tag{322}$$

this is half of the deflection occurring in advancing a distance *gap* in the interior of the bend. (The angle $\theta^{(FF)}$ is implicitly assumed to be positive, irrespective of whether the orbit is clockwise or counterclockwise.) Consider a particle approaching the fringe field region at radial displacement x. At the longitudinal center of the fringe field region the kinetic energy of this particle deviates from its "proper" (i.e. fully-inside value at radial displacement x) by the amount

$$\Delta\gamma^{(FF)}(x) \approx \frac{1}{2}\,\frac{\Delta V(x)}{m_p c^2/e} \approx -\frac{1}{2}\,\frac{E\,x}{m_p c^2/e}, \tag{323}$$

where $\Delta V_{\rm tot}$ is the total voltage increase from inner electrode to outer electrode. (The electric field points radially inward in order for positive particles to bend toward negative x but, by convention, E is positive.) Here, for simplicity, we are neglecting the fact that the actual electric field will have more complicated x-dependence depending, for example, on the value of the field index m. Our assumed fringe field spatial dependence is also simplistic.

According to Eq. (318) the leading effect of passage through a bend region with γ deviation from magic $\Delta\gamma$, is a rate of change of spin angle α per unit deflection angle θ given by

$$\frac{d\alpha}{d\theta} \approx \left(\frac{g}{2} - 1 + \frac{g/2}{\gamma_0^2}\right)\Delta\gamma \quad \Big(\stackrel{\rm for\ proton}{=} 3.586\,\Delta\gamma. \Big) \tag{324}$$

Combining equations, the excess angular advance occurring while entering the bend at displacement x is

$$\boxed{\widetilde{\Delta\alpha}^{\rm FF} = +\left(\frac{g}{2} - 1 + \frac{g/2}{\gamma_0^2}\right)\frac{1}{2}\,\frac{E\,x}{m_p c^2/e}.} \tag{325}$$

(**Aside:** it may be appropriate to keep another term in expansion (324) in order to include the effect that dispersion introduces a correlation between γ and x which, after averaging, leaves a finite precession, even if $< x >$ vanishes in Eq. (325) .)

In our initial treatment of this edge effect we are assuming this precession lies in exactly the same plane as the orbit plane of the particle in the bend element, justifying the notation $\widetilde{\Delta\alpha}^{\rm FF}$ Entrance (and, later, exit) values can simply be added to the main precession through the bend element. Meanwhile, in the fringe field region the advance of the tangent to the orbit is $\theta^{(FF)}$ as given by Eq. (322). The + sign on the rhs of Eq. (325) reflects the fact that, for a particle displaced radially outward, the particle momentum is completing some of its rotation in the fringe field where its magnitude is more positive than in the bend interior.

Though the fringe field precession occurs continuously over the range *gap* it is applied discontinuously at the bend edge. This is consistent with our hard edge treatment of the particle's momentum evolution. Because $\widetilde{\alpha}$ is measured relative to the orbit direction, Eq. (325) gives the spin angle precession over and above the advance of the tangent to the orbit.

The fact that spin and momentum angular advances do not match has come about because the particle has bent appreciably while its speed deviates from the magic value. On exiting the bend element the particle also bends appreciably while its γ deviation is given by the same formula (323). Eq. (325)

therefore applies to both entrance and exit. Unfortunately this means that excess input precession and excess output precession combine constructively rather than tending to cancel (as edge focusing sometimes does.)

The largest magnitude $\Delta\gamma^{(FF)}$ can have is

$$|\Delta\gamma^{(FF)}_{\max}| = \frac{1}{4}\,\frac{E\,gap}{m_p c^2/e} \quad \left(\overset{\text{e.g.}}{=} \frac{1}{4}\,\frac{(10.5\times10^6)\times 0.03}{0.938\times10^9} = 0.84\times10^{-4}.\right) \tag{326}$$

For a particle with magic velocity skimming the outer electrode, where the effect is maximum, the angular runout is given by

$$\begin{aligned}|\Delta\alpha^{(FF)}_{\max}| &\approx \left(\frac{g}{2} - 1 + \frac{g/2}{\gamma_0^2}\right)\Delta\gamma_{\max}\,\Delta\theta^{(FF)} \\ &= 3.586\times(0.84\times10^{-4})\times(0.375\times10^{-3}) \\ &= 1.13\times10^{-7}\,\text{radians/edge.}\end{aligned} \tag{327}$$

With perhaps 50 edges in the lattice, and revolution frequency of about 1 MHz, the maximum spin runout will be about one revolution per second. This vastly exaggerates the spin decoherence, of course, because it does not account for the averaging effect of synchrotron oscillations. A challenge for lattice design is to perfect the synchrotron oscillation averaging to zero.

10.5 Spin Evolution Through Thin Elements

In ETEAPOT the only "thick" elements are bends. Spin evolution through them has already been discussed. All other elements are treated as thin element kicks. Rearranging Eq. (324) produces, for spin evolution through a thin element,

$$\boxed{|\widetilde{\Delta\alpha}| \approx \left(\frac{g}{2} - 1 + \frac{g/2}{\gamma_0^2}\right)\Delta\gamma\,\widetilde{\Delta\theta}} \tag{328}$$

where $\widetilde{\Delta\theta}$ is positive by definition and $\widetilde{\Delta\alpha}$ is the angular deviation of the bend plane spin coordinate relative to the orbit. The absolute value sign in this equation eventually has to be removed; it is included here so that the discussion of signs can be deferred. In paraxial approximation, for a particle with transverse position (x, y), the magnitude of the (not necessarily horizontal) angular deviation $\widetilde{\Delta\theta}$ in a quadrupole of strength q is given by

$$\widetilde{\Delta\theta} = |q|\sqrt{x^2+y^2}, \tag{329}$$

where q is the inverse focal length of the quadrupole.

The magnitude of the angular deflections in sextupoles and higher order multipoles are also functions only of the combination $r = \sqrt{x^2+y^2}$. Eq. (329) generalizes to

$$\begin{aligned}\widetilde{\Delta\theta}_{\text{quad}} &= |q|r, \\ \widetilde{\Delta\theta}_{\text{sext}} &= \frac{|S|}{2}\,r, \\ \widetilde{\Delta\theta}_{\text{oct}} &= \frac{|O|}{6}\,r,\end{aligned} \tag{330}$$

where S is the conventionally defined sextupole strength and O is the conventionally defined octupole strength. The element strengths appearing in an SXF lattice description file include the numerical factors. That is, the quad parameter is $b_1 = q$, the sextupole parameter is $b_2 = S/2$, the octupole parameter is $b_3 = S/6$, and so on.

A significant complication concerns the sign of the $\widetilde{\Delta\alpha}$. For a *horizontally focusing or defocusing quadrupole* there is no ambiguity, since the bend plane in the quadrupole is the same as the overall

(horizontal) lattice design plane. In this case, with $y = 0$, Eq. (328) can be made more explicit;

$$\widetilde{\Delta\alpha}_h \approx \left(\frac{g}{2} - 1 + \frac{g/2}{\gamma_0^2}\right) \Delta\gamma \, q \, x. \tag{331}$$

where, by convention, a horizontal *focusing* quad has $q > 0$. The sign in Eq. (331) reflects the fact that, for $x > 0$ and $q > 0$, the quadrupole "helps" by bending the momentum in the same sense as the bending elements. This formula makes it clear that reversing the sign of q reverses the sign of $\widetilde{\Delta\alpha}$.

For obtaining the proper sign for vertically focusing quadrupoles it is necessary to handle consistently the transformation from laboratory to bend frame spin coordinates, which is why the sign issue has been deferred until after discussing this transformation.

Most of the elements in a storage ring cause spin precession which approximately conserves the vertical component of spin $s_y\hat{\mathbf{y}}$. The leading exceptions to this in a proton EDM storage rings are the vertically focusing or defocusing quadrupoles present in the lattice to keep β_x magnageably small. Particles having non-vanishing vertical betatron amplitude are deflected vertically which causes $s_y\hat{\mathbf{y}}$ to precess. (As an aside it can be mentioned that there is a very strong tendency for this precession to cancel in subsequent quadrupoles and, therefore, probably not contribute significantly to spin decoherence. Nevertheless it is important for the precession to be modeled correctly.) All quadrupoles and sextupoles in the lattice cause similar precession to at least some degree.

The planes of deflection for particles incident on a quadrupole are shown in Figure 11. In a perfect multipole field the magnitude of the total deflection angle is constant on a contour of fixed radius (i.e. a circle centered on the origin.) For a particle incident at (x_0, y_0) the equation of the line of intersection of the deflection plane with the transverse plane is

$$y = y_0 - \frac{y_0}{x_0}\,(y - y_0), \tag{332}$$

As shown if the figure, the roll-angle of the deflection plane (with counter-clockwise roll taken as positive) is $\phi_0 = \tan^{-1}(y_0/x_0)$, irrespective of quadrant and whether the quadrupole is focusing or defocusing. However the inverse tangent function is, itself, multiple valued. To make it single valued one can determine ϕ_0 using

$$\phi_0 = \text{arctan2}(qy_0, qx_0). \tag{333}$$

Along with Eq. (328), this establishes both the sign and magnitude of $\widetilde{\Delta\alpha}$, while preserving the sign reversal when the sign of q reverses. This should be checked numerically in all quadrants. For sextupoles,

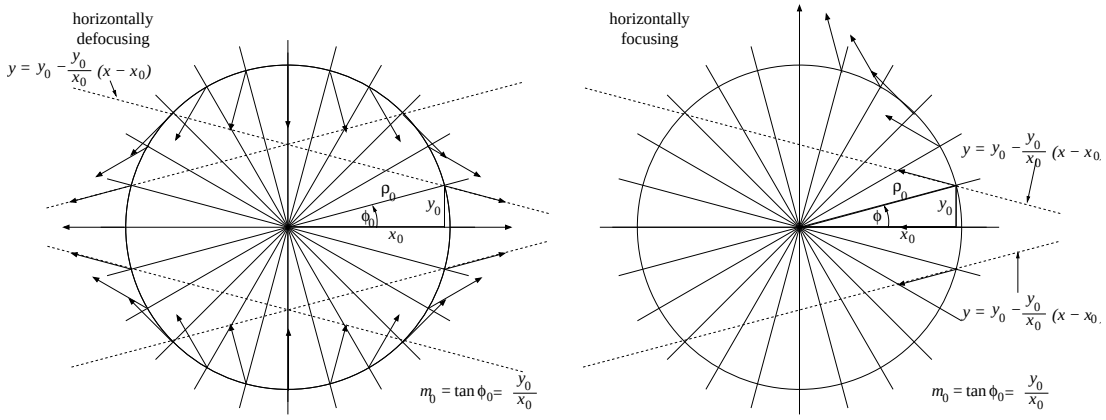

Figure 11: The broken lines shows the deflection planes for particle with dispacements x_0, y_0 in various quadrants, incident on an erect quadrupole. The roll-angle of the deflection plane (with counter-clockwise roll taken as positive) is $\phi_0 = \tan^{-1}(y_0/x_0)$ irrespective of quadrant, and irrespective of whether the quadrupole is focusing or defocusing.

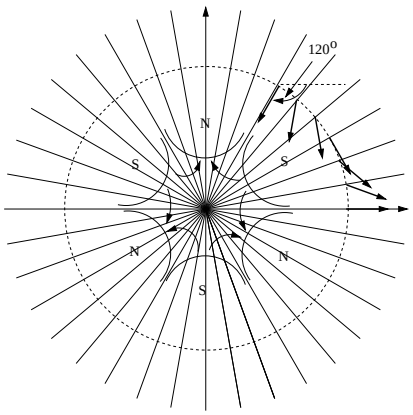

Figure 12: Pole profiles for a sextupole element are shown. By comparison with Figure 11, this figure is intended to help in generalizing Eq. (333) to sextupoles, octupoles, and other multipoles.

octupoles and other multipoles it is also necessary to generalize Eq. (333). Figure 12 is intended to be helpful. The results are

$$\begin{aligned}\phi_{0,\mathrm{quad}} &= 1\arctan2(qy_0, qx_0),\\ \phi_{0,\mathrm{sext}} &= 2\arctan2(Sy_0, Sx_0),\\ \phi_{0,\mathrm{oct}} &= 3\arctan2(Oy_0, Ox_0).\end{aligned} \tag{334}$$

With roll angles of the bend plane determined this way, the following formulas apply to all multipoles.

Substitution into Eq. (302) and setting $\phi_0 = \phi$ produces

$$\begin{pmatrix} s_x'' \\ s_y'' \\ s_z'' \end{pmatrix} = \begin{pmatrix} \cos\phi & \sin\phi & 0 \\ -\sin\phi & \cos\phi & 0 \\ 0 & 0 & 1 \end{pmatrix} \begin{pmatrix} \cos\widetilde{\Delta\alpha} & 0 & -\sin\widetilde{\Delta\alpha} \\ 0 & 1 & 0 \\ \sin\widetilde{\Delta\alpha} & 0 & \cos\widetilde{\Delta\alpha} \end{pmatrix} \begin{pmatrix} \cos\phi & -\sin\phi & 0 \\ \sin\phi & \cos\phi & 0 \\ 0 & 0 & 1 \end{pmatrix} \begin{pmatrix} s_x \\ s_y \\ s_z \end{pmatrix} \tag{335}$$

It is appropriate, to improve numerical precision, to break the central matrix into two terms, $\mathbf{I}+\mathbf{\Delta}$ where $\mathbf{I}$ is the identity matrix and $\mathbf{\Delta}$ is a small deviation. Then, since $\mathbf{I}$ commutes with the outer matrices, and their product is $\mathbf{I}$, the final result is equal to $\mathbf{I}$ plus a small deviation. The matrix product is

$$\begin{aligned}&\begin{pmatrix} \cos\phi & \sin\phi & 0 \\ -\sin\phi & \cos\phi & 0 \\ 0 & 0 & 1 \end{pmatrix} \left(\begin{pmatrix} 1 & 0 & 0 \\ 0 & 1 & 0 \\ 0 & 0 & 1 \end{pmatrix} + 2\sin(\widetilde{\Delta\alpha}/2) \begin{pmatrix} -\sin\widetilde{\Delta\alpha}/2 & 0 & -\cos\widetilde{\Delta\alpha}/2 \\ 0 & 1 & 0 \\ \cos\widetilde{\Delta\alpha}/2 & 0 & -\sin\widetilde{\Delta\alpha}/2 \end{pmatrix} \right) \begin{pmatrix} \cos\phi & -\sin\phi & 0 \\ \sin\phi & \cos\phi & 0 \\ 0 & 0 & 1 \end{pmatrix} \\ &= \begin{pmatrix} 1 & 0 & 0 \\ 0 & 1 & 0 \\ 0 & 0 & 1 \end{pmatrix} + 2\sin(\widetilde{\Delta\alpha}/2) \begin{pmatrix} \cos\phi & \sin\phi & 0 \\ -\sin\phi & \cos\phi & 0 \\ 0 & 0 & 1 \end{pmatrix} \begin{pmatrix} -\sin\widetilde{\Delta\alpha}/2 & 0 & -\cos\widetilde{\Delta\alpha}/2 \\ 0 & 1 & 0 \\ \cos\widetilde{\Delta\alpha}/2 & 0 & -\sin\widetilde{\Delta\alpha}/2 \end{pmatrix} \begin{pmatrix} \cos\phi & -\sin\phi & 0 \\ \sin\phi & \cos\phi & 0 \\ 0 & 0 & 1 \end{pmatrix}.\end{aligned} \tag{336}$$

Calculation of the *changes* in spin coordinates requires only the second term, which is

$$2\sin(\widetilde{\Delta\alpha}/2) \begin{pmatrix} -\cos(\phi)^2\sin(\widetilde{\Delta\alpha}/2) & \cos(\phi)\sin(\widetilde{\Delta\alpha}/2)\sin(\phi) & -\cos(\phi)\cos(\widetilde{\Delta\alpha}/2) \\ \cos(\phi)\sin(\widetilde{\Delta\alpha}/2)\sin(\phi) & -\sin(\phi)^2\sin(\widetilde{\Delta\alpha}/2) & \sin(\phi)\cos(\widetilde{\Delta\alpha}/2) \\ \cos(\phi)\cos(\widetilde{\Delta\alpha}/2) & -\sin(\phi)\cos(\widetilde{\Delta\alpha}/2) & -\sin(\widetilde{\Delta\alpha}/2) \end{pmatrix}. \tag{337}$$

As mentioned before, all components in this matrix are small, of order $\widetilde{\Delta\alpha}$ or smaller, even if the angle ϕ is as great as $\pi/2$. Multiplying this matrix on the right by $(s_x, s_y, s_z)^T$ produces deviations $(\Delta s_x, \Delta s_y, \Delta s_z)$ which, added to (s_x, s_y, s_z), give the output spin coordinates.

10.6 Formulas Sensitive to Precession Sense

Hardly anything can be more confusing than what constitutes positive sense of precession of momentum and spin, especially in a storage ring in which there are both CW and CCW beam directions. One can haggle whether or not the sign choices in Fig. (10) were chosen advisedly. But, for better or worse, we define the sense of momentum precession in that figure to be *positive*. We also define the vertical axis to be always the same, and specified by the unit vector $\hat{\mathbf{y}}$.

In electric bending elements, for momenta close to the magic momentum the rates of precession of spin and momentum are approximately equal, which makes it easy to establish the signs of contributions to the spin precession. The same was true, in Eq. (331), for horizontally focusing quads. But for vertically focusing quads, and multipoles in general it seems advisable to develop and algebraic test, based on dot products and cross products of vectors, in order to specify precession senses.

The sense of momentum precession in Fig. (10), which we have defined to be positive, can also be defined to be the sign of the scalar product

$$\Big(\frac{d\mathbf{p}}{dt}\times\mathbf{p}\Big)\cdot\hat{\mathbf{y}}>0. \tag{338}$$

with the momentum $\mathbf{p}$ always lying approximately in the horizontal plane, which is normal to $\hat{\mathbf{y}}$. When expressed in terms of the electric field using Newton's law, the same condition for positive sense precession can be expressed

$$e\Big(\mathbf{E}\times\mathbf{p}\Big)\cdot\hat{\mathbf{y}}>0, \tag{339}$$

with $\mathbf{E}$ also approximately horizontal.

Similarly, the positive sense for spin precession can be defined by

$$\Big(\frac{d\mathbf{s}}{dt}\times\mathbf{s}\Big)\cdot\hat{\mathbf{y}}>0. \tag{340}$$

Using Jackson's Eq. (11.170), the spin precession in electric field $\mathbf{E}$ is given by

$$\frac{d\mathbf{s}}{dt}=-\frac{e}{m^2c^2\gamma}\,\mathbf{s}\times(\frac{g}{2}-\frac{\gamma}{\gamma+1})(\mathbf{p}\times\mathbf{E}) \tag{341}$$

Substituting this expression into Eq. (340) produces

$$-\frac{e}{m^2c^2\gamma}\,(\frac{g}{2}-\frac{\gamma}{\gamma+1})\Big(\Big(\mathbf{s}\times(\mathbf{p}\times\mathbf{E})\Big)\times\mathbf{s}\Big)\cdot\hat{\mathbf{y}}>0. \tag{342}$$

Simplifying the triple cross product and using the fact that $\mathbf{s}$ is a unit vector, this reduces to

$$\frac{e}{m^2c^2\gamma}\,(\frac{g}{2}-\frac{\gamma}{\gamma+1})\Big(\Big(-\mathbf{s}\cdot(\mathbf{E}\times\mathbf{p})\Big)\mathbf{s}+\mathbf{E}\times\mathbf{p}\Big)\cdot\hat{\mathbf{y}}>0. \tag{343}$$

For any spin vector $\mathbf{s}$ lying in the plane perpendicular to $\mathbf{E}\times\mathbf{p}$ (which, in the pEDM experiment is always approximately parallel to the y-axis) the condition reduces to

$$\frac{e}{m^2c^2\gamma}\,(\frac{g}{2}-\frac{\gamma}{\gamma+1})\,\mathbf{E}\times\mathbf{p}\cdot\hat{\mathbf{y}}>0. \tag{344}$$

11 Electrostatic Lattice Design

11.1 Lattice Function Evolution in Focusing Elements

Twiss function evolution through a focusing element with focusing coefficient K is described by

$$\boldsymbol{\beta}(z) = \begin{pmatrix}\alpha(z)\\ \beta(z)\\ \gamma(z)\end{pmatrix} = \begin{pmatrix} \cos 2\sqrt{K}\,z & \frac{\sqrt{K}}{2}\sin 2\sqrt{K}\,z & -\frac{1}{2\sqrt{K}}\sin 2\sqrt{K}\,z \\ -\frac{1}{\sqrt{K}}\sin 2\sqrt{K}\,z & \cos^2\sqrt{K}\,z & \frac{1}{K}\sin^2\sqrt{K}\,z \\ \sqrt{K}\sin 2\sqrt{K}\,z & K\sin^2\sqrt{K}\,z & \cos^2\sqrt{K}\,z \end{pmatrix} \begin{pmatrix}\alpha(0)\\ \beta(0)\\ \gamma(0)\end{pmatrix}$$
$$= \mathbf{M}_E(K,z)\,\boldsymbol{\beta}(0), \tag{345}$$

where $\gamma = (1+\alpha^2)/\beta$. The most promising candidate for bend element for the proton EDM experiment has curved-planar electrodes for which there is no vertical focusing. From Eq. (216), with $K_{x,1} = 0$, the focusing coefficients for x and y motion are

$$K_{x,1}^{(E,\text{eff.})} = \frac{1}{r_0^2} + \frac{1}{r_0^2\gamma_0^2},$$
$$K_{y,1}^{(E,\text{eff.})} = 0. \tag{346}$$

In a field free region $K = 0$ and the Twiss evolution matrix reduces to

$$\boldsymbol{\beta}(z) = \begin{pmatrix}\alpha(z)\\ \beta(z)\\ \gamma(z)\end{pmatrix} = \begin{pmatrix} 1 & 0 & -z \\ -2z & 1 & z^2 \\ 0 & 0 & 1 \end{pmatrix} \begin{pmatrix}\alpha(0)\\ \beta(0)\\ \gamma(0)\end{pmatrix} = \mathbf{M}_D(z)\,\boldsymbol{\beta}(0). \tag{347}$$

By definition, at a "beam waist" the α-function vanishes.

11.2 A Basic Lattice Building Block

A relatively simple lattice building block consists of a drift of length $L_d/2$, followed by a thin quad of strength q, followed by two indentical electric bends of focusing strength K and length $l_E/2$, followed by another thin quad of strength q and another drift of length $Ld/2$. The matrix describing Twiss function evolution through the first half of this sequence is

$$\mathbf{M}_h = \mathbf{M}_E(K, L_e/2)\,\mathbf{M}_Q(q)\,\mathbf{M}_D(L_d/2) \tag{348}$$

The matrices all have the form shown in Eq. (345), though with elements specific to the particular element and applicable to x or y motion. The matrix for the full block is

$$\mathbf{M}(L_d, L_e, K, q) = \mathbf{M}_h^{-1}\mathbf{M}_h. \tag{349}$$

Let us suppose this sequence describes evolution from a waist to an identical waist. A transfer matrix $\mathbf{M}(z)$ describing waist-to-identical-waist evolution satisfies

$$\begin{pmatrix}0\\ \beta(0)\\ 1/\beta(0)\end{pmatrix} = \mathbf{M}(L_d, L_e, K, q) \begin{pmatrix}0\\ \beta(0)\\ 1/\beta(0)\end{pmatrix} = \begin{pmatrix} M_{11} & M_{12} & M_{13} \\ M_{21} & M_{22} & M_{23} \\ M_{31} & M_{32} & M_{33} \end{pmatrix} \begin{pmatrix}0\\ \beta(0)\\ 1/\beta(0)\end{pmatrix}. \tag{350}$$

This equation applies separately to both x and y planes though with different values of β_x and β_y (where the argument 0 has been suppressed). This yields four equations,

$$\beta_x^2 = \frac{M_{23,x}}{1 - M_{22,x}}, \quad \beta_x^2 = \frac{1 - M_{33,x}}{M_{32,x}},$$
$$\beta_y^2 = \frac{M_{23,y}}{1 - M_{22,y}}, \quad \beta_y^2 = \frac{1 - M_{33,y}}{M_{32,y}}. \tag{351}$$

If β_x and β_y are specified, this yields four equations for the four unknowns. On physical grounds, if β_x and β_y are chosen sensibly, one expects to find unique, sensible values for $L_d,\ L_e,\ K$,and q.

A more useful solution results from regarding L_e and K as being given length and strength parameters of the electric bending element. Then one should be able to find β_x and β_y as functions of L_d and q.

11.3 Full Ring Transfer Matrices and Dispersion Function

Orbit evolution from the origin at $s = 0$ to a general position s can be expressed by a transfer matrix $\mathbf{M}(s, 0)$:

$$\begin{pmatrix} x(s) \\ x'(s) \\ \Delta \end{pmatrix} = \begin{pmatrix} M_{11}(s,0) & M_{12}(s,0) & M_{13}(s,0) \\ M_{21}(s,0) & M_{22}(s,0) & M_{23}(s,0) \\ 0 & 0 & 1 \end{pmatrix} \begin{pmatrix} x(0) \\ x'(0) \\ \Delta \end{pmatrix}. \tag{352}$$

After associating one of the transfer matrices derived above with each of the elements in the ring, $\mathbf{M}(s, 0)$ is found by "concatenating" (i.e. multiplying) these matrices. A transfer matrix $\mathbf{M}(s_2, s_1)$ describing evolution from s_1 to s_2 can be found similarly.

Since the transfer matrix includes a description of the influence of energy offset, it can also be used to find the dispersion function $D(s)$, in terms of which the off-energy closed orbit displacement is given by

$$x_{\Delta,\text{c.o.}}(s) = D(s)\Delta, \tag{353}$$

where Δ is a fractional offset appearing in Eq. (227). Evolution once around the ring, starting from the origin, of an off-energy particle on the closed orbit corresponding to its energy is described by the "once-around" transfer matrix $\mathbf{M}$:

$$\begin{pmatrix} D(0)\Delta \\ 0 \\ \Delta \end{pmatrix} = \begin{pmatrix} M_{11} & M_{12} & M_{13} \\ M_{21} & M_{22} & M_{23} \\ 0 & 0 & 1 \end{pmatrix} \begin{pmatrix} D(0)\Delta \\ 0 \\ \Delta \end{pmatrix}. \tag{354}$$

This has assumed the lattice is mirror symmetric about the origin, which is why the slope of the off-energy orbit has been set to zero at the origin. This provides two equations determining $D(s)$:

$$D(0) = \frac{M_{13}}{1 - M_{11}} = -\frac{M_{23}}{M_{21}}, \tag{355}$$

one of which can be used as a consistency check. Evolution around the ring of $D(s)$ and $D'(s)$ is then given by

$$\begin{pmatrix} D(s) \\ D'(s) \\ 1 \end{pmatrix} = \begin{pmatrix} M_{11}(s) & M_{12}(s) & M_{13}(s) \\ M_{21}(s) & M_{22}(s) & M_{23}(s) \\ 0 & 0 & 1 \end{pmatrix} \begin{pmatrix} D(0) \\ 0 \\ 1 \end{pmatrix}. \tag{356}$$

Spelled out explicitly this yields

$$\begin{aligned} D(s) &= D(0)\, M_{11}(s) + M_{13}(s), \\ D'(s) &= D(0)\, M_{21}(s) + M_{23}(s). \end{aligned} \tag{357}$$

where $\widetilde{\mathcal{C}}$ is the circumference of the ring and the length over which all lattice functions have to be periodic.

12 Refraction at Wedge Faces (Introduction Only)

(Like most accelerator tracking codes,) TEAPOT represents entrance and exit magnetic fringe fields by thin multipoles. Simplest, and usually adequate, especially for normal incidence, is the "hard edge" model that treats the magnetic field discontinuously from its uniform value inside the magnet to zero outside. This preserves symplecticiy. The leading effect is the "wedge focusing" that accompanies pole face rotation (non-normal entrance or exit).

For the EDM experiment the central proton will enter and exit the bend elements normally, and the same will be approximately true for all protons. There will, however, be two effects specific to the electric (as contrasted with magnetic) field. One is the change ΔK in kinetic energy resulting from the change in potential energy.

$$\begin{aligned} \Delta K &= \sqrt{p^2c^2 + m_p^2c^4}\Big|_{\text{after}} - \sqrt{p^2c^2 + m_p^2c^4}\Big|_{\text{before}} \\ &= -eV\Big|_{\text{after}} + eV\Big|_{\text{before}} = -e\Delta V(x, y). \end{aligned} \tag{358}$$

This would be exact for changes from well inside to well outside. But we have assumed "hard edge" discontinuous change of potential at the wedge face in the last step with (x, y) being the intersection point of the orbit with the face of the wedge. Since the transverse momentum components are conserved

The other effect is a refractive deflection resulting from the impulsive change in longitudinal momentum while the transverse momentum is conserved. Keeping track of the particle direction by evolving the momentum components (p_x, p_y, p_s), since p_x and p_y are conserved, we need only solve for Δp_s in the equation

$$\sqrt{p_x^2 + p_y^2 + (p_s + \Delta p_s)^2 + m_p^2 c^4} - \sqrt{p_x^2 + p_y^2 + p_s^2 + m_p^2 c^4} = -e\Delta V(x, y), \tag{359}$$

12.1 Orbit Evolution Through Multipole Elements

Transverse electrostatic fields can be expanded using the same multipole series as is used for transverse magnetic multipole elements. Electric multipoles will therefore be treated the same way magnetic elements are presently treated in TEAPOT. Sufficiently thin slicing one should provide a fully satisfactory model. Refractive effects could be treated the same way as was just described for bend elements. This will probably be unnecessary, at least initially.

References

[1] C. Møller, *The Theory of Relativity,* Clarendon Press, Oxford, 1952,

[2] G. Muñoz and I. Pavic, *A Hamilton-like vector for the special-relativistic Coulomb problem,* Eur. J. Phys. **27**, 1007-1018, 2006

[3] R. Talman, *Accelerator X-Ray Sources,* John Wiley and Sons, 2006

[4] R. Talman, *Geometric Mechanics,* John Wiley and Sons, 2000

[5] J. Aguirregabiria et al., Archiv:physics/0407049v1 [physics.ed-ph] 2004,

[6] U. Torkelsson, Eur. J. Phys., **19**, 459, 1998,

[7] T. Boyer, Am. J. Phys. **72** (8) 992, 2004

[8] N. Malitsky, J. Talman, and R. Talman, *Ring Lattice for Proton EDM Measurement,* pEDM collaboration document, 11 January, 2011. Another chapter submitted to the March 2011 BNL pEDM Project Review.

[9] Review of the Storage Ring EDM experiment at BNL, December, 2009, `http://www.bnl.gov/edm/review/EDM Review`.

[10] R. Talman, *Miscellaneous Calculations for a Fully Electrostatic Proton EDM Experiment, Version II,* `http://www3.bnl.gov/muonedm/ Matters_of_interest/RTalmanElectrostaticEDM.2.pdf`.

[11] Proton EDM Storage Ring Collaboration, *R&D Development Plan for a Proton EDM Experiment with Sensitivity of* $!)^{29}$ *e.cm,* BNL Report Proton_RD_091125.pdf, 2009

[12] H. Wollnik, *Optics of Charged Particles,* Academic Press, p. 124, 1987

[13] *Ring Lattice for Proton EDM Measurement*, chapter in report to March, 2011, BNL Review of Proton EDM experiment, February 10, 2011. Available at the same source as the present report.

[14] J. Jackson, *Classical Electrodynamics,* 3rd edition, John Wiley, 1998

[15] G. Zhong and J. Marsden, *Lie-Poisson Hamilton-Jacobi Theory and Lie-Poisson integrators,* Phys. Lett. A **133**, 134-139, 1988

[16] J. Sanz-Serna and M. Calvo, *Numerical Hamiltonian Problems,* Chapman and Hall, 1994

[17] L. Schachinger and R. Talman, *TEAPOT: A Thin Element Program for Optics and Tracking,* Part. Accel. **22**,35(1987)

[18] Y. Yan, G. Bourianoff, and L. Schachinger, Proc. Workshop on Nonlinear problems in Future Particle Accelerators, Capri, Italy, 1990

[19] N. Malitsky and R. Talman, *Unified Accelerator Libraries,* Proceedings of Conference on Accelerator Software, Williamsburg, VA, 1996, *The Framework of Unified Accelerator Libraries,* ICAP98, Monterey, 1998

[20] R. Engelke and C. Chandler, *Planetary Perihelion Precession with Velocity-Dependent Gravitational Mass,* Am. J. Phys. **38**, 90, 1970

[21] *Ring Lattice for Proton EDM Measurement*, chapter in report to March, 2011, BNL Review of Proton EDM experiment, February 10, 2011. Available at the same source as the present report.

[22] Y. Semertzidis, *Horizontal Tune as a Function of E-Field Functional Form,* BNL note, 10 January, 2011

[23] H.B. Dwight, *Tables of Integrals and Other Mathematical Data,* MacMillan Publishing Co., Inc., 1961